THE UNIVERSITY
of EDINBURGH

Hydrophobic and fire retardant treatment with functionalised silica particles applied on hemp shiv

Marion Agathe Bourebrab

A thesis submitted for the degree of
Doctor of Philosophy

THE UNIVERSITY
of EDINBURGH

2019

Hydrophobic and fire retardant treatment with functionalised silica particles applied on hemp shiv

Marion Agathe Bourebrab

This thesis has been supervised by

Dr Alan Taylor

Dr Géraldine G. Durand

Dr Rory M. Hadden

Prof Luke A. Bisby

The examining committee consisted of

Prof Maude Jimenez

Université de Lille

Dr Ricky Carvel

The University of Edinburgh

To my nephew Timmu-rakas, may you never stop exploring and questioning the world around you.

Declaration

I declare that this thesis has been solely composed by myself, under the supervision of Dr Alan Taylor (TWI Ltd.), Dr Géraldine G. Durand (TWI Ltd.), Dr Rory M. Hadden (The University of Edinburgh) and Prof Luke A. Bisby (The University of Edinburgh). The experimental work was carried out either at the National Structural Integrity Research Centre (NSIRC) within TWI Ltd. facilities, or at the BRE Centre for Fire Safety Engineering, in the School of Engineering of the University of Edinburgh. The work described herein has not been submitted for any other degree qualification. I confirm that the work is my own, and where some work was carried out as part of a collaborative project, contributors are explicitly mentioned and acknowledged.

Marion A. Bourebrab

20th December 2018

Abstract

With an ever growing population, increased air pollution, and decrease of natural resources, the construction sector requires new sustainable solutions. Bio-materials, usually crop by-products, are considered a strong alternative to conventional building materials, and their use is not a direct competition in other supply chains like food crops can be. On top of their lower cost of manufacture (from both an economic and resource perspectives), they present attractive acoustic and thermal insulation properties. Specifically, the woody core of the hemp plant (*Cannabis sativa L.*), also named hemp shiv, acts as a moisture buffer due to its micropores, which allow water vapour to permeate. A wider adoption of this material as part of a building envelope is however hindered by the intrinsic chemical characteristics of hemp shiv. Made up mostly of cellulose and other sugar-derived polymeric groups, hemp shiv deteriorate in warm and humid environments, giving rise to microbial growth, and present a non-negligible fire risk. Their combustibility and predisposition to absorb liquid water are two issues which need to be addressed in order to enable their use in the built environment.

This thesis presents the development of a silica particle technology to limit the biodegradation and improve the fire performance of hemp shiv. A rational design approach was followed for the synthesis of silica particles, by changing reactions parameters and the ratios of reagents. Better understanding of the effect of the reagents proportions and temperature on the synthesis allowed the size, porosity, and surface chemistry of the resultant silica particles to be tailored. Specifically, it was found that keeping the quantity of water between two boundary conditions enabled the con-

trolled synthesis of discrete particles which diameters ranged from 120 to 820 nm with a defined pore shape distribution. Select formulations of particles of different sizes were then functionalised to make them hydrophobic, which was successfully assessed when functionalised silica particles were deposited on glass slides. Hemp shiv were then coated with selected formulations of functionalised silica particles, and their water repellence was equally verified, as well as the limitation of their water uptake, which increased from a few seconds to beyond 20 minutes. The samples also demonstrated delayed biodegradation when exposed to a humid environment, whilst retaining their moisture buffering and hydrophobic properties. Finally, silica was shown to act as a heat sink, by absorbing part of the radiant heat thus more energy was required for the onset of pyrolysis to occur. They also protected the hemp shiv against further oxidation, and consequently reduced their combustion rate. Composite structures made from hemp shiv in which the silica particles were introduced displayed improved fire performance, and similar response (although physical rather than chemical) when compared to composites treated with conventional fire retardant solutions. The approach followed here proved that silica particles can prevent moisture and thermally induced deterioration of hemp shiv, at laboratory scale.

Lay Summary

With an ever growing population, increased air pollution, and decrease of natural resources, the construction sector requires new sustainable solutions. Bio-materials, usually crop by-products, are considered a strong alternative to conventional building materials, and their use is not a direct competition in other supply chains like food crops can be. On top of their lower economic and resource cost, they present attractive thermal insulation properties to reduce energy use in buildings. Specifically, parts of the hemp plant, also named hemp shiv, have the ability to regulate moisture from its environment due to its micropores which act as a buffer. Like most plant based materials, hemp shiv are combustible, and present fire risks, and are also susceptible to rotting if kept in moist environment. These issues need to be addressed before widely adopting hemp shiv as an insulation material.

This thesis presents the development of a silica particle technology to address these issues. The synthesis of silica particles was carried out by changing reactions parameters and measuring their influence on the physical and chemical characteristics of the resultant particles. Specific formulations of particles of different sizes were then functionalised to make them repel liquid water, which was successfully assessed when functionalised silica particles were deposited on glass slides. Hemp shiv were then coated with selected formulations of functionalised silica particles, and their water repellence was equally verified. The samples also demonstrated decay limitation when exposed to a humid environment. The presence of silica on the surface of hemp shiv delayed the onset of ignition of the material. The silica treatment displayed a similar performance to conventional fire retardant solutions. The approach followed here

proved that silica particles can prevent deterioration of hemp shiv, at a laboratory scale.

Acknowldegments

First and foremost, I would like to express my gratitude towards my supervisors at TWI Ltd., Dr Alan Taylor and Dr Géraldine Durand, for their support, advice, discussions about silica particles and science in general. I am grateful that I could start building my career from such opportunity of work. Many thanks to my other two supervisors at the University of Edinburgh, Dr Rory Hadden and Prof Luke Bisby, for having shared with me your extensive knowledge of anything fire-related.

Financially, this work was funded by TWI Ltd. through the ISOBIO project (European Union's Horizon 2020 research and innovation programme, under grant agreement N°636835). I feel privileged to have had the opportunity to work on this project, and would like to acknowledge the consortium partners involved.

Great work is never a single person making, and I am deeply grateful to many contributors for their help in the labs: from TWI side, Chris and the TCE section at TWI Middlesbrough for the countless samples you have run for me on the TGA, Alex and Jacob for showing me how to best use some pieces of equipment (and fixing them), Steve who taught me how to synthesise the silica particles in the early days and helped me out throughout the last three years, Angelo for the BET experiments you carried out for me, Sheila for allowing me to see my particles for the first time by SEM; Juan P. (now at UQ) for showing me how to tame the cone calorimeter in the Fire Lab at the University of Edinburgh and Michal for helping me with it; Valentin at Cavac Biomatériaux for the numerous hemp shiv composite samples you have manufactured for me to test.

Having a great team to work with was equally as important in and out of the

lab. I would like to thank the best team of TWI, the Functional Coatings and Resins section (Adam, Alan, Alex, Ana, Angelo, Anna, Christina, Eu, Géraldine, Gillian, Jacob, Marta, Mehrnaz, Nadia, Shenghui, Steve, Taraneh, Victoria), for their help, support, discussions, and the welcome distractions over lunchtime walks. Even though I haven't spent so much time there, the Fire Group at the University of Edinburgh has been an amazing second team, and I greatly appreciated their support when I was visiting.

Carrying out a PhD can be a daunting experience, especially towards the write up when willpower is very much needed. I do believe in the Latin motto *Anima sana in corpore sano*, and I am so grateful to have had an amazing crew to train with at the Tsunami Gym in Cambridge, to keep me sane by letting me hit the pads. I would like to slip a little note to the CVG Army, who empower each other in and out the gym to achieve one's goals, be it in personal or professional life.

Many of my friends have been an amazing support during those three years, whom I would like to thank. Thanks to all the friends I have made at work, in no particular order: Sofía, Nico, Ángela, Oli, Craig, Evelyne, Pedro, Kamer, Gaby, Farnoosh, Amina, and the whole Tipper Group, and I will probably have missed a few. You surely have made the days go faster! All the generations of Holbrook Girls: Sarah, Becca, Kirsten, Daisy, Marisa, thank you for your patience and having to deal with me, my mood swings, and my broken ankle, for feeding me, for all our amazing times together, you have been, and still are my family. Lisa, we've been through this journey together, and we'll finish it together (although you a bit earlier than me)! Many thanks for the numerous weekends spent at the library or the Espresso Library (thanks to the staff there!), the bike rides, the mud runs, the gym sessions, the spontaneous dinners, and many many more moments spent together. Mis cariños in Edinburgh Uli and Martina, thanks for the 50 mila lacrime and the great memories I made with you in Scotland, Lund, Malmö, and Copenhagen. Thank you my almost-sister Alex for encouraging me, for being by my side depuis le lycée dans la Yaute, for coming to visit my other home country, and for being such an inspiring, strong-willed person. Thank you Claire "Voodoo" for having been (and still being) my role model, for our long con-

versations on quantum physics and your life advice, I am so grateful I get to call you my friend. Saying thank you to my Quad Squad – Deanna, Mell, and Birgit – would not be enough: I don't know how I would have carried on without your unconditional moral support, the runs, the drinks, the trainings, the dinners, the painting, the trips, for always being there in (many) good and (much fewer) bad times. You are the best.

Kiitos minun suomalaisperheelle, kun opetitte minulle suomalaisista perusarvoista, ja erityisesti sisusta, kun olitte vieressäni ajatuksissa vaikka kaukana. Kiitän myöskin minun skeittitytölle Lilo siitä, että olet sinä.

Merci aux PDG pour ces nombreuses années d'amitié, de m'avoir fait rire avec vos conneries sur WhatsApp, pour les Skypéros, les craquages, les partages, mais particulièrement votre soutien. Merci à la fameuse Shadow Girl Estelle pour les rires depuis la Gold Coast. Je tiens à glisser un mot à ma cousine Zoé, d'avoir été présente malgré la distance entre le Laos et le Mexique. Tantísimas gracias a Pauline por estar a mi lado durante más años que me atrevo a decir, pour tous ces moments partagés sur les skis, et tes mots d'encouragement dans les derniers moments de cette thèse.

Finally, les mots ne seraient pas suffisants pour décrire combien je vous dois Äiti et Papa. Vous m'avez toujours soutenue et comprise, appris à persévérer et à être forte, tout en m'insufflant la soif de savoir et de comprendre. Merci de m'avoir laissée partir au loin pour grandir, et d'avoir été là, tout simplement. Merci aussi ma Cam, pour tout, et plus encore!

Contents

List of Figures

List of Tables

List of Acronyms

APP Ammonium polyphosphate

BA Boric acid

BET Brunauer-Emmett-Teller theory

BJH Barrett-Joyner-Halenda theory

DCA Diiodomethane contact angle

DLS Dynamic light scattering

DSA Drop shape analyser/analysis

DSC Differential scanning calorimetry

DTG Derivative thermogravimetric (curve)

EDX Energy-dispersive x-ray spectroscopy

FEGSEM Focussed electron gun SEM

HC Humidity chamber

HET Humidity exposure test

HRR Heat release rate

HRT Hydrolytic resistance test

HSB Hemp shiv board

IMS Industrial methylated spirit

MgS Magnesium sulfate

MKP Monopotassium phosphate

MLR Mass loss rate

nPTMS N-propyl trimethoxysilane (IUPAC name: trimethoxy(propyl)silane)

NVC Non-volatile content

OC Oxygen consumption

OWRK Owens, Wendt, Rabel, and Kaelble method

PA Phosphoric acid

PdI Polydispersity index

PMMA Poly(methyl)methacrylate

RH Relative humidity

SEM Scanning electron microscopy

SFE Surface free energy

TEM Transmission electron microscopy

TEOS Tetraethoxysilane (IUPAC name: tetraethyl silicate)

TG Thermogravimetric (curve)

TGA Thermogravimetric analysis

THC Tetrahydrocannabinol

TTI Time to ignition

WCA Water contact angle

Chapter 1

Introduction

1.1 Context of research

As of 2010, industrial and residential buildings in the European Union account for over 40 % of the total energy demand and 36 % of CO_2 emissions. New regulations were put into place to achieve a 20 % reduction of energy consumption across all sectors in the EU by 2020, with a reduction of CO_2 and greenhouse gases emissions, and specifically Directive 2010/31/EU (European Parliament 2010) for the development of energy efficient buildings. To enable such challenging changes, new environmentally friendly solutions and materials needs to be developed, with the aim of providing new sustainable solutions such as nearly-zero energy buildings, following Directive 2012/27/EU (European Parliament 2012).

Extensive research on bio-based materials derived from agricultural crop have demonstrated their potential viability as building materials (Pacheco-Torgal and Jalali 2011; Amziane and Collet 2017; Arup 2017). Bio-based materials can capture and store CO_2 through photosynthesis, can be harvested annually (Jones 2017), and are biodegradable at their end of service life. Notably, wheat straw, flax, hemp, and many others present attractive acoustic (Glé et al. 2011) and thermal insulation properties (Korjenic et al. 2011), besides being easy to harvest in moderate climates (Ansell and Mwaikambo 2009). Additionally, such cellulosic insulation exhibits a higher propensity of moisture absorption (Kymäläinen and Sjöberg 2008), which is one of the reason

why the Museovirasto (2000) recommended their use over inorganic insulation materials to refurbish old timber houses. Hemp shiv in particular exhibit a hygrothermal behaviour as they can buffer heat and moisture owing to their microporosity (Lawrence et al. 2013). As part of an insulation panel, they can regulate indoor air environment, therefore reducing the need for air conditioning, thus less energy is required to maintain the indoor air quality of the building. This was the basis for the ISOBIO project[1], which aimed at developing and implementing new bio-based insulation panels and renders from renewable resources (forestry, agricultural crop by-products, waste) for more energy-efficient buildings. The ISOBIO products aim at delivering 50 % reductions in embodied energy and carbon levels, a 20 % improvement in insulation properties, and 30 % reduction in cost throughout the lifetime of the building or retrofitted wall.

Two drawbacks of such cellulosic materials which would hinder their wider utilisation are that they easily absorb liquid water (Arnaud and Gourlay 2012), which leads to rotting via microbial growth and thus biodegradation (Sedlbauer 2001), and they are combustible, which presents a significant fire risk when introduced in a built environment (Mngomezulu et al. 2014). The bio-materials can be treated in order to alleviate these issues. A unique solution was sought and described in this thesis, which is based on silica particle technology. They were chosen for their versatility, low cost, availability, and potential to provide a dual functionality. The particle size can be designed to be smaller than those of the micropores of hemp shiv and so should not block them, thus allowing air permeation. The surface of the particles can be functionalised to make them hydrophobic and limit degradation caused by liquid water. Finally, being an inorganic material, silica acts as a heat sink to protect the hemp shiv beneath from oxidation. Thermal degradation is thus limited, which in turn reduces the release of flammable gases, which consequently improve the fire performance of treated hemp shiv.

[1]This PhD research was made possible by the ISOBIO project, funded by the EU's Horizon 2020 research and innovation programme, under grant agreement N°636835.

1.2 Aim, approach, and objectives

The research reported in this thesis was carried out to determine the potential for functionalised silica particles to achieve a dual-property performance: to limit decay in a humid environment and to limit the thermal degradation of hemp shiv in the event of a fire.

In order to demonstrate this concept, various steps were followed (as illustrated in the flow chart in Figure 1.1), which spanned a broad range of scientific disciplines. Firstly, the treatment was designed, by following the Stöber method to synthesise various sizes of silica particles. The design rules were investigated and key parameters were identified to produce consistent materials. Following a patented route (Taylor et al. 2017), the silica particles were functionalised as to change their outer surface from hydrophilic to hydrophobic.

This approach enabled the manufacture of versatile particles, as they can then be employed for different applications, such as anti-fouling and anti-icing coatings, corrosion protection, fillers in polymeric matrices, etc. The functionalised particles were deposited by dip-coating on glass slides to assess their repellent properties, and then on hemp shiv. This material had previously demonstrated interesting insulation properties, and was a strong candidate material within the ISOBIO project. Because such bio-materials are highly absorbent, they need to be protected against liquid water to prevent microbial growth during their handling period at the construction phase (e.g. if it rains). The liquid water repellence of the coated surface of hemp shiv was therefore assessed, which was linked to the complete coverage provided by several layers of particles deposited. Composite structures made with hemp shiv and bio-based binder (derived of polysaccharides) were manufactured, to resemble more conventional insulation panels. As such bio-materials were to be employed in housing settings, in which warmth and humidity can be common (in a bathroom for instance), the repellent properties were also verified on materials kept in an environment that is favourable for microbial growth, hence rotting.

Finally, the behaviour of coated loose hemp shiv and derived composites under radiant heat was estimated, as to demonstrate the fire retardant effect of silica. This

was compared with composites in which conventional fire retardants were added, to prove that the silica-based coating, and the presence of inorganic species in general, can be considered an option to reduce the effects of thermal degradation. Existing regulations and codes in the building industry do not yet capture the risks associated with bio-materials. Instead, functional tests were carried out, with an aim of understanding the behaviours of degradation observed. In that sense, knowledge on the structural response of those materials can be built upon evidence.

Therefore, the approach followed aimed at proving that the silica particle technology could be a solution to a dual problem of degradation. The work described in this thesis was thus divided in several objectives to achieve the overall aim:

- To consistently synthesise silica particles and to carry out their morphological assessment;
- To modify the repellence properties of hemp shiv to delay the rate of biodegradation;
- To measure the impact that silica may have on the flammability of bio-materials.

1.3 Thesis layout

The work covers different topics, from sample manufacture to their characterisation. It is presented from a nanoscale perspective to macroscale effects, which is illustrated in Figure 1.1. This should allow the reader to get an overview of the work in the most flowy way, even though carried out in a more iterative manner.

After this introductory chapter, **Chapter 2** presents the background information relating to the three main topics: bio-based materials used in insulation, silica particle technology, and fire retardants for bio-based materials. The knowledge gap which exists between these topics is highlighted, which forms the thesis.

Chapter 3 describes how the treatment based on silica particle technology was developed. Extensive characterisation work was carried out in order to understand the underpinning parameters for synthesis of silica Stöber spheres. This chapter is

based on the work published in *Journal of Sol-Gel Science and Technology* (Bourebrab, Oben, et al. 2018).

Chapter 4 describes how adding functionalities to silica particles changes their chemical properties, namely how they can become hydrophobic. The deposition method, characterisation of coated glass slides, and water repellence assessment were depicted. Part of this chapter was published in a scientific article (Bourebrab, Durand, et al. 2018).

Chapter 5 introduces methods of assessing how the developed treatment protects the surface of bio-materials against liquid water and humidity. This chapter is based on the work published in the journal *Materials* (Bourebrab, Durand, et al. 2018). A different functionalisation formulation of the same technology was described by Jiang, Bourebrab, et al. (2018) and published in *ACS Sustainable Chemistry & Engineering*, although not extensively discussed in this thesis.

Chapter 6 examines the thermal degradation of hemp shiv, which was affected by coating silica particles as it delayed the onset of pyrolysis, thus reduced the combustion rate of hemp shiv.

Chapter 7 is a follow-up of the previous chapter, for which the fire performance of treated composite structures with hemp shiv was evaluated, in order to validate the developed treatment as solution to provide bio-materials with improved fire performance. Some of the results presented in this chapter have been submitted as a joint scientific article with Valentin Colson of Cavac Biomatériaux to *Construction and Building Materials* (Colson, Bourebrab, et al. 2019).

Finally, **Chapter 8** presents a summary of the conclusions drawn in each chapter. A holistic view of the thesis is given, specifically how the characteristics of a unique coating can influence two different aspects of degradation of hemp shiv, as well as recommendations for future work.

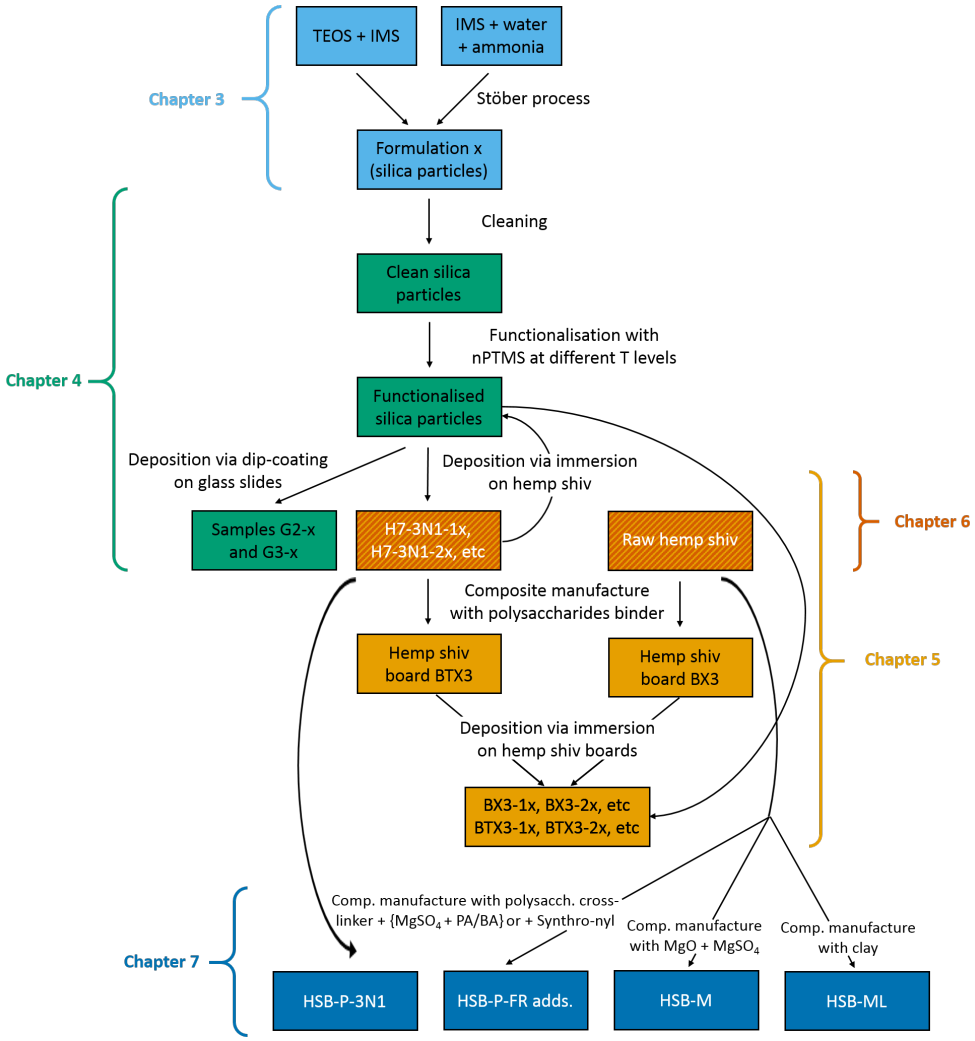

Figure 1.1: Flow chart representing the work carried out in this thesis and the associated chapters.

1.4 Contributions to knowledge

The work presented in this thesis and the ISOBIO project have been disseminated at various occasions over the course of these PhD studies. This industrial research was carried out with scientific rigour, which is highlighted by the publication of three peer-reviewed articles. The following record aims at reflecting on how this research contributed to the body of knowledge, either via publications or conference presentations, listed in chronological order.

1.4.1 Scientific report and peer-reviewed articles

Marion A. Bourebrab. Enhancing bio-materials properties: bringing hydrophobicity and fire retardancy. (2016). Internal report. *Awarded Best 1st year NSIRC PhD Student, presented by the Armourers & Brasiers Gauntlet Trust.*

Marion A. Bourebrab, Géraldine G. Durand, Alan Taylor. (2018). Development of Highly Repellent Silica Particles for Protection of Hemp Shiv Used as Insulation Materials. *Materials*. Peer-reviewed article. (Bourebrab, Durand, et al. 2018)

Yunhong Jiang, Marion A. Bourebrab, Nadia Sid, Alan Taylor, Florence Collet, Sylvie Pretot, Atif Hussain, Martin Ansell, Michael Lawrence. (2018). Improvement of water resistance on hemp woody substrates by deposition of functionalised silica hydrophobic coating that enhance moisture buffering properties. *ACS Sustainable Chemistry & Engineering*. Peer-reviewed article. (Jiang, Bourebrab, et al. 2018)

Marion A. Bourebrab, Delphine T. Oben, Géraldine G. Durand, Peter G. Taylor, James I. Bruce, Alan R. Bassindale, Alan Taylor. (2018). Influence of the initial chemical conditions on rational design of silica particles. *Journal of Sol-Gel Science and Technology*. Peer-reviewed article. (Bourebrab, Oben, et al. 2018)

Valentin Colson, Marion A. Bourebrab, Olivier Jadeau, Christophe Lanos. (2019). Formulation of novel fire retardant additives for biobased insulation material. Submitted to *Construction and Building Materials*.

1.4.2 Conferences

Marion A. Bourebrab, Alan Taylor. Advanced functional additives: Introducing hydrophobicity and fire retardancy into bio-based construction materials. ISOBIO workshop "Science and technology solutions for bio-based insulation", Rennes (France), February 2016. Oral presentation.

Marion A. Bourebrab, Géraldine G. Durand, Alan Taylor, Rory M. Hadden, Luke A. Bisby. Development of fire retardant treatment with silica nanoparticles to apply onto bio-based composite materials. Nanotech France 2016, Paris (France), June 2016. Oral presentation.

Marion A. Bourebrab. Hydrophobic and fire retardant treatment for insulation materials. NSIRC Conference, Cambridge (UK), June 2016. Poster.

Marion A. Bourebrab, Rory M. Hadden, Luke A. Bisby, Alan Taylor, Géraldine G. Durand. Fire retardant and hydrophobic treatment of bio-based insulation materials. School of Engineering Post-Graduate Conference, Edinburgh (UK), April 2017. Poster.

Marion A. Bourebrab, Rory M. Hadden, Luke A. Bisby, Alan Taylor, Géraldine G. Durand. Dual-functionalised silica particles treatment for improved fire performance and hydrophobicity of insulating bio-materials. Infrastructure & Environment Student Conference, Edinburgh (UK), May 2017. Poster.

Marion A. Bourebrab, Rory M. Hadden, Luke A. Bisby, Alan Taylor, Géraldine G. Durand. Dual-functionalised silica particles treatment for improved fire performance and hydrophobicity of insulating bio-materials. 12th International Association of Fire Safety Science Symposium, Lund (Sweden), June 2017. Poster.

Marion A. Bourebrab, Alan Taylor, Géraldine G. Durand, Rory M. Hadden, Luke A. Bisby. Tailoring silica particle size with Stöber process. NSIRC Conference, Cambridge (UK), June 2017. Oral presentation. *Awarded Best presentation.*

Marion A. Bourebrab, Nadia Sid. Development of highly repellent silica nanoparticles for protection of bio-based insulation composite materials. Applied Nanotechnology and Nanoscience International Conference, Rome (Italy), October 2017. Oral presentation. *Awarded Best presentation in the field of Environmental Science: Nano, presented by the Royal Society of Chemistry.*

Marion A. Bourebrab. A fire- and rain-proof straw house? Yes please!...Or how using silica particles can delay biodegradation and improve the fire performance of bio-materials used in insulation. Younger Members' Committee of The Welding Institute Seminar, Cambridge (UK), February 2018. Oral presentation.

Marion A. Bourebrab, Alan Taylor, Géraldine G. Durand, Rory M. Hadden, Luke A. Bisby. Enhanced water resistance and fire performance of bio-based insulation materials via silica particles treatment. International Symposium on Inorganic and Environmental Materials, Ghent (Belgium), June 2018. Oral presentation.

Marion A. Bourebrab, Alan Taylor, Géraldine G. Durand, Rory M. Hadden, Luke A. Bisby. Enhanced fire performance and delayed biodegradation of bio-material composites. NSIRC Conference, Cambridge (UK), July 2018. Oral presentation.

Chapter 2

Literature Review

2.1 Introduction

The research conducted and reported in this thesis covers a wide range of topics and technologies: bio-materials used as insulation in buildings, hydrophobic materials, and fire retardant solutions. This chapter reflects on each topic and associated literature to provide a broad understanding of the problem. The aim of this literature review is to provide an overview of the fundamentals and state-of-the-art of each topic, and to demonstrate how the current research was carried out to fill the gap identified.

2.2 Hemp shiv: a new insulation bio-material

The hemp plant *Cannabis sativa L.* has been used by mankind for millennia, for its narcotic properties, fibres, and seeds. The plant is divided in three phenotypes, each presenting various concentrations of tetrahydrocannabinol (THC), which is a psychoactive chemical used for recreational and medicinal drugs. Phenotype III possesses the lowest THC content and is harvested for its fibres (Chandra et al. 2017). Those are mainly exploited for paper production, as insulation materials, and transformed into bio-composites for the automotive sector (Carus et al. 2013). The fibres are mechanically extracted after retting, which is a biological process which partially degrades the hemp plant to facilitate fibre extraction from the stem (Nykter 2006). Shiv (Figure

2.1), fines, and dust are thus by-products of this separation process. Particularly, hemp shiv are used in particle boards for their light weight. In fact, Magniont et al. (2012) highlighted their low bulk density, and Jiang, Lawrence, et al. (2018) determined that approximately 76.7 % of the material correspond to their accessible porosity, (as measured by mercury intrusion porosimetry). These features make it a valuable candidate as insulation materials. Glé et al. (2011) classified the sound absorption of hemp shiv as excellent (0.8 on average on a scale from 0 to 1 for the frequency range 400 Hz to 2000 Hz), which demonstrates its potential for acoustic insulation applications. Extensive research was carried out to determine how hemp shiv could be used as thermal insulation (Nykter 2006; Kymäläinen and Sjöberg 2008; Korjenic et al. 2011; Lenormand et al. 2014), which is further described in Section 2.2.2.

Figure 2.1: Hemp shiv and a few fibres visible in the upper middle part of the photograph.

Similar to any biomass, hemp shiv are made from cellulose, hemicellulose, lignin, and other secondary components, which are reported in Table 2.1 according to various sources. Their relative quantities vary depending on the species of hemp, where, and how the plant was harvested: the soil, climate, retting process, and measuring methods, all can affect the given compositions (Thomsen et al. 2005; Nykter 2006). The hemp shiv provided by Cavac Biomatériaux and used in the work reported in this

thesis were characterised by Viel et al. (2018) via the Van Soest method.

Table 2.1: Chemical composition of hemp shiv in the literature, in wt%.

Source	Cellulose	Hemicellulose	Lignin	Ashes	Fat and wax	Other	Extraction method
Vignon et al. (1995)	44	18	28	2	1	7	Steam explosion
Thomsen et al. (2005)	47–48	21–25	16–19	1–2	8–9		Steam explosion
Diquélou et al. (2015)	46–49	18–21	22–23	3–4	–	–	Soxhlet extraction
Kidalova et al. (2015)	44	27	22	2	–	–	Soxhlet extraction
Viel et al. (2018)	49–51	21–22	9–10	1	17–18		Van Soest method

2.2.1 Economical benefits and accessibility

Hemp and other bio-materials possess a huge potential for a wider use, due to their relative low cost, light weight, and availability (Campilho 2017). As regards hemp, the major producer has been (and still is) China, specialising in the production of hemp fibre for textiles. Since 1980s, hemp harvesting has become more common in the EU, especially for the production of non-woven hemp fibres (Small 2017). Nykter (2006) indicates that the fibres are detached by retting in the field, which facilitates their subsequent mechanical extraction. No chemicals are required for this process, called hammering, which separates the fibres from the shiv and dust (also named fines) (Hirst 2013). The decortication of fibres from hemp plant yields 1.7 kg of hemp shiv per kilogram of fibres produced, according to Carus et al. (2013), or 55 wt% of shiv and 30 wt% fibres extracted according to Lenormand et al. (2014). When they are not burnt as waste (Nunes 2017), the shiv are considered as a by-product with only half the value to that of fibres, and are used as bedding material for animals (Carus et al. 2013). Developing their range of applications would be extremely beneficial for the hemp industry. Moreover, the hemp plant is very easy to harvest with low demands of water (Ebskamp 2002), therefore can be grown in moderate climates (Ansell and Mwaikambo 2009).

2.2.2 Physical properties and moisture buffering

Common insulation materials present very low thermal conductivities (λ) and thus U-value, also called the thermal transfer coefficient. It is calculated by the inverse of the thermal resistance (R) of a material. The lower the thermal conductivity, the lower the U-value (and greater R), and the better insulator the material is. The Energy Saving Trust (2006) recommends aiming for a U-value of 0.30 $W/m^2.K$ for wall insulation. As a comparison, a non-insulated wall made of poured concrete which thickness is four inches exhibits a U-value=0.86 $W/m^2.K$ (Combustion Research Corporation 2018). The thermal conductivities and thermal transfer coefficients of commercially available insulation materials, as well as some bio-based materials used for insulating are collated in Table 2.2. Cérézo (2005) and Gourlay (2014) reported the thermal conductivities from various bulk densities of loose hemp shiv obtained from different suppliers. Their densities are comparable to those of straw bales, between 89 kg/m^3 and 155 kg/m^3. They however displayed lower thermal conductivity values, between 0.048 W/m.K and 0.058 W/m.K. The U-value can be calculated, which comes to between 0.48 W/m^2 and 0.58 $W/m^2.K$ if an insulation layer thickness of 100 mm is considered.

The reason why hemp shiv presents a lower thermal conductivity than straw bales can be explained by their microporosity. They are a naturally porous material owing to their intrinsic microstructure. Jiang, Lawrence, et al. (2018) carried out extensive characterisation of this material, and determined by mercury intrusion porosimetry an accessible porosity of approximately 76.7 % and a total surface area of 57.6 m^2/g. For comparison, another bio-based building material, untreated wood, exhibits a total surface area of 16.5 m^2/g (D. Wang et al. 2014). Typically, the microstructure of hemp shiv exhibits both micro- (3–10 nm) and macropores (1–2 µm and 20–80 µm) (Jiang, Lawrence, et al. 2018). The microscale cell structure presents pits which diameter were measured at approximately 2 µm, which can be seen in the A and B images in Figure 2.2, extracted from Jiang, Bourebrab, et al. (2018). The highly porous nature of hemp shiv allows air permeation, thus water vapour permeation. Based on experiments carried out by Hill et al. (2009) on flax fibres, Lawrence et al. (2013) explained this phe-

nomenon, and described this as also being characteristic of hemp shiv. Water vapour is adsorbed on the structure of the shiv and its pores where it condenses (exothermic reaction) and evaporates (endothermic). This hygric exchange is also called moisture buffering, and was explained by Tran Le et al. (2010) in the case of a hemp-lime assembly. Such materials can therefore regulate humidity and temperature in a building preventing sudden changes.

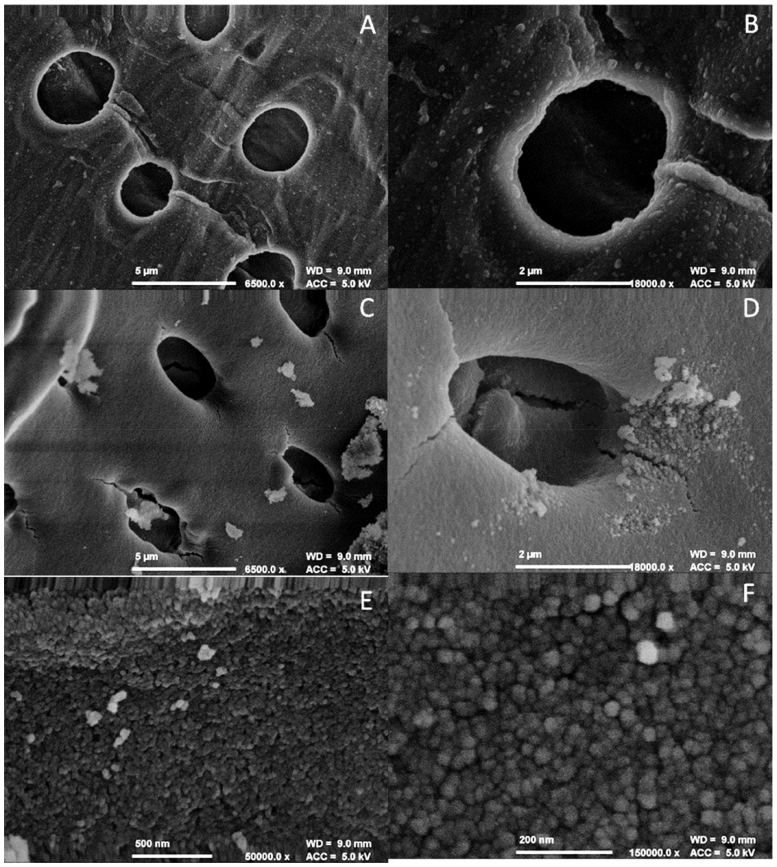

Figure 2.2: Field emission SEM micrographs of (A) and (B) untreated hemp shiv and (C–F) coated hemp shiv. Reprinted with permission from Jiang, Bourebrab, et al. (2018). Copyright 2018 American Chemical Society.

2.2.3 The example of hemp-lime wall assemblies

Currently, the most common use of hemp shiv as a building material is for hemp-lime (also called hemp-concrete, or hempcrete). It was developed in France in the early

1990s for non-load bearing elements of a construction, e.g. wall partitions supported by a timber frame. Hemp-lime is considered a more sustainable alternative to traditional concrete owing to the hemp component, also benefiting from a much lower density (400 kg/m^3 against 2000–2600 kg/m^3) (Gourlay 2014).

The main research carried out has been focussed on the hygrothermal properties of hemp-lime. Amongst the reported research work, Tran Le et al. (2010) simulated the transient hygrothermal behaviour of such assembly over various climatic cycles, suggesting the propensity of the wall to absorb and desorb moisture, therefore to attenuate the effect of air humidity on the indoor relative humidity compared to a more traditional concrete. Shea et al. (2012) analysed the same phenomenon on a test building (Hempod, located at the University of Bath, UK) for 11 days. Despite the external variations of temperature (6.5 °C of daily amplitude), the internal measures remained fairly constant over the course of the experiment (amplitude of only 0.9 °C), and a similar result was obtained for the relative humidity. Hemp-lime assemblies seem like a strong alternative to conventional concrete, however it is interesting to note that the thermal conductivity and thermal transfer coefficient were lower for hemp shiv alone than for hemp-lime (Table 2.2). The hygroscopic feature of the assembly was also associated to the presence of the bio-aggregates. However, lime acts as a binder to form bricks, and Hirst (2013) explained that the highly alkaline nature of lime would protect the hemp-lime assembly against biodegradation. This makes its presence necessary, unless an alternative binder is used, and another compound or treatment is added to limit biodegradation.

2.2.4 The biodegradation problem

Cellulose, a polysaccharide, is the main compound of hemp shiv, and generally of biomaterials originating from crop. Cellulose is a strong natural polymer, which keeps its integrity via the hydrogen bonds between the different hydroxyl groups of two glucose units, forming a solid microcrystalline structure (Ciechańska et al. 2009). Despite its name, hemicellulose is not a type of cellulose as it contains different sugar units, and exhibits a high degree of branching with other groups, making it a non-crystalline

structure (John and S. Thomas 2008). Both components can however be hydrolysed by acid agents, which makes them prone to microbial growth and rotting, especially when exposed to humidity and warmth. Sterling et al. (1985) introduced the eponymous graph, which summarises the ideal humidity conditions at room temperature for a healthy living environment, between 40 % and 60 % of relative humidity. However, insulation materials – especially when used in housing – might be exposed to greater relative humidity and temperature. Under such conditions, bio-material such as hemp shiv can incur biodegradation thus leading to viruses and bacteria proliferation which can be harmful to human health.

The hydrophilic surface and hygroscopic behaviour of hemp shiv imply a very high water uptake. Tavisto et al. (2003) measured that a 40 μL droplet of water was absorbed by a hemp shiv in four to five seconds. Gourlay (2014), and it was later confirmed by Hussain, Calabria-Holley, Jiang, et al. (2018), quantified this water absorption to be equivalent to 400 % of the initial dry weight of the shiv. In a review, Mokhothu and John (2015), described the biodegradation phenomenon of natural fibres when exposed to water, and the need to develop treatments for composites containing them. Specifically, they mentioned coating bio-materials with hydrophobic compounds (particles and thin-films amongst other solutions) to protect their hydrolysable surface against liquid water. Effectively, these solutions reduced the surface tension between the substrate and water, thus increased the hydrophobic behaviour. The effects of biodegradation from water exposure were therefore limited. Most treatments applied on natural fibres and described here were however based on fluorosilanes, which enabled superhydrophobicity (water contact angle greater than 150°), but overlooked potential environmental hazards caused by the halogen-based silane used in the formulation.

Table 2.2: Physical characteristics of cement (for comparison) and common synthetic and bio-based insulation materials, for 100 mm thickness unless stated otherwise.

Material	Density (kg/m^3)	λ (W/m.K)	U-value (W/m^2.K)
Cement concrete[1]	2243	0.086$*$	0.86
Polyisocyanurate (PIR) or polyurethane (PUR) foam[2]	50–800	0.023	0.16–0.26 (thk=140–80 mm)
Phenolic foam[2]	35–200	0.022	0.16–0.25 (thk=140–80 mm)
Rock wool[3]	60	0.040	0.14
Silica aerogel[4]	100	0.003	0.03$*$
Straw bale[5]	70–150	0.060–0.080	0.60–0.80$*$
Wood fibre[6]	160–240	0.038–0.050	0.38–0.50$*$
Wood wool[6]	50	0.038–0.040	0.38–0.40$*$
Hemp fibre[6]	40	0.038–0.040	0.38–0.40$*$
Hemp-lime[3]	440	0.115	0.44 (thk=300 mm)
Hemp shiv	110–155[7] 89–106[8]	0.048–0.058[7] 0.052–0.055[8]	0.48–0.58$*$ 0.52–0.55$*$

[1] Data extracted from Combustion Research Corporation (2018), converted from lbs/ft^3 for a 4" wall (101.6 mm).

[2] Data extracted from Energy Saving Trust (2006) for wall insulation (only values achieving best practice are reported).

[3] Data extracted from Evrard and De Herde (2010).

[4] Data extracted from CRC Handbook of Chemistry and Physics (2018), although commercial flexible aerogels exhibit a thermal conductivity of 0.015 W/m.K (ISOBIO 2015).

[5] Data extracted from Costes et al. (2017).

[6] Data extracted from Lawrence et al. (2013).

[7] Data reported by Cérézo (2005) from two independent experiments.

[8] Data extracted from Gourlay (2014).

$*$ Determined by calculation considering a wall which thickness is 100 mm.

2.3 Hydrophobic silica particles

2.3.1 Hydrophobicity and associated solutions

There are many possibilities to make the surface of a material repel liquid water, the two main ones being creating a physical repellence between the substrate and a water droplet, and the other a chemical repellence. Extremely high repellence is commonly known as the lotus leaf effect (Barthlott and Neinhuis 1997; Marmur 2004), for which the substrate presents a microstructure, with a certain roughness so that a water cannot wet to the surface. The wax present on the leaves contributes to the hydrophobic character due to its lack of affinity with water, which could be described as the chemical repellence of water (IUPAC 1997).

Basic principles of water repellence

The wettability property of a substrate with a liquid, specifically water, is given by the Young-Laplace equation (Equation 2.1), which links the surface energies between the solid, liquid, and gaseous phases, as represented in Figure 2.3. There is complete wetting of the surface by the liquid when $\theta = 0°$. The greater the contact angle θ formed between the liquid and solid at the liquid/solid/vapour interface, the more the surface repels the liquid. In the case of water, a surface is said to be hydrophilic for $\theta < 90°$, hydrophobic when $\theta > 90°$, and superhydrophobic when $\theta > 150°$ (θ is called the water contact angle (WCA) when the liquid of interest is water).

$$\gamma_{sv} = \gamma_{sl} + \gamma_{lv} \times cos\theta \tag{2.1}$$

Fowkes (1964) explained that it is hard for a liquid to spread onto a substrate which has a low surface free energy (SFE). This parameter can be measured by the means of probe liquids of different polarities to create a wetting envelope. It is calculated by the Owens, Wendt, Rabel, and Kaelble (OWRK) method (Owens and Wendt 1969; Rabel 1971; Kaelble 1970), which combines the polar part (surface free energy due to polar interactions) and the disperse part (dispersive interactions) of the SFE. For

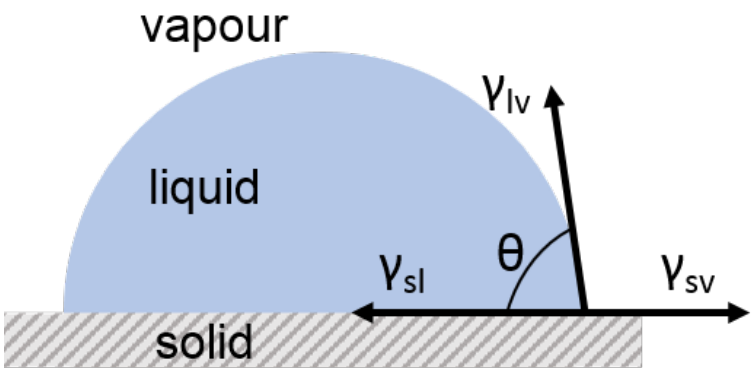

Figure 2.3: Illustration of the Young-Laplace Equation 2.1, adapted from Fowkes (1964).

example, polytetrafluoroethylene (PTFE, mostly used and known for Teflon™coated surfaces) exhibits a SFE value of 20 mN/m on average, as reported by Jańczuk and Białłopiotrowicz (1989) from various literature data and their own experimental ones. This value is typical of surfaces with low wetting (high liquid repellence).

Wenzel (1936) found that the Young-Laplace approach to wetting was only representative of an idealised homogeneous state, and from his empirical observations, roughness should be taken into account (Figure 2.4). Cassie and Baxter (1944) on the other hand employed a weighted approach to the wetting phenomenon by considering air which might be trapped between the asperities of the material (also called re-entrant features). Considering these statements, the repellent properties of a surface can be improved by:

- decreasing the surface free energy of the substrate;
- creating roughness: by removing some material ('top-down' method, such as etching), or adding some ('bottom-up', with using single molecules or entities as building blocks).

Industrial need: hydrophobic coatings

According to the *Web of Science*, the number of published research articles for "hydrophobic coatings" has increased tenfold in 20 years (until 2015), showing the ever-

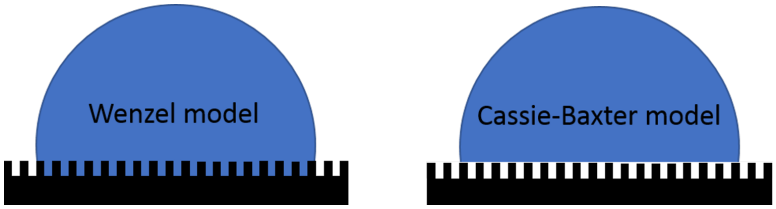

Figure 2.4: Schematic of the Wenzel and Cassie-Baxter models of wetting phenomenon, after Wojdyla et al. (2015).

growing demand in research in this field (Figure 2.5). The need for such coatings has significantly increased in the last three decades, across all sectors of industry. They can be named easy-clean, anti-fouling, anti-icing, anti-corrosion, amongst other propositions, but represent a unique aim: ensuring surfaces effectively repel liquid water to limit its damaging effect. Wojdyla et al. (2015) reviewed the state of the art in terms of low energy (low surface tension) coatings used for anti-fouling applications. For example, fluoropolymers and polysiloxanes are commonly used in the formulations of such coatings, but these however present low mechanical durability, and thus are prone to damage. New solutions for durable low-energy coatings emerged as nanostructured surfaces, which can be created by 'bottom-up' methods, which means that (usually) inorganic material are deposited on the substrate to build a rougher surface. Due to its low cost of manufacture, nanosilica is considered a strong candidate to be used in the formulation of low-energy durable coatings (Wojdyla et al. 2015), as well as transparent and superhydrophobic coatings (Bravo et al. 2007).

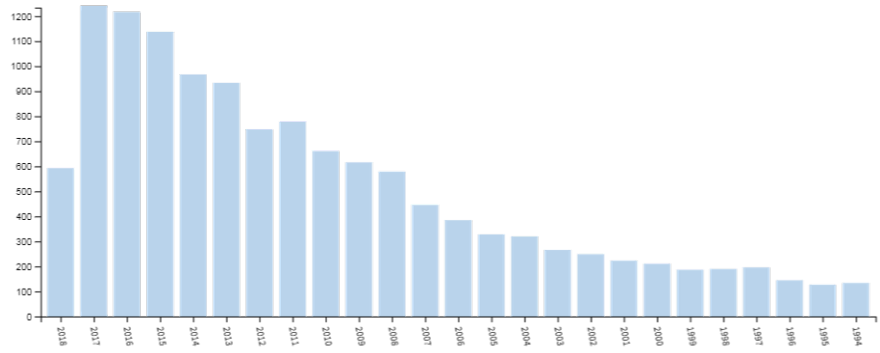

Figure 2.5: Recorded research articles corresponding to "hydrophobic coatings" according to the *Web of Science* in the last 25 years (data retrieved on 15th June 2018).

2.3.2 Silica particles

Commercial silica is widely produced by two main routes: pyrogenic silica is obtained from flame pyrolysis which allows a good control of the viscosity of the final product, and precipitation/ion-exchange method, which involves the use of various chemicals (Iler 1979). Those two methods, although being cost-effective, do not allow complete control of the surface of the particles. On the other hand, sol-gel methods are a good alternative to produce purer materials (Lim et al. 2010), whilst reducing the energy required during manufacture (Hyde et al. 2016). Additionally, the surface chemistry of the resultant material can be controlled (Rahman and Padavettan 2012), which leads to the development of more complex structural hierarchies (Perro et al. 2006; Tsai and Lee 2007), such as the raspberry-like shapes (Carcouët et al. 2014). The design routes fo such materials can be tuned by varying the synthesis parameters. The composition of the initial systems and the relative ratios of reagents strongly influenced the final products, by modifying the rates of hydrolysis and condensation occurring during synthesis.

Chemistry of Stöber silica particles synthesis

The first reported example of controlled and simultaneous reactions of hydrolysis and condensation of alkoxysilanes with an aim of producing silica particles in solution is usually attributed to Stöber et al. (1968). Brinker (1988) and Ibrahim et al. (2010) described the well-known reactions of hydrolysis and condensation as follows:

$$\mathrm{Si(OC_2H_5)_4} + x\mathrm{H_2O} \rightarrow \mathrm{Si(OC_2H_5)_{4-x}(OH)_x} + x\mathrm{C_2H_5OH} \tag{2.2}$$

$$\equiv \mathrm{Si{-}OC_2H_5} + \mathrm{HO{-}Si} \equiv \rightarrow \equiv \mathrm{Si{-}O{-}Si} \equiv + \mathrm{C_2H_5OH} \tag{2.3}$$

$$\equiv \mathrm{Si{-}OH} + \mathrm{HO{-}Si} \equiv \rightarrow \equiv \mathrm{Si{-}O{-}Si} \equiv + \mathrm{H_2O} \tag{2.4}$$

Equation 2.2 represents the hydrolysis reaction, Equations 2.3 and 2.4 correspond to the condensation reactions, liberating alcohol and water respectively. Silicon tetraalkoxides (e.g. tetraethoxysilane, TEOS, $\mathrm{Si(EtOH)_4}$) are transformed into silica ($\mathrm{SiO_2}$) following series of chemical reactions presenting subtle interdependencies. Assink and

Kay (1984) postulated that 15 intermediates existed between the precursor and silica, all of each exhibiting slightly different hydrolysis and condensation reaction rates. The general formula $\mathrm{Si(OC_2H_5)}_x\mathrm{(OH)}_y\mathrm{(OSi)}_z$ can describe these 15 intermediate species, where $x + y + z = 4$ (the composition of the intermediates can be seen in Figure 3.3). Each intermediate created from the inter-dependent hydrolysis and condensation reactions can also become new intermediates themselves capable to react further. This suggests that any combination of $(x; y; z)$ can be formed for any initial concentration of reagents. Particularly, the degree of hydrolysis would be increased with increments of water content, which would lead to species defined by a smaller value of x.

Mechanisms of particle growth

The mechanisms of particle formation and growth still create debate. In their review, Hyde et al. (2016) focussed on three of the most popular models which explain how colloidal silica can be synthesised: monomer addition and growth, aggregation, and a combination of both.

The first is supported by Flory (1941), Stockmayer (1944), LaMer and Dinegar (1950), and Matsoukas and Gulari (1988) amongst others. The number of nuclei present in the system upon starting the hydrolysis reaction is equivalent to than the number of particles at the end of the reactions, which means that each nucleus grew into a particle. Bailey and Mecartney (1992) mentioned that this phenomenon would occur as long as the particles would be colloidally stable in their medium.

On the other hand, some nuclei would collide with each other creating bigger entities (aggregation model), which is a theory supported and explained by Bogush, Tracy, et al. (1988), Nagao et al. (2000), and Seyfaee et al. (2015) as well as other research groups.

Finally, M. T. Harris et al. (1990) and Giesche (1994) described how those two mechanisms could be valid a different stages of growth, and specifically that the shift from aggregation to monomer addition would occur at a 135 nm threshold of particle size, and in low-ammonia and low-water concentrations, which was specified by M. T. Harris et al. (1990).

Those proposed mechanisms (or a combination of both) and their details are still to be elucidated, as too many parameters of reaction (initial concentrations, temperature, feeding rates, etc.) can interfere in the synthesis, therefore conducting a thorough comparison between the work of each research groups is not an easy task.

Varied initial conditions but similar behaviour

The synthesis of Stöber silica particles involves a silane source (typically tetraethoxysilane, TEOS) introduced into a mixture of alcohol, water, and a catalyst such as ammonia. The Stöber process seems to have been studied thoroughly since it was proposed in 1968. Researchers have tried to determine which was the influence of each parameter on the silica spheres synthesised. Jafarzadeh et al. (2009) studied the influence of the addition sequences and feed rates, with smaller particles produced when the addition rate of ammonia was lower. Park et al. (2002) determined that the temperature influenced the most the final particle size, more than the concentration of reagents or the feeding rates. Rao et al. (2005) analysed how the final particle size depended on the concentrations of the reagents. They explained that ammonia evaporates at higher temperatures (around 70 °C), therefore its concentration decreases, which leads to a medium richer in water than it should have been. Consequently, particles tend to be bigger in those water-richer systems. Tan et al. (1987), Bogush, Tracy, et al. (1988), and H.-C. Wang et al. (2006) demonstrated that smaller particles were synthesised with increased temperatures of reaction, which contradicts the results obtained by Rao et al. (2005). A firm comparison of the effect of temperature could only be carried out if the initial chemical and physical conditions of the systems are kept identical, which is hard to find in the literature. Almost every research group used different set ups, such as variation of temperature, change in the process from a single pot to two-pot, various concentrations of reagents and type, amongst others. Similarities in particle shape, size and characteristics were however visible despite many different input parameters.

Nevertheless, despite the breadth of studies on Stöber silica particles, it is possible to extract some general patterns regarding the link between particle growth and

water content. When works from Bogush, Tracy, et al. (1988), Sato-Berrú et al. (2013), and Greasley et al. (2016) are plotted on the same graph, the pattern of particle size evolution with increasing water content is similar, irrespective of the other reagents' concentration. The general behaviour shows that the particles were bigger with an increased initial water content, up to a maximum after which the size decreased despite the water content further increasing, which is illustrated in Figure 2.6. Overall, the biggest particles were synthesised when the water content was included between 10 wt% and 30 wt%, and the size decreased past 35 wt%. This feature suggests that beyond a specific initial water content, particles are not stabilised in their medium. In a Stöber system in which methanol was the solvent, Bridger et al. (1979) introduced the notion of a saturation limit of water in the system at 15 mol/L (which would correspond to 34 wt%). Similarly to the phenomena observed in Figure 2.6, the particles rose to a peak in size with increased water contents, until this saturation limit, after which the size decreased.

Interestingly, researchers seem to have focussed their studies on systems for which water contents represented only up to half of the whole system. The study led by Sato-Berrú et al. (2013) covered a broader range of water contents, up to 60 wt%, but they overlooked the miscibility gap which occurred beyond 50 wt% of water. As the TEOS is soluble in ethanol but degrades in water, when the initial systems become more water-rich than alcohol-rich, the TEOS remains at the interface where part of it slowly reacts with the ethanol. The ammonia remains in the aqueous phase and does not participate as a catalyst of the hydrolysis reaction. Over ten days, enough TEOS would have reacted and produced ethanol so that it would auto-catalyse its reaction of hydrolysis.

2.3.3 Adding functionalities

Silica particles made from the Stöber process are inherently hydroxyl rich, with a silanol ($-\mathrm{Si}-\mathrm{OH}$) density between 4 and 6 $\mathrm{OH/nm^2}$ (Zhuravlev 1993). Alkoxysilanes can be grafted onto the particle surface by reaction with the silanols, in the presence of a catalyst and heat, as it was demonstrated by Lin et al. (2001), Carrot et al. (2002), Liu

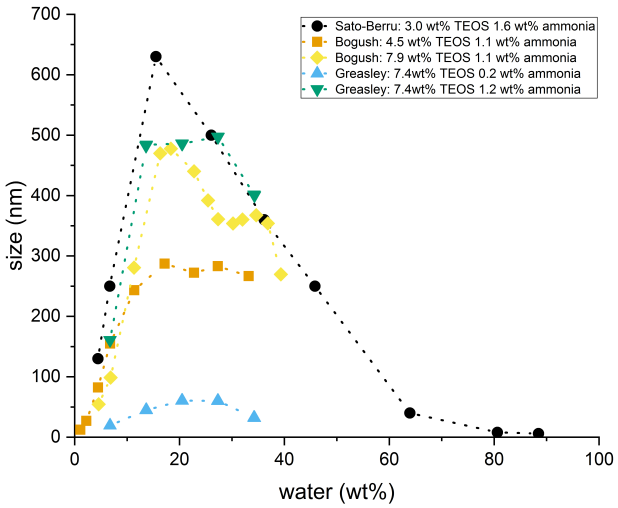

Figure 2.6: Particle size evolution with water content, as reported by Sato-Berrú et al. (2013), Bogush, Tracy, et al. (1988), and Greasley et al. (2016). The data was replotted in wt% of water for this graph.

et al. (2003), and Posthumus et al. (2004) and is illustrated in Figure 2.7. The presence of alkoxysilanes thus limits aggregation of the particles due to sterical stabilisation, and also facilitates their dispersion into organic media. Bauer et al. (2003) and Posthumus et al. (2004) described a way of functionalising silica particles with methacryloxypropyltrimethoxysilane, for which the rate of reaction between the silane and the particles was faster than the homocondensation of the trialkoxysilane.

Most common functionalising agents for hydrophobicity are halogen-based (Bravo et al. 2007; Cho et al. 2017; Barati Darband et al. 2018; Jeevahan et al. 2018), such as fluoroalkyl groups (Hikita et al. 2005). Such silanes can provide great water repellence, characterised by high water contact angle (above 150°) and very low sliding angles (below 10°). Wojdyla et al. (2015) however proved their low durability against abrasion, and Xue et al. (2014) mentioned the increased environmental hazards associated to halogen-derived silanes compared to others. The Danish Environmental Protection Agency (2016) submitted a proposal to the European Chemical Agency to restrict the use of polyfluorosilanes in aerosol consumer products due to potential harm to human

health by inhalation. This suggests that such chemicals and their derivatives might be phased out in the near future, their manufacture might be more regulated, therefore safer alternatives are required.

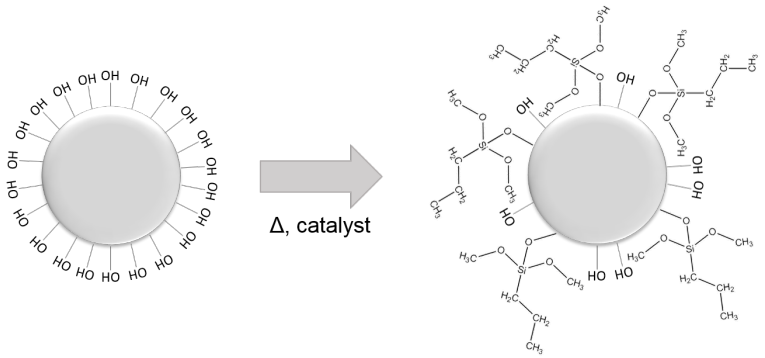

Figure 2.7: Schematic representation of silane grafting onto the surface of silica particles (the silane represented here is n-propyl trimethoxysilane, used in Chapter 4).

2.4 Fire retardant solutions for bio-based materials

2.4.1 Combustion of bio-based materials

All bio-based materials are natural polymeric materials, made from cellulose as a backbone, and other carbohydrates (specifically, the composition of hemp shiv is detailed in Table 2.1). They normally contain absorbed moisture from their environment. When exposed to heat, water vapour is the first component to evaporate, after which the bio-compounds decompose, as they undergo various depolymerisation reactions. These chemical decomposition reactions are commonly known as burning or combustion process when the bio-based solid fuel degrades in presence of oxygen. Based on the theory of wood combustion explained by Browne (1958), Roberts (1970) indicated that the components of wood release volatiles at different temperatures, namely hemicellulose between 200 °C and 260 °C, cellulose between 240 °C and 350 °C, and lignin between 280 °C and 500 °C. Above 450 °C, most of the cellulose volatilised whilst only 50 % of lignin did, the remaining being char residue (Drysdale 2011). The char yield

depends on the heating rate and thus on the temperature at which depolymerisation occurs (Madorsky 1964). Indeed, a slow heating produces more tar, whereas higher heating more gaseous compounds.

Depending on the concentration of oxygen available for the fuel to burn and with sufficient energy, combustion of materials can be complete or not. With plentiful of oxygen, the fuel can burn easily and its decomposition reaches greater extents. Fully oxidised compounds are released, such as CO_2. With limited oxygen supply, combustion cannot be sustained and is usually incomplete. It is characterised by the release of greater concentrations of partially oxidised compounds, CO, amongst other oxidation gas products, as well as greater residual mass. Under inert atmosphere, pyrolysis occurs.

Pyrolysis

Pyrolysis comes from the Greek words $\pi\upsilon\rho$ (fire) and $\lambda\upsilon\sigma\iota\varsigma$ (decomposition). It describes the irreversible, endothermic process by which solid fuel made from organic material is converted to flammable gases, in inert atmosphere (or very limited oxygen supply). Although a very complex process, the accepted and simplified explanation is based on combined heat and mass transfers occurring within the solid phase, and at the boundary conditions, which are usually the interface between the solid material and the local atmosphere (Torero 2016). When sufficient heat from an external source radiates on the exposed surface of the solid phase, the local temperature increases until reaching the pyrolysis temperature of the material, which triggers this endothermic process. Gases are released by the chemical decomposition reactions, which creates a mass loss in the solid phase. As oxygen enters the bulk material via the same pathways the pyrolysis gases were released, further oxidation reactions are generated, such as charring, and the bulk material gains mass. When the volatile products of pyrolysis are released from the surface of the solid, they mix with air and oxidise. In turn, oxidation reactions produce energy, which is released at the boundary conditions. The products of pyrolysis of a solid fuel primarily made of carbon-based compounds are therefore the carbonaceous residue (char), and the flammable gas phase.

Flaming

Shortly after the onset of pyrolysis of solid materials, gases are released from the solid fuel. Thereupon and in the presence of a pilot source (flame or spark), the released gases will more rapidly oxidise, provided the mixture can sustain combustion. This means that sufficient fuel gases needs to be released to exceed the critical mass flux value, and enough oxygen is present in the local atmosphere for near-stoichiometric oxidation reactions to occur (Drysdale 2011). The gas phase combustion forms the flame, which is almost always a diffusion process and therefore production of soot is expected if the fuel is a carbon-based material. In addition to undergoing flaming combustion, many materials derived from natural products are capable of sustaining smouldering combustion.

Smouldering

Smouldering occurs in solid materials that yield a solid char upon heating. This phenomenon is characterised by being a flameless, slower, low-temperature, incomplete form of combustion (Ohlemiller 1995; Rein 2009). Palmer (1957) is one of the first reported and widely acknowledged works on smouldering, which remains quite recent compared to the combustion theory formulated by Lavoisier at the end of the 18^{th} century. Smouldering combustion occurs within the solid fuel and is an heterogeneous reaction involving oxygen from the air and the solid carbon-rich char produced by pyrolysis. A particular challenge associated with smouldering is that it is a volumetric phenomenon and therefore can occur within a material and proceed unseen for extended periods. Oxygen supply to the material and heat losses to the local environment are the two major mechanisms which control this type of combustion rate (Ohlemiller 1995). Smouldering can occur on its own should enough heat be provided to the solid fuel to reach its pyrolysis temperature. This case presents an additional risk associated with this type of combustion as ignition is relatively easy to occur with low heat sources which would not otherwise produce a flame (Ohlemiller 1995). The transition to flaming can be caused by slight variations in heat and oxygen supplies as the phenomenon is very sensitive to local changes in the energy balance. In his study

of smouldering combustion of dust beds and fibrous insulating boards, Palmer (1957) demonstrated that variation of air flow could either not be sufficient to sustain combustion, or accelerate its rate if increased, as more oxygen was supplied to the fuel. In this latter case, air draught could also induce transition to flaming combustion. Reciprocally, smouldering can be subsequent to flaming if the heat source is removed or the oxygen supply diminished.

The example of a bio-based material primarily exposed to a heat flux of 11.5 kW/m^2 for 40 min is shown in Figure 2.8. Initially, flaming combustion occurred, but smouldering combustion took over within the material and carried on, despite having removed the heating source. It means that enough heat and oxygen were present in the bulk of the sample to sustain combustion. Huang and Rein (2014) described the shape of the smouldering front as an ellipsoid (or pan). The top layer of the smouldering material is exposed to air, which is much colder than the bulk, leading to heat losses by convection thus creating the pan-shape on the external sides. An ash layer builds up, insulating the material beneath, which smouldering front propagates deeper.

2.4.2 Building regulations on the use of bio-based materials

Hadden (2011) carried out several studies of smouldering fire at various scales to better understand its mechanisms, yet it remains still an under-researched phenomenon. The increased use of bio-based materials in construction – such as cellulosic, or potentially hemp shiv in insulation – means that this mode of combustion may increase in prominence in the built environment. The risks associated with smouldering, such as unseen, creeping burning front, should be considered when such materials form part of the building.

Steen-Hansen et al. (2018) highlighted that there are only limited test methods to assess smouldering fires and their associated risks. The procedure to evaluate continuous smouldering for building materials described in Standard BS EN 16733:2016 (British Standards Institution 2016) indicates that the materials tested are exposed to a burner flame for 15 min, and then to evaluate if flaming combustion continues on the material or sustained smouldering occurs. Other heat sources are used as igniters,

Figure 2.8: Photograph of a bio-based material smouldering and characteristic pan-shaped smouldering front, as described by Huang and Rein (2014).

such as a lighted cigarette on cellulosic fibres in Standard C739 (ASTM 2017a), or a wooden crib (NORDTEST 1988). None of these standards however describe the mechanisms of smouldering combustion of these types of insulation materials, and only provide a binary outcome. For this reason, Steen-Hansen et al. (2018) developed a bench-scale test method to evaluate smouldering of a wood-fibre insulation material, and indicated that some types of specimen showed propensity of not only smouldering but subsequent flaming combustion as a secondary oxidation occurred.

The fire safety of cellulosic-based insulation material is often overlooked as the problem is not yet taken into account in building codes. In addition, common fire retardant additives or coatings used in house settings, generally applied on furniture and in the insulation panel, are typically developed for flaming fires (acting both in the gaseous and condensed phases) but would not be specifically targeted to smouldering fires, which occur mainly in the condensed phase.

2.4.3 Overview of commercially available fire retardant solutions: *modi operandi*

Levan (1984) described extensively the chemistry behind fire retardancy of components deposited on wood, the most common bio-based material used in construction. Owing to their similarities of chemical composition, wood can serve as a good case study for other bio-based materials used in the built environment, such as hemp shiv.

Broadly, there are two modes of actions for fire retardants: by chemical and physical action. The first corresponds to compounds for which chemical reactions occur under heat exposure to form new products. These can act either in the gaseous phase (flame retardants), or in the condensed phase by altering the thermal properties of the material. The second category groups compounds which affect combustion by being present on the combustible material and by modifying the energy balance (e.g. by increasing the thermal mass of the whole system). The different fire strategies are shown in Figure 2.9 and were explained in details by Witkowski et al. (2016).

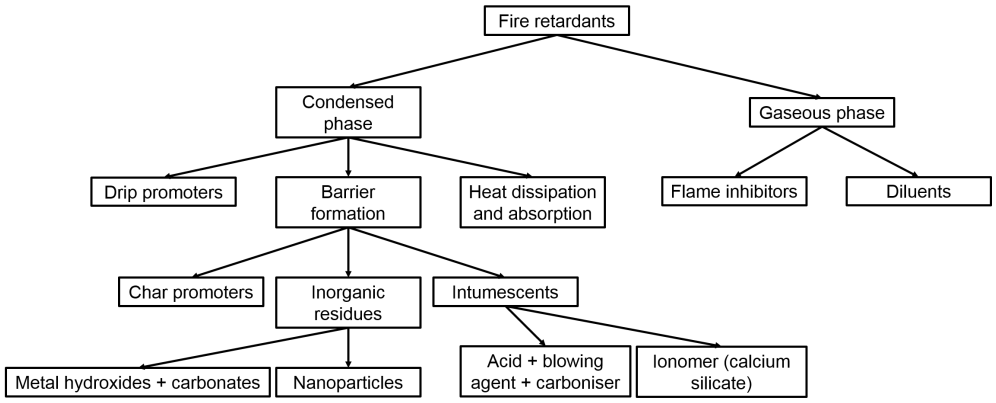

Figure 2.9: Schematic of fire retardants strategies, adapted from Witkowski et al. (2016).

Typically, flame retardants act in the gaseous phase by releasing free radicals, as it is the case for halogen-based flame retardants, especially those containing bromine (Georlette 2001). Upon burning polymers, high-energy radicals $H^{\bullet}$ and $HO^{\bullet}$ are released, as well as $X^{\bullet}$ from the halogen flame retardant (where X represents the halogen molecule). The latter recombines with the very reactive $H^{\bullet}$ to form HX gases (Troitzsch 1998). Similar recombinations also occur with the use of phosphorus-based

compounds, such as $HO^{\bullet}$, $PO^{\bullet}$, and $HPO_2^{\bullet}$ as described by Schartel (2010). The recombination reactions are highly endothermic thus use heat, which in turn decreases the temperature of the flame. Flame retardants can also produce additional gases, such as water vapour, which dilute the gaseous phase, reducing the flame temperature impeding the chain reactions to persist. Formulations made with boron or phosphorus elements (for example boric acid and borate, monopotassium phosphate, etc.) are an example, as they decompose past their boiling point, thus releasing water (Lally 2005; Tsuyumoto and Oshio 2009).

Some of the flame retardants mentioned previously can also be fire retardant, when they also act in the condensed phase, which is the case of boron-based and phosphorus-based compounds. When heated, these compounds chemically react with oxygen to form water vapour and acid, and the latter promotes char formation (Troitzsch 1998). This layer presents low thermal properties therefore cannot transport heat as effectively as the initial polymer. Char thus forms an insulating barrier which also prevents the release of volatiles from the core material (Bourbigot and Duquesne 2007). Intumescent coatings contain blowing agents, acid, and a carbon source which when reacting under heat form an intumescent char layer (Jimenez et al. 2006). Ammonium polyphosphate (APP) is typically used as the acid source in intumescent coatings, therefore protecting the substrate by chemical action, additionally to charring promotion.

A final type of fire retardant additives promoting a heat barrier are inorganic materials, which can protect the combustible material. Inorganic elements are not flammable, withstand high temperatures and tend to absorb heat owing to their low thermal conductivities (λ). For instance, Gourlay (2014) measured this parameter for lime on its own at λ=0.273 W/m.K, and silica presents also a relatively low value, at λ=1.4 W/m.K (CRC Handbook of Chemistry and Physics 2018), close to that of concrete (Table 2.2). Kandola (2001) and Wilkie and Morgan (2008) reviewed the addition of nanoscale silicates in various polymer matrices, and concluded overall that these inorganic additives would insulate the polymer beneath from radiant heat. For a modified polyamide with nanoclay, Kashiwagi, R. H. Harris, et al. (2004) remarked that

originally well-dispersed clay nanoparticles migrated towards the polymer surface upon heating, where they aggregated as part of the char layer. As lower heat release rates were monitored for the polyamide/clay samples, they suggested that the clay-reinforced char formed a thermal insulating protection, which shielded the polyamide from external radiation, which was also the conclusion drawn by Gilman et al. (2006) for layered silicates in polystyrene. In turn, the release of pyrolysis gases was limited by the presence of silicates on the outer surface of the modified polymer. Another explanation for the observed phenomenon is that the thermal mass of the whole composite is greater than the pristine polymer, therefore more heat is required to bring the composite to its pyrolysis temperature. This mechanism is not specific to a type of material (e.g. nanoclay) but rather observed for any inorganic material (Wilkie and Morgan 2008). The size of the additives only influences aggregation within the matrix, whereas the chemical nature of the compound is selected for its availability, cost, and potential for other functionalities (for instance functionalised silica particles).

2.4.4 Silica as a fire retardant

Research has already demonstrated the use of silica as a fire retardant, notably on polymers. For instance, Hshieh (1998) studied silicone-based intumescents which degraded forming a silica ash layer. It shielded the polypropylene beneath and limited its degradation by protecting it from radiant heat both of the flame and of the adjacent burning material. Kashiwagi, Gilman, et al. (2000) observed the same effect of silica deposited on the same polymer and on polyethylene oxide, although they noted that fused silica did not give as good results as silica gel. Specifically, they mentioned the importance of silica near the exposed surface of the polymers to insulate it from radiant heat. Further research on another polymer, poly(methylmethacrylate) (PMMA), concurred with these conclusions, with silica gel considerably decreasing the peak heat release rate when the silica-PMMA mix was exposed to a radiant heat flux of 40 kW/m^2 (Kashiwagi, Shields, et al. 2003). In addition, Kashiwagi, Morgan, et al. (2003) remarked that the shielding effect of silica was clearly exhibited when the surface of the condensed phase was completely covered. Mercado Roca (2005) utilised

modified epoxy resins with silica, which formed an insulating layer on the polymer upon burning and limited the production of volatiles by barrier effect. Similarly, Roenner et al. (2017) confirmed that nanosilica could improve the mechanical toughness of the epoxy matrix as well as limit flame spread, as the silica migrated to the surface of the substrate thus diffusing heat which led to a lower surface temperature.

Alongi et al. (2014) reported the thermal shielding effect of silica-based coatings on cotton fibres, by cone calorimetry analysis under exposure to a heat flux of 35 kW/m^2. The residue increased from <1 wt% to 3.5 wt% with as little as 1.6 wt% silica in the formulation, and up to 13 wt% when the coating contained both phosphorus (char promoter by release of phosphoric acid) and silica (thermal shield). Branda et al. (2016) impregnated fabric made from hemp fibres with silicate waterglass (sodium silicate), after which the treated hemp fibres were added to a matrix of epoxy resin to fabricate composites. The waterglass treatment on the fibres slightly decreased the peak of mass loss rate and final mass loss value (from 22 wt% to 30 wt%) as measured by thermogravimetric analysis (TGA). A greater shift in the residual value at 800 °C was recorded between the composite hemp/epoxy when treated hemp fibres were utilised (from 9.9 wt% to 23 wt%). They obtained even better results when the epoxy matrix contained an additional fire retardant agent, ammonium polyphosphate (APP) (up to 32 t% residual mass at 800 °C). They observed similar shifts in the residue after cone calorimetry (radiant heat flux of 35 kW/m^2), with less heat released when the hemp fabrics were coated (with and without the presence of APP).

2.4.5 Toxicity problem

Generalities

Purser (2001) explored the toxicity of various fire retardant solutions, which might hinder their future utilisation as regulations for toxic products become stricter. For example phosphorus-based compounds, such as APP and other organophosphorus fire retardants, might decompose into the neurotoxic trimethylol propane phosphate.

Toxicity of halogenated flame retardants is a major issue in the current flame retardant market, especially since they have been proven to accumulate in the environment

and were found in human tissue, as was summarised by Alaee and Wenning (2002). Chemical authorities both in Europe and the USA have pushed for a total ban of halogenated fire retardants (Directive 2003/11/EC, European Parliament (2003) and Assembly Bill 706, California Legislature (2007)). Further studies added more evidence to the case, for instance Babrauskas and Stapleton (2015) mentioned the toxicity of this class of flame retardants which are usually found in domestic settings (upholstered furniture, bedding material, curtains, etc.). Some of the halogenated compounds can accumulate in house dust, and potentially create a health hazard, especially for young children (Ward et al. 2014).

Since the use of halogenated fire retardants is being ruled out by governing bodies, alternatives are sought such as boric acid derivatives. However, teratogenicity was measured in several mammal foetuses as a consequence of boric acid exposure, which also led to skeletal modifications and organ dysfunction (European Chemical Agency 2010). Stronger regulations of boric acid compounds have been put into place so that the associated potential risks for humans (R60 and R61 risk phrases) appear on the substance safety data sheets as per recommended by the Regulation (EC) 1271/2008 (European Parliament 2008).

Safer alternatives fire retardant solutions are now being developed and tested to replace their more toxic counterparts, which were summarised by Wakelyn (2008) for textile products. Such solutions should not be persistent nor bioaccumulative, which could be the case of inorganic materials (clay, silica).

Silica additives

Hemp in construction is still a niche application of fire retardants to find recent thorough studies on their fire protection. This is the reason why the silica solution mentioned and studied in this thesis is based on experimental assessment of the fire performance of material with silica particles instead of assessment against standardised testing methods. This route was chosen to ensure that the underpinning mechanisms of delayed and/or reduced pyrolysis were better understood. Moreover, it can be argued that testing frameworks should be put into place to assess the mechanism in-

duced by specific fire retardant additives, and their associated hazards when released in the local environment. So far, a study by Napierska et al. (2010) evaluated the hazards on humans linked to nanosilica presence, concluding that the latter could cause harm only if the crystalline form of SiO_2 was used, or if it enters the respiratory system. More research is still required to fully validate silica as a non-toxic alternative to conventional fire retardants, such as for example by monitoring its release in the local atmosphere upon exposing coated material to heat. Further to this, all components used in the formulation of the final fire retardant solution (catalyst, functionalising agent, etc.) should be verified not to be harmful either.

2.5 Knowledge gap

Several methods permit to modify the surface of bio-materials to improve their properties. Chemical vapour deposition (CVD) methods, or the plasma-enhanced version (PECVD), are commonly used in the semiconductor industry to deposit TEOS as a silica precursor, although they require specific equipment. However, such methods tend to only chemically modify the substrate, and hydrophobicity can only be sustained for long periods if the surface roughness is enhanced as well.

When silica-derived thin-film gels were applied on hemp shiv, Hussain, Calabria-Holley, Schorr, et al. (2018) successfully demonstrated the gained hydrophobic properties by chemical modification. However by its nature, the coating was a dynamic system which might be prone to gelling, which induces shelf-life requirements that might hinder its industrialisation. Alongi et al. (2014) also proceeded with the sol-gel method to improve the thermal stability of coated bio-materials, such as cotton. Sol-gel technologies are indeed highly versatile and simple to carry out. When the outputs are stable sols, these can be deposited as such to physically modify the surface of the substrate, or the sols can be modified, which would provide the substrate with different functionalities (chemical modification).

As regards fire retardant solutions applied on bio-materials, borate (and boric acid) derivatives (Lazko et al. 2013) are still widely used to treat cellulose materials despite

their probable harm. Palumbo et al. (2017) also used boric acid to both delay mould growth, and limit the extent of combustion of corn pith insulation panels.

Considering the potential use of bio-based materials as insulation, and their inherent issues due to their chemical nature (water absorption leading to moisture and fire risk), new less toxic protective solutions are being sought. Ideally, such alternatives should address these two major problems conjointly with a simple to design approach in anticipation of industrialisation. More specifically, several aspects were identified in each part of this chapter:

- Key parameters to ensure consistent manufacture and quality control of the treatment should be known, to facilitate potential industrialisation.
- The developed treatment should not block the pores of the shiv to maintain moisture buffering.
- Hemp shiv need to be treated with a hydrophobic agent to limit their biodegradation, and withstand water exposure. This solution should not involve halogen-based silanes due to their potential toxicity.
- Pyrolysis of hemp shiv needs to be delayed and/or limited, by the means of a fire retardant, both during the flaming (if it occurs) and smouldering modes of combustion. This solution should protect the bio-material by physical action instead of chemical action to limit the potential toxicity of the smoke released (as it tends to be the case with conventional fire retardant additives).

Based on the characteristics exhibited by silica and demonstrated in this review, it appeared that the solution could be functionalised (for repellent properties) silica (protective layer) particles (tailored size which do not block the pores of hemp shiv).

Chapter 3

Silica particle synthesis

3.1 Introduction

Silica particles can be synthesised via numerous methods, via both dry and wet processes (Hyde et al. 2016). In this chapter, only the Stöber method (Stöber et al. 1968) is described. This approach has been chosen by the Coatings Team at TWI Ltd. for its simplicity, relatively low cost, and versatility for producing particles of different sizes and in a chemical environment facile for subsequent functionalisation. The size of particles can be tailored for the required application, and functionalities (such as water repellence) can be added in a simple manner (see Chapter 4). Multiple parameters, such as the time of reaction, the temperature, the reagents and their relative quantities (see Chapter 2), can influence the final particle size and their physical characteristics. Here, a set of formulations for which the water content increased whilst the initial alcohol content decreased was synthesised. This approach was followed so that the final total weight of each solution prepared would remain constant across all the set, similarly to the volumetric method of Sato-Berrú et al. (2013). There are two main objectives to this study:

- To analyse how the water content influences the size, porosity, and characteristics of the silica particles (part of this work was published by Bourebrab, Oben, et al. (2018);

- To develop a consistent method of fabrication and analysis for synthesising particles in anticipation of scaling up for industry application.

3.2 Experimental approach

3.2.1 Synthesis methodology

The silica particles were all synthesised following the Stöber process (Stöber et al. 1968), which is commonly used at TWI Ltd. in the coating technologies they provide. This method only requires a silane precursor, an alcoholic solvent, water, and a base catalyst. Seventeen formulations were synthesised, for which tetraethoxysilane (TEOS, IUPAC name: tetraethyl silicate) was chosen as the silica precursor. This alkoxysilane was favoured over alternatives for its availability and lower cost. The TEOS was thoroughly mixed with 28 % of the solvent, industrial methylated spirit (IMS, 99 % ethanol, 1 % methanol). Similarly to Stöber et al. (1968), ammonia was chosen as the catalyst, which was reduced in-house to a 25 wt% grade. Ammonia, selected quantities of water, and the remaining of IMS were mixed in a second pot, which was then added to the first, following by vigorous shaking for two minutes. The process is represented in Figure 3.1. The exact compositions of the formulations are described in Table 3.1. The final total weights of the formulations were made to be equal to 636 $\pm$ 1 g by decreasing the IMS content whilst the water content increased. The quantity of ammonia was deliberately set constant across the formulations to remove a degree of freedom. The formulations were then left to react for 48 h, either at room temperature (23 °C) or in the oven at 65 °C for the case where the effect of a higher temperature on the particle size was analysed. Room temperature can mean 23 °C or up to 27 °C depending on the location of manufacture, which therefore would induce variations in the process should this one be reproduced by other research groups. In this study, the samples were made in a laboratory regulated at 23 $\pm$ 1 °C to ensure reproducibility, as well as reducing the energy demand for the manufacturing steps for a more environmentally friendly approach in anticipation of potential industrialisation.

Samples were taken to examine the particle growth (via Dynamic Light Scatter-

ing) and reaction progress (via the measure of non-volatile content) as a function of time during synthesis. Figure 3.2 represents a flow chart of the particle synthesis and associated characterisation steps carried out in this study.

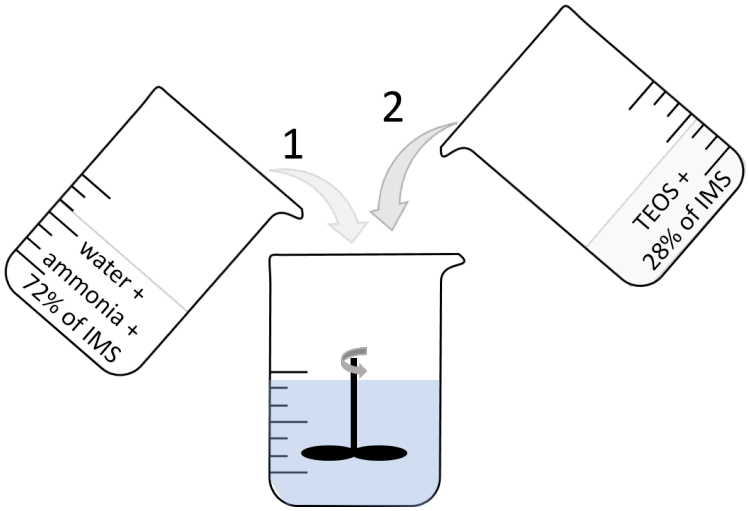

Figure 3.1: Schematic representation of the Stöber process followed for this study

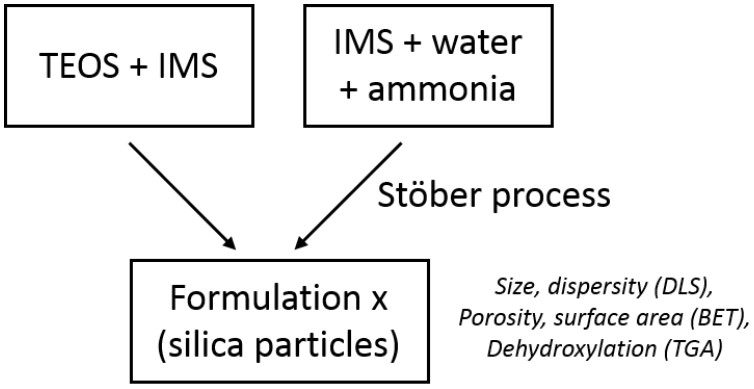

Figure 3.2: Flow chart representing the synthesis process of silica particles. The characterisation methods employed are shown in italic.

From a stoichiometric point of view, silica formation occurs from TEOS if the molar ratio between TEOS and water is 2:1 (Equation 3.1). Considering the amount of TEOS used in this set of formulations, this ratio corresponds to having 2.28 wt% of water in the initial system, which is a value between that of Formulations 1 and 2. However, in order to have complete and simultaneous hydrolysis of the four ligands of TEOS

Table 3.1: Relative quantities (in weight percentage (wt%)) of the reagents for the Stöber synthesis of silica

Formulation #	TEOS	IMS	Ammonia	water
1	13.19	84.89	0.48	1.44
2	13.21	82.52	0.47	3.79
3	13.24	77.76	0.47	8.53
4	13.21	73.12	0.48	13.20
5	13.25	68.35	0.48	17.91
6	13.24	65.15	0.48	21.14
7	13.21	61.25	0.48	25.06
8	13.18	57.26	0.47	29.09
9	13.20	53.46	0.47	32.86
10	13.23	49.48	0.48	36.81
11	13.20	45.57	0.48	40.75
12	13.23	37.64	0.48	48.65
13	13.19	29.92	0.47	56.42
14	13.22	22.05	0.48	64.26
15	13.18	14.23	0.48	72.11
16	13.23	6.32	0.48	79.98
17	13.25	0.05	0.48	86.23

for these systems, four moles of water per mole of TEOS is necessary, assuming the water liberated during condensation is not reused. This 4:1 molar ratio corresponds to a water content of 4.56 wt% for the quantity of TEOS present in these formulations. This value is just above that of Formulation 2. This means that Formulations 1 and 2 are substoichiometric, their products being intermediate silica species in the Assink and Kay's nomenclature (Assink and Kay 1984) which are not fully hydrolysed silica particles ($x > 0$). The reactions for Formulations 3 and beyond are not limited by stoichiometry. The intermediates produced during the subsequent hydrolysis and

condensation reactions are schematically represented in Figure 3.3.

$$\mathrm{Si(OEt)_4 + 2H_2O \rightarrow SiO_2 + 4C_2H_5OH} \tag{3.1}$$

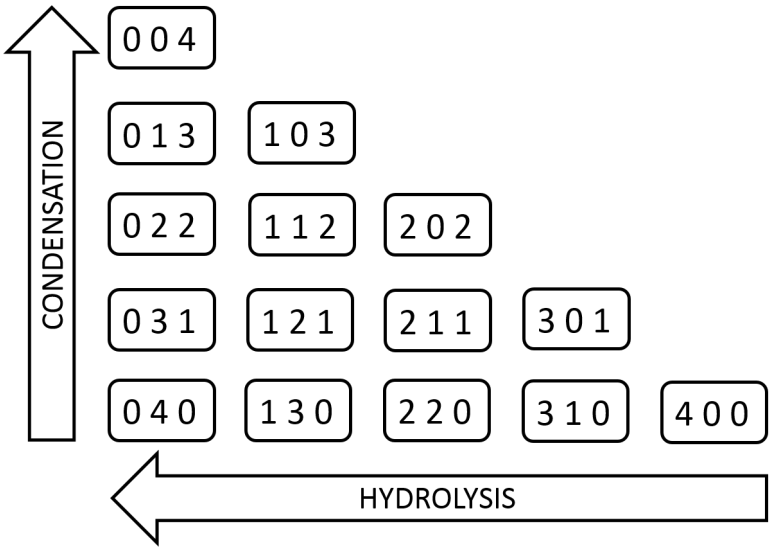

Figure 3.3: Schematic description of the 15 intermediates produced by the subsequent hydrolysis and condensation reactions, from TEOS to siloxane, according to Assink and Kay (1984). The general formula is given as $\mathrm{Si(OC_2H_5)}_x\mathrm{(OH)}_y\mathrm{(OSi)}_z$, where $x+y+z=4$ and the numbers represented in the schematic correspond to the values x, y, and z can be. The triplet $(4,0,0)$ therefore corresponds to TEOS, whilst $(0,0,4)$ represents a silica entity.

3.2.2 Characterisation methods

Particle size distribution

The Dynamic Light Scattering (DLS) method allows the determination of the distribution of particle diameters. These measurements were carried out at room temperature (23 ± 1 °C) with a Zetasizer Nano-S (Malvern Instruments, UK) (Figure 3.4), equipped with a laser beam of λ=632.8 nm and a backscatter detector positioned at 173°. Particles diffract the light from the laser source in all directions as long as they are in Brownian motion. This creates fluctuations in the intensity measured, which can then be tracked back to the hydrodynamic diameter of the particles via the correlation data

over time (Hassan et al. 2015). A measurement which distribution is given by intensity only necessitates information on the dispersant viscosity and refractive index values, whereas the particle optical properties are required for volume and number distributions of particle size (according to recommendations from the instrument manufacturer Malvern Instruments (2014)).

Here, an aliquot (approximately 2 μL) of each formulation was sampled from the parent solution without any modification, and its particle size distribution was measured three times. The sampling was repeated several times during the reaction process (between 0.22 h and 80 h) to monitor particle growth. The Z-average value was reported as it corresponds to the measurement of the hydrodynamic diameter of the particles (also named the cumulants mean), which is the most stable parameter produced by the DLS method (J. C. Thomas 1987; International Organization for Standardization 2008). The polydispersity index (PdI) gives indication on the dispersity of size within a distribution. When the PdI value is smaller than 0.1, the distribution is considered monodisperse (Stetefeld et al. 2016).

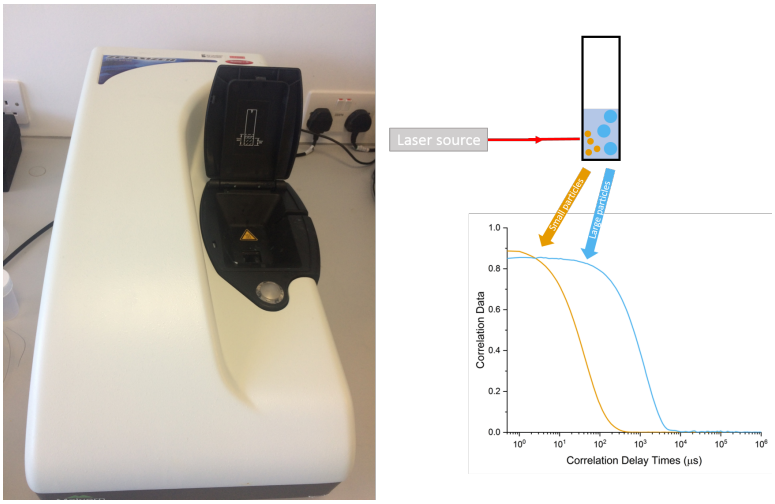

Figure 3.4: Zetasizer Nano-S at TWI Ltd. for particle size measurements and schematic explanation of the DLS method.

Porosity and surface area

In order to assess the pore size distribution and surface area of mesoporous samples, nitrogen adsorption and desorption was carried out. This approach allows determination of a wide range of pore sizes, including the complete range of micropores (< 2 nm) and mesopores ($2 < x < 50$ nm) (Rouquerol et al. 1994). A combination of two methods was employed to estimate the effective pore size distribution: the semi-empirical and analytical Horvath-Kawazoe method (HK) (Horvath and Kawazoe 1983; Haghighatju et al. 2017) considers a slit-pore shape geometry of materials, whilst its extension the Saito-Foley model (Saito and Foley 1991; Lowell et al. 2004; Haghighatju et al. 2017) uses a cylindrical pore geometry approach. The Brunauer-Emmett-Teller (BET) theory (Brunauer et al. 1938) was employed to calculate the specific surface area of each dried sample within the BET range ($0.05 \leqslant P/P_0 \leqslant 0.3$). The pore size analysis was conducted by implementing a modified Kelvin equation, which is known as the Barrett-Joyner-Halenda (BJH) method (Barrett et al. 1951), and commonly used for mesoporous materials.

The experiments were carried out with a Micromeritics ASAP 2060 (Micromeritics Instrument Corporation, Norcross, GA, USA) (Figure 3.5), and the results analysed with the software Micromeritics MicroActive™Ȧn aliquot of each formulation of silica particles was dried for 72 h at 65 °C in air. Each sample weighed between 0.10 g and 0.15 g. The samples were first degassed under vacuum, at 90 °C for one hour, followed by 16 h at 150 °C. Following this gradual degassing protocol avoided damaging the samples by preventing dehydroxylation, according to Li et al. (2015). The BET analysis was carried out by subsequent adsorption and desorption of nitrogen at the gas/solid interface within the sample. The experiment was carried out at -196 °C (77 K) by immersing the flask containing the dried particles in a dewar filled with liquid nitrogen.

Solid contents

The non-volatile content (NVC) calculation is traditionally used in the coatings industry to measure the proportion of inorganic matter to solvents in a solution (ASTM

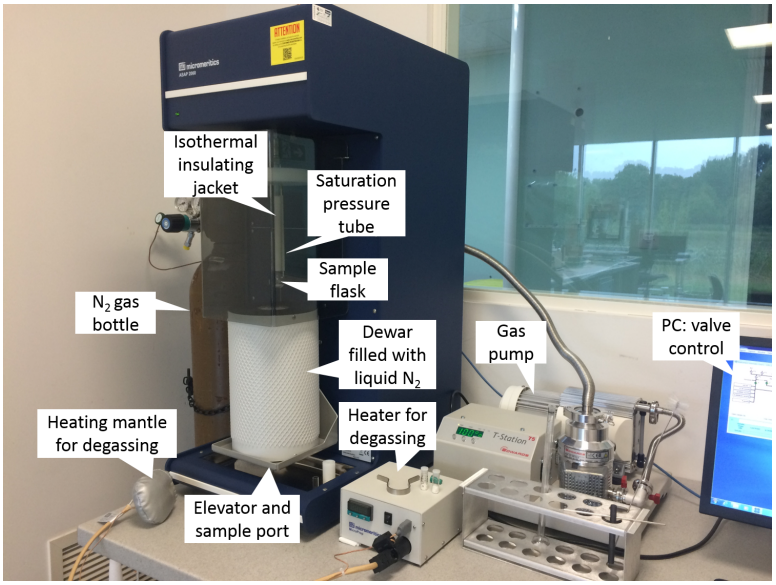

Figure 3.5: Photograph of the Micromeritics ASAP 2060 BET equipment at TWI Ltd.

2013). In order to track the progress of the reactions leading to silica particles synthesis, samples were collected at various times of reaction for up to 80 h after mixing the reagents. A sample consisted of an aliquot of each silica dispersion which was dried for 72 h at 65 °C. The NVC value was calculated according to Equation 3.2. The hydrolysis reactions were presumed to have progressed to completion 48 h after mixing, which is given as the final NVC value (reported in Table 3.2). Monitoring the evolution of NVC over time was done to determine whether any volatile silica species (most likely unreacted or partially reacted TEOS) were still present in the mixture at a given time.

$$NVC\% = \frac{\text{weight of dried silica particles}}{\text{weight of dispersion sampled}} \times 100 \tag{3.2}$$

The same aliquots of each formulation which had been dried for 72 h at 65 °C were also used for characterisation via thermogravimetric analysis (TGA, Netzsch STA 449 F3 Jupiter equipped with silicon carbide furnace, Netzsch, Germany, shown in Figure 3.6). Such characterisation method and chosen parameters allowed evaluating the final solid content as well as the steps of degradation of the samples, such as dehydroxylation. These analyses were carried out in a Pt-Rh crucible, from room temperature to 1000 °C at a rate of 10 °C/min, in air. This heating rate was selected under the

hypothesis that the sample and the apparatus are at thermal equilibrium (Witkowski et al. 2016).

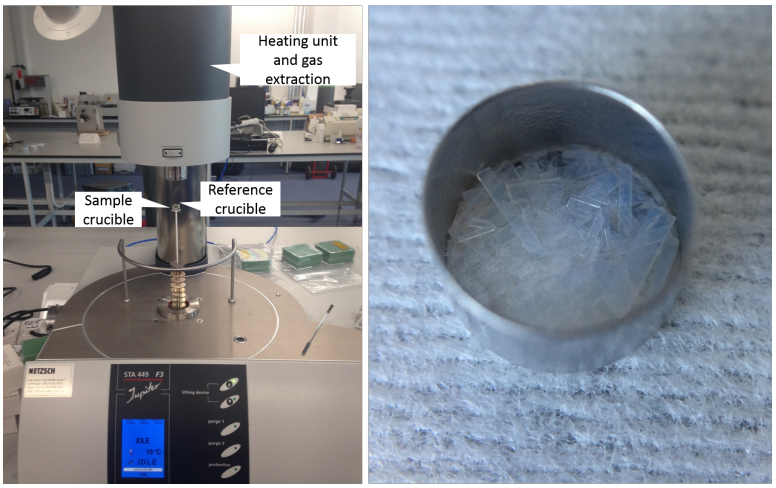

Figure 3.6: Image of the TGA kit (Netzsch STA 449 F3 Jupiter) at TWI Middlesbrough, and close-up view of silica solids in the crucible.

3.3 Physical characteristics

3.3.1 Overview

The different characteristics of the 17 formulations of silica particle dispersions are summarised in Table 3.2, and an image of the vials after 48 h of reaction is shown in Figure 3.7. More details on the mechanisms behind those results are given in the following subsections: the particle size distributions (Size and PdI) are discussed in Section 3.3.2; the BET surface area, total pore volume, and isotherm hysteresis type in Section 3.3.4; the mass residue by TGA in Section 3.3.5; the NVC in Section 3.3.3.

3.3.2 Size dependence with water content

Modifying the reagents concentration has an influence on the resulting particle size and characteristics of the synthesised silica (Bogush, Tracy, et al. 1988; Sato-Berrú et al. 2013; Greasley et al. 2016). In this study, the emphasis was placed on increasing

Table 3.2: Summary of the characteristics of the prepared suspensions and their dried solids. The standard deviations are not shown for clarity.

Formulation #	Size, Z-average (nm)	PdI	BET surface area (m^2/g)	Total pore volume (cm^3/g) at $0.99 \times P/P_0$	Isotherm hysteresis type (Sing et al. 1985)	Mass residue TGA (wt%)	NVC (%)
1	12.50	0.35	549.92	0.51	H2	71.93	4.28
2	32.01	0.20	347.31	0.41	H2	85.37	4.30
3	122.50	0.06	233.69	0.34	H1	87.50	4.28
4	234.35	0.05	165.08	0.32	H1	86.94	4.26
5	351.75	0.06	103.78	0.18	H4	88.23	4.25
6	579.20	0.15	197.58	0.18	H4	85.17	4.23
7	727.05	0.05	220.37	0.15	H4	88.59	4.23
8	754.00	0.09	283.74	0.19	H4	90.89	4.15
9	818.95	0.07	295.03	0.19	H4	88.73	4.18
10	676.70	0.05	307.86	0.21	H4	88.52	4.17
11	451.15	0.02	290.54	0.35	H4	86.02	4.11
12	198.13	0.41	251.74	0.67	H2	91.05	4.08
13	*	*	444.92	0.60	H2	90.70	4.05
14	*	*	453.09	0.59	H2	91.02	4.11
15	*	*	468.15	0.60	H2	91.82	3.77
16	*	*	447.85	0.57	H2	92.22	3.93
17	*	*	464.71	0.55	H2	92.22	3.87

$*$ Those values could not be measured by the DLS method due to the two-phase nature of the systems.

the water content from one formulation to the next, whilst decreasing the alcohol content to keep a constant total weight at 636 $\pm$ 1 g. In Figure 3.8, the average particle diameter is plotted against the water content: the size increased with each water increment, until peaking at 818 nm for approximately 33 wt% of water, after which the size reduced. Past Formulation 12, the DLS method could not be used for particle size measurements due to the two-phase nature of the dispersions.

A photograph of all the vials of the 17 formulations after 48 h of reaction is shown in Figure 3.7. One can clearly see that particles made from Formulation 2 presented Rayleigh scattering, which is characteristic of materials whose size is smaller than 10 % of the wavelength of light to which they are exposed. This clear blue haze is typical of silica nanoparticles in suspension and was seen especially for vial of Formulation 2. Formulations 3 to 11 were white/opaque, which is typical of Mie scattering, meaning

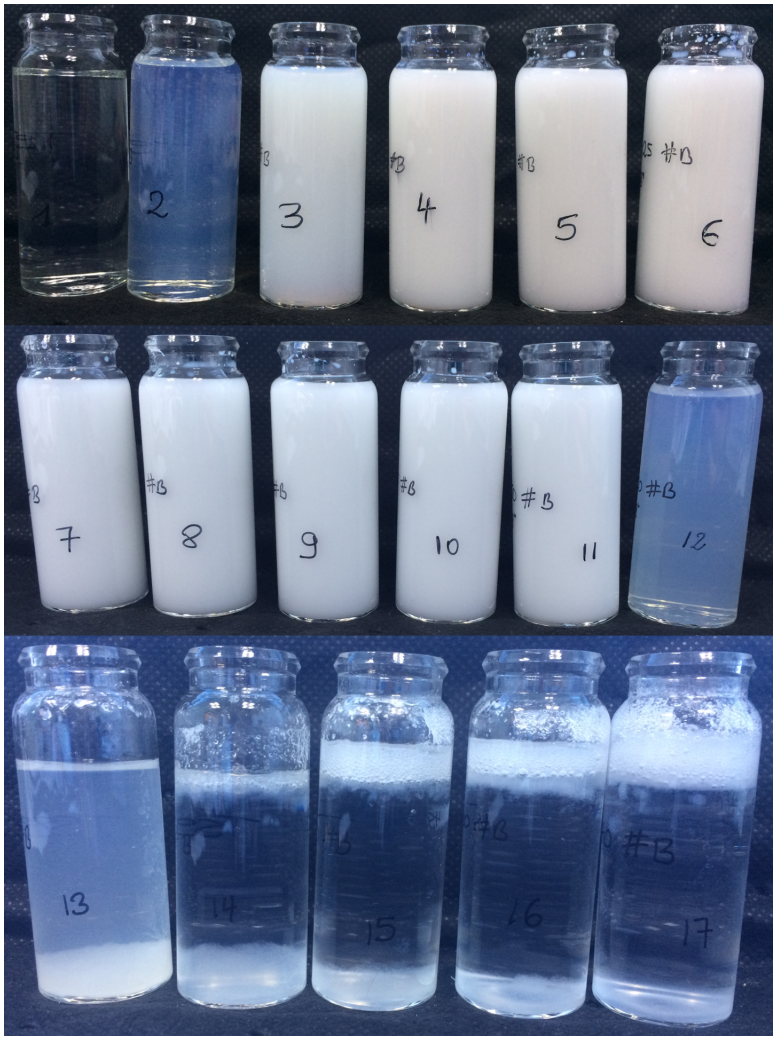

Figure 3.7: Visual assessment of the 17 formulations after 48 h of reaction.

that the particles in those vials have a diameter approaching that of the wavelength of visible light (400 nm to 800 nm). Vials of Formulations 13 to 17 presented a clear phase separation with some sedimentation. Half or more of the content of the formulations being water, it is likely that a TEOS-rich phase in ethanol with a foam-like appearance was floating on top of an aqueous phase. Finally, due to its visual aspect, Formulation 12 seemed to present nanoparticles of roughly the same size than those of Formulation 2, but the average value obtained from DLS data refutes this. Indeed, the error bars for this formulation are greater than any other, covering a range from 90 nm to 215 nm. The image of Formulation 12 used for Figure 3.7 had a correspond-

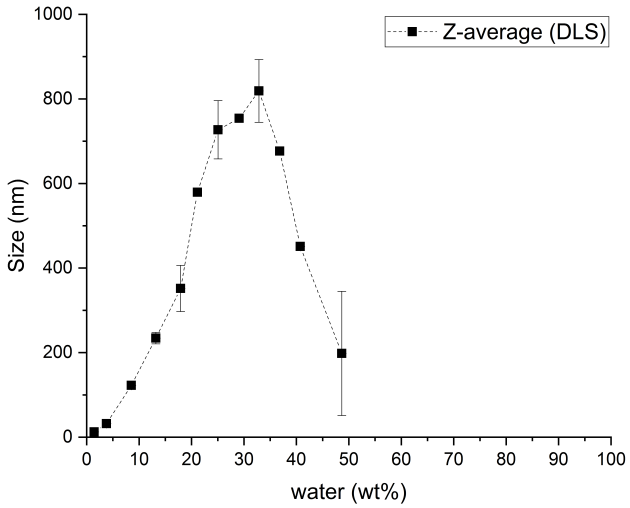

Figure 3.8: Particle size evolution with water content from Formulation 1 to 12.

ing Z-average measurement of 93 nm, with two main peaks of intensity at 246 nm and 42 nm (hence the blue haze).The PdI value was however over 0.53, describing a very low quality and polydisperse sample (PdI >0.2), and indicating that the DLS was not the adequate method for such sample.

In order to reach full hydrolysis of the precursor, 4.56 wt% of water are needed for the quantity of TEOS introduced in the mix, which is greater than the water content of Formulation 2. This suggests that Formulations 1 and 2 were insufficient in water, and therefore the hydrolysis reactions did not go to completion. The materials synthesised from Formulations 12 and over demonstrated multiple phase systems: it is thought that partially reacted TEOS formed aggregated structures rather than discrete particulates, as it can seen from the TEM images h to j in Figure 3.9 by Bourebrab, Oben, et al. (2018).

As it has been reported by others (Bogush, Tracy, et al. 1988; Sato-Berrú et al. 2013; Greasley et al. 2016), the particle size peaked for a composition of approximately 33 wt% of water (also plotted in Figure 2.6). The obtained measurements of particle size in this study compared with those of other research groups demonstrates that irrespective of the initial quantities of reagents, similar pattern of size increase and

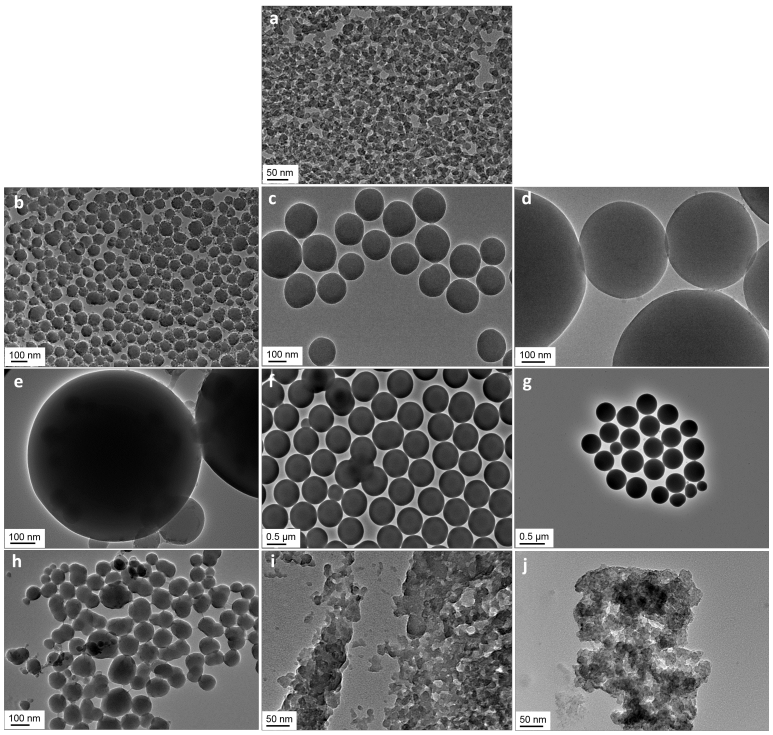

Figure 3.9: TEM images of silica particles of different sizes with increasing water content. Reprinted with permission from Bourebrab, Oben, et al. (2018). Copyright 2018 Springer.

decrease was observed. Reaching a peak indicated that the stability of the siloxane intermediates might have changed around this water content. Silicon alkoxides such as TEOS degrade in water, which is why co-solvents such as ethanol are used. In the lower range of water contents, the mixtures appeared homogeneous, thus the expected reactions hydrolysis and condensation are likely to occur to produce particles of narrow size distributions. At higher water contents, the mixtures are more heterogeneous, due to the greater quantity of water over that of alcohol, until some ethanol has been liberated during hydrolysis at the water/TEOS interface (Equation 2.2). The hydrolysis and condensation reactions (Equation 2.4) occur simultaneously, with the chemical environments favouring one or the other (Brinker 1988). The competition between the two reactions also relies on the high pH of the systems: condensation is likely to occur more rapidly than hydrolysis due to the presence of ammonia as catalyst; therefore an even greater quantity of water will make up the majority of the

medium, which means that there will be a point at which a single phase mixture cannot be achieved anymore.

The formation of silicon intermediates can be considered by using the nomenclature of Assink and Kay (1984) $\mathrm{Si(OC_2H_5)}_x\mathrm{(OH)}_y\mathrm{(OSi)}_z$ (Figure 3.3). The silica precursor TEOS ($x = 4$; $y = z = 0$) is insoluble in water, and in a medium of water/alcohol above a critical value of water content. Close to this value, the composition changes to $x \neq 4$ and $y > 0$, followed by $z > 0$. Because these x, y, and z evolve over the course of the two reactions, and the composition of the associated media change as both ethanol and water are liberated, the solubility characteristics of the 13 intermediate species between TEOS and $\mathrm{Si(OSi)}_4$ (more conventionally written as $\mathrm{SiO_2}$) will change as well. These alterations in the nature of the intermediate rely on the availability of partially hydrolysed silane to participate in further condensation reaction, which would be dependent on local compositional considerations. The homogeneity of the initial mixture and the composition of its medium are then critical to determine the structural and compositional characteristics of the resultant material synthesised.

3.3.3 Induction time and influence of temperature

The mechanisms dictating particle growth are still subject to debate. In a thorough review, Hyde et al. (2016) summarised that three mechanisms could explain particle growth following synthesis via the Stöber process: the aggregation model, where small nuclei aggregate to form a bigger entity; the nucleation growth model, where small nuclei grow over time; or a combination of both. In order to understand which model better describes particle growth with the parameters set for this study, the particle size (Z-average) and solid content (NVC) values of the dispersions were measured over time, up to 80 h after initial mixing of the reagents. The average diameter of particles made from Formulation 3 over time is reported in Figure 3.10. During an induction period, the Z-average showed a pattern which could be attributed to the nucleation growth model, as the nuclei grew from 69 nm at 0.22 h to 117 nm after 5 h. After, this, the Z-average value plateaued at this value without further major fluctuation (in the range of an uncertainty of 3 nm due to the measuring technique). This

phenomenon concurs with the findings of Topuz et al. (2015), although they analysed particles of greater diameters (310 nm and 520 nm), and with Bogush and Zukoski IV (1991) for 390 nm, 410 nm, and 550 nm particles. The similarity for different sizes of particles would suggest that this model is valid across a range of size.

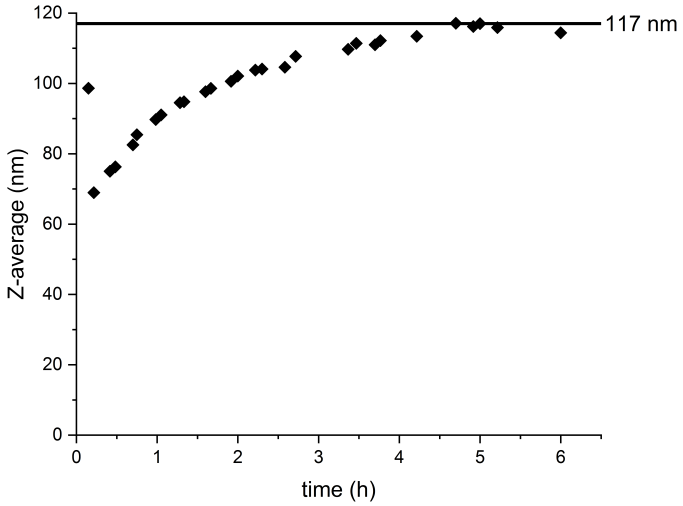

Figure 3.10: Induction period of particle growth, example of Formulation 3, with a particle size plateauing at 117 nm after 5 h of reaction.

The availability of the volatile precursor (TEOS) is another parameter that gives an indication on the progress of nucleation growth. The total time required for TEOS to be converted into non-volatile species can be estimated by measuring the NVC value throughout the particle synthesis. According to Equation 3.1, the complete reaction from TEOS to silica involves one mole of TEOS to produce one mole of silica SiO_2. The NVC can therefore be calculated following the simple calculation shown in Equation 3.4, which results in a final NVC value of 3.8 % (based on the initial quantity of TEOS used in these formulations). However, obtaining a greater NVC value than the 3.8 % calculated suggests that not all potential reactions have occurred, and some species formed still contained ethoxy (unhydrolysed) and silanol (uncondensed) groups ($x >$

0 and $y > 0$ in Assink and Kay's formulation (Assink and Kay 1984)).

$$\begin{aligned} & n(\mathrm{TEOS}) = n(\mathrm{SiO_2}) \\ \Leftrightarrow\ & \frac{m(\mathrm{TEOS})}{M(\mathrm{TEOS})} = \frac{m(\mathrm{SiO_2})}{M(\mathrm{SiO_2})} \\ \Leftrightarrow\ & m(\mathrm{SiO_2}) = m(\mathrm{TEOS}) \times \frac{M(\mathrm{SiO_2})}{M(\mathrm{TEOS})} \end{aligned} \tag{3.3}$$

with M(SiO_2)=60.09 g/mol and M(TEOS)=208.33 g/mol.

Therefore if we replace m(SiO_2) from Equation 3.3 in the NVC Equation 3.2, we obtain Equation 3.4:

$$\begin{aligned} NVC\% &= \frac{m(\mathrm{SiO_2})}{m(solution)} \times 100 \\ &= \frac{m(\mathrm{TEOS})}{m(solution)} \times \frac{M(\mathrm{SiO_2})}{M(\mathrm{TEOS})} \times 100 \\ &= \frac{84}{636} \times \frac{60.09}{208.33} \times 100 \\ &= 3.8 \end{aligned} \tag{3.4}$$

Different batches of Formulation 2 were synthesised, one batch put in the oven at 65 °C to react, whilst three others were left at room temperature, similarly to the procedure followed earlier on. The reaction was monitored by measuring the NVC value at different times, until it reached a plateau at 4.3 %, as is displayed in Figure 3.11. The NVC plateaued after 44 h of reaction for the room temperature batches, which is far longer than the 5 h required to establish the final particle size. This suggests that the hydrolysis and condensation reactions were still continuing even after nucleation finished. When the sols were aged at a higher temperature, the final NVC value of 4.3 % was reached after 15 h, which illustrates the influence of temperature on the kinetics of reaction. However, the particles synthesised at 65 °C were smaller than those at room temperature, with a final diameter measured at 18 nm, which is in accordance with the findings of Bogush, Tracy, et al. (1988) and H.-C. Wang et al. (2006). The particle size distribution was, however, much broader with a PdI value at 0.33 (see results in Table 3.3). The plot of the particle size distribution for both temperatures of synthesis (Figure 3.12) suggests a normal distribution for both cases, centred around the values of Z-average shown in Table 3.3. The distribution of the 65 °C batch, however, dis-

plays what resembles a second population overlapped with the main one, probably centred around 100 nm. This means that increasing the temperature of reaction for the same initial composition leads to either aggregated entities or bigger particles in a polydisperse system.

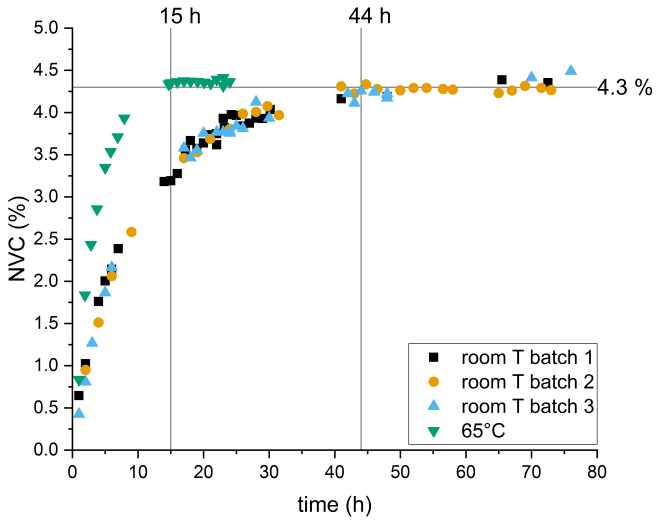

Figure 3.11: Influence of temperature on the non-volatile content value

Table 3.3: Size measurements for Formulation 2 particles synthesised at room temperature and 65 °C. The standard deviation was calculated from five samples of each type of batch.

Temperature	time (h) to NVC=4.3 %	Z-average (nm) ± stdev	PdI ± stdev
room T	44	32.4 ± 0.5	0.21 ± 0.01
65 °C	15	18.1 ± 0.6	0.33 ± 0.04

Therefore, in order to produce consistent monodisperse silica particle suspensions, the parameters of reaction are key. It is also a compromise between rapidity and consistency: industrially, fast reactions tend to be cheaper as they require less energy to produce over time, but having consistently the same materials produced should prevail. This is the reason why for this thesis, unless stated otherwise such as in this particular study, all silica particles were synthesised at room temperature, in a two-pot process with a rapid addition of TEOS to the other reagents, in order to obtain

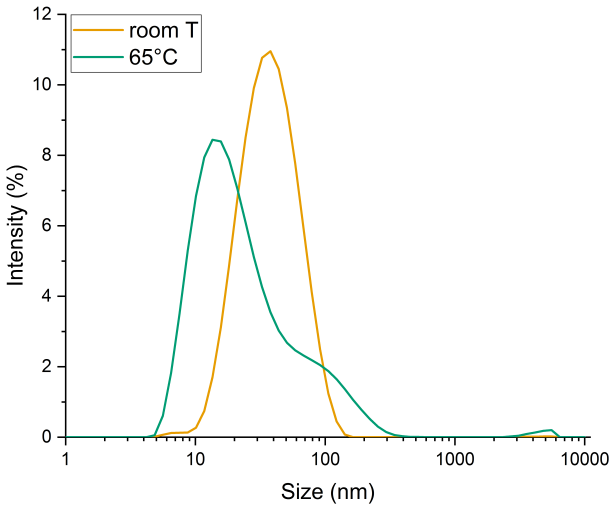

Figure 3.12: Particle size distributions of Formulation 2 particles synthesised at room temperature and 65 °C. The distributions are the averaged values of five samples measured for each type of batch.

monodisperse silica particles of a given consistent size.

3.3.4 Micro- and mesoporosity and surface area

The porosity and specific surface area characteristics of the dried samples synthesised from the 17 formulations were analysed using nitrogen sorption methods. Overall, type IV isotherms were obtained for all samples according to the IUPAC classification (Sing et al. 1985). This is typical of mesoporous materials which exhibit a uniform surface. The values of total pore volume and specific surface area are shown in Table 3.2 and displayed in graphical form in Figure 3.13. The data suggests that the dried materials produced could be grouped in three categories:

- materials from Formulations 1 and 2, made from substoichiometric water contents, which can be described as disordered materials with high specific surface area and total pore volume values;

- materials from Formulations 3–11, with an average specific surface area of approximately 230 m^2/g and an average total pore volume of 0.23 cm^3/g;

- materials from Formulations 13–17, for which the water contents were greater than 56 wt%, presented an average specific surface area of approximately 450 m^2/g and an average total pore volume of 0.58 cm^3/g.

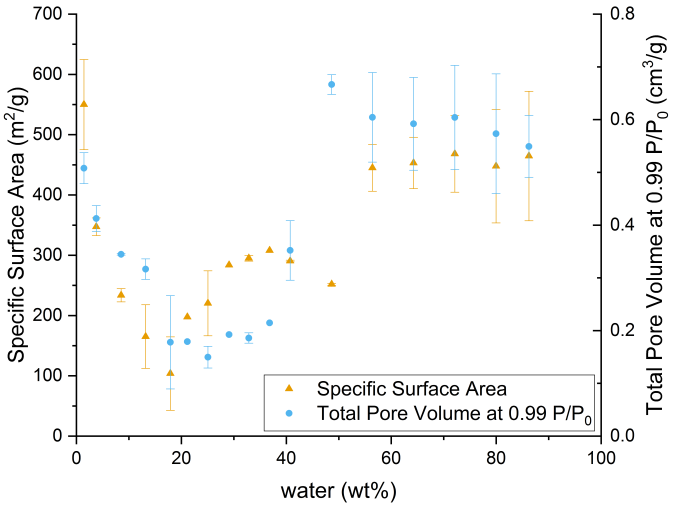

Figure 3.13: Specific surface area and total pore volume measurements for the dried materials of the 17 formulations.

As was suggested in Section 3.3.2, samples of the first category presented sub-stoichiometric water contents (below 4.56 wt%), which were insufficient for the hydrolysis/ condensation reactions to go to completion. The materials might still have presented some ethoxy groups ($x \neq 0$), and were generally disordered, which is demonstrated by the H2 type of hysteresis loop of their isotherms (according to the IUPAC classification (Sing et al. 1985)), which is illustrated in Figure 3.14. The second category, which corresponds to Formulations 3 to 11, demonstrated lower values of surface area and total pore volume. The isotherm curves of those samples either demonstrated a hysteresis loop H1 (Formulations 3 and 4) or H4 (Formulations 5 to 11). The H1 type is characteristic of a narrow pore size distribution, which pore shape

is more cylindrical. The H4 type is representative of narrow slit pores. The surface area and total pore volume values obtained for the third category were higher than those of the second category. Such increase would mean that the materials are more porous. Additionally, they also presented type H2 hysteresis loops, which are often found for disordered materials with less defined pore shape. Finally, the sample issued from Formulation 12 seemed to be in an intermediate between the second and third categories: the low specific surface area at 251 m^2/g is similar to that of the second category of materials, whilst the higher total pore volume at 0.67 cm^3/g and the shape of the hysteresis loop suggest this material should belong to the third category.

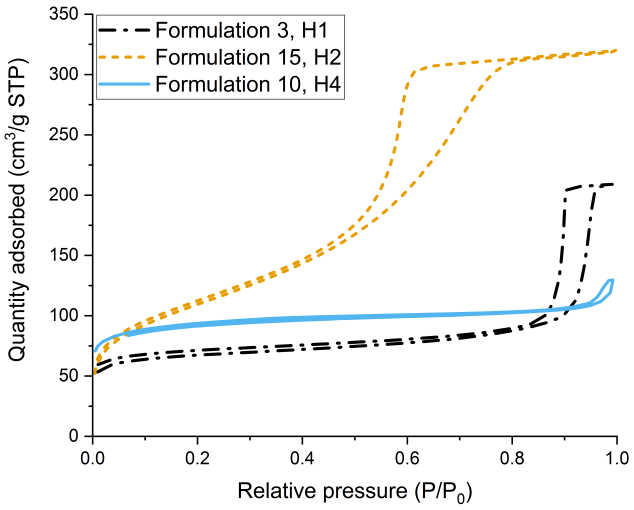

Figure 3.14: The three different types of hysteresis loops of the isotherm curves obtained.

Usually, the choice for mesoporous materials over non-porous ones is led by the increased available surface area, which means more reactive sites accessible. If this aspect alone were considered, materials from the third category would be preferred. However, these formulations yielded disordered materials with less well defined pore shapes. Materials which present defined pore shape and size distribution (second category, with initial water contents ranging from stoichiometric level 4.56 wt% to 40.75 wt%) were favoured.

3.3.5 Prediction of surface chemistry following degradation of silanols

Considering the general formula $\mathrm{Si(OC_2H_5)}_x\mathrm{(OH)}_y\mathrm{(OSi)}_z$ to describe the species formed by subsequent hydrolysis and condensation according to Assink and Kay (1984), it is clear that some intermediates present groups which are degradable at lower temperatures than others. Silicon dioxide is inorganic, therefore no thermal degradation occurs below 1000 °C for the final moiety $\mathrm{Si(OSi)}_4$. Nevertheless, the materials synthesised in this study showed thermal degradation, which can be analysed to better understand their chemical nature, and evaluate their x, y, and z values.

The thermogravimetric curves of this experiment are presented in a consolidated manner in Figure 3.15. The materials were categorised in a different way than in Section 3.3.4.

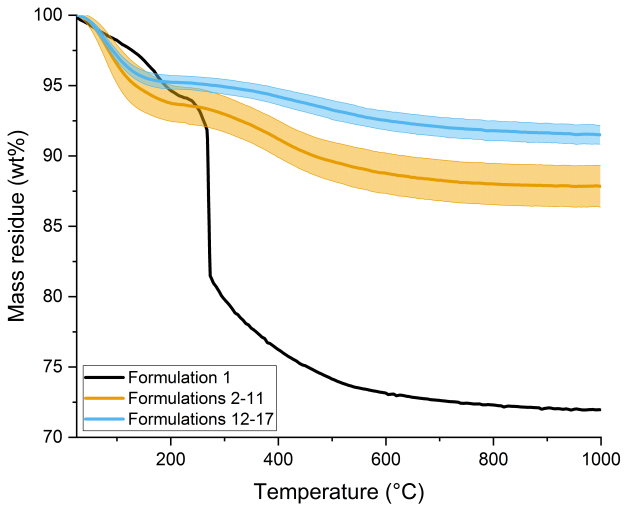

Figure 3.15: Thermogravimetric analysis of the 17 formulations, showing the difference between the three categories of formulations here: 1, 2–11, and 12–17. The shaded areas around the curves represent the standard deviation within each category of formulations.

The dried material produced from Formulation 1 clearly underwent more important degradation upon heating to 1000 °C compared to the other samples, which is why it is represented on its own. The initial weight loss occurring at 70 °C is likely to be associated with the evaporation of physisorbed species which have not been

removed during the preceding drying process (Dzis'ko et al. 1950). The most significant weight loss at about 270 °C can be interpreted by considering the initial water content in the formulation. Being substoichiometric, not all the alkoxy groups have been hydrolysed, and so the resultant material would present residual ethoxy groups chemically bonded to the surface. In anticipation of a further utilisation of silica particles as inorganic solid, it is important to reduce the number of volatile ethoxy groups as much as possible (reducing x value), and drive the condensation reactions further towards the most $-\mathrm{OSi}$ groups (greater z).

The second and third categories represented in Figure 3.15 demonstrated a similar behaviour but to a lesser extent. The lower temperature weight losses up to approximately 200 °C can be related to the removal of volatiles and physisorbed species; whereas dehydroxylation is most probably the cause of the second weight losses, between 200 °C and 700 °C (Armistead et al. 1969; Effati and Pourabbas 2012; Zhuravlev 2000). The final residual weight of each category can give some indications on the z value, which ought to be very close to zero for Formulation 1, and slightly greater for the third category (12–17) than for the second (2–11): $z_{(1)} \simeq 0 < z_{(2-11)} \leqslant z_{(12-17)}$.

The main difference between the second and third categories of dried materials was the absolute weight loss over the complete temperature range. Effectively, the materials from Formulations 2–11 lost on average 6.5 % of their initial weight on heating to 200 °C, and an additional 6 % by what is supposed to be dehydroxylation, leading to a final residual weight of 87.5 %. As regards the third category of materials, the initial weight loss was of approximately 4.8 %, followed by 3.7 % by removal of silanols, which equates to a final residual weight of 91.5 % on average across the category. The specific surface area for the third category was greater than for samples of the second one (see Section 3.3.4), which appears contradictory with exhibiting a lesser weight loss by dehydroxylation, which would suggest a lower silanol density. One possible explanation would be that the dried materials of the second category still present a higher residual alkoxy content (non negligible x), although the weight loss between 300 °C and 400 °C would have been greater than the one observed here (closer to that of Formulation 1). Another potential interpretation would be that these

two categories of materials present different silanol populations (Figure 3.16). The materials from the second category made with lower water contents could be richer in geminal silanols, which would induce a higher Q^2/Q^3 ratio, whereas a lower ratio would be valid for the third category, whose materials could be richer in vicinal or isolated silanols. Indeed, more complete hydrolysis and condensation reactions (reducing the x and y values) would mean that more silicon atoms of the surface have bound with oxygen towards more Q^3 and eventually Q^4 species (thus increasing the z value). Such behaviour will be validated in future work by analysing this set of dried samples via solid state ^{29}Si NMR (Nuclear Magnetic Resonance) spectroscopy.

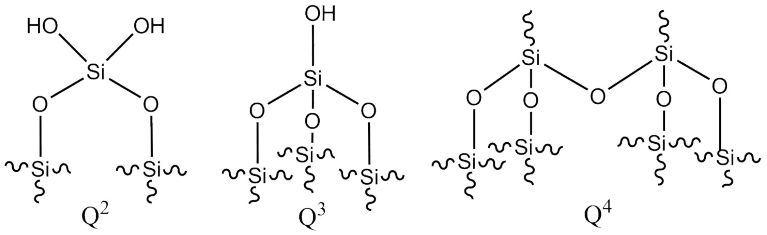

Figure 3.16: Schematic representation of silanol types present on silica spheres surface. Q^2 refers to geminal silanol, Q^3 to vicinal silanol (the isolated case is not represented here), and Q^4 to siloxane (Zhuravlev 2000).

3.4 Towards industrialisation: introduction of specifications following statistical distributions

The silica particle suspensions made according to Formulations 2 and 3 are standard materials for further development and applications within the Coatings team at TWI Ltd. Over the course of this thesis, a large number of batches have been synthesised and analysed by different members of the team. Reproducibility of the same material is key for an industrial application, regardless of the person manufacturing them. The materials should all be part of a same population of monodisperse silica particles with hydrodynamic diameters of either ∼30 nm or ∼120 nm (Formulations 2 and 3 respectively) before the cleaning process (to remove the ammonia) and before functionalisation (see Chapter 4).

Both formulations display Gaussian distributions, which are illustrated by the example of the DLS outputs in Figure 3.17. Formulation 2 demonstrates a mean Z-average of 30.8 nm and mean PdI value of 0.20, whereas Formulation 3 has a mean Z-average of 123.2 nm and mean PdI of 0.07 (see Table 3.4a). The lower the PdI, the narrower the distribution and the higher the intensity peak, which is clearly observable from Figure 3.17. Statistically, the mean and standard deviation of a population give a good estimate of the distribution in size across a population. However, if belonging to a certain population of material relies on statistical data, median and interquartile range values are more relevant, as they concede less weight to outliers (Upton and Cook 1996) (Table 3.4b).

The statistical distributions of particle size for each formulation is shown in Figure 3.18. The output from these distributions can then become a quality control tool for when a new batch is synthesised (Table 3.4). For example, when a batch of silica particles is produced according to Formulation 2, it is visually assessed by verifying the presence of the slight blue haze, and the particle size distribution is measured by the DLS method. If the Z-average is outside the range Z-average (median) $\pm$ iqr, the batch is considered non-conform as out of the specifications given. When the Z-average is within the aforementioned range, the PdI value is checked to be in its own range as well. Outside it on the greater side, the particles might be of the expected size, but their distribution is too polydisperse. If outside on the smaller side, the batch is considered more monodisperse than the rest of the population of Formulation 2 samples, which is still considered a good batch.

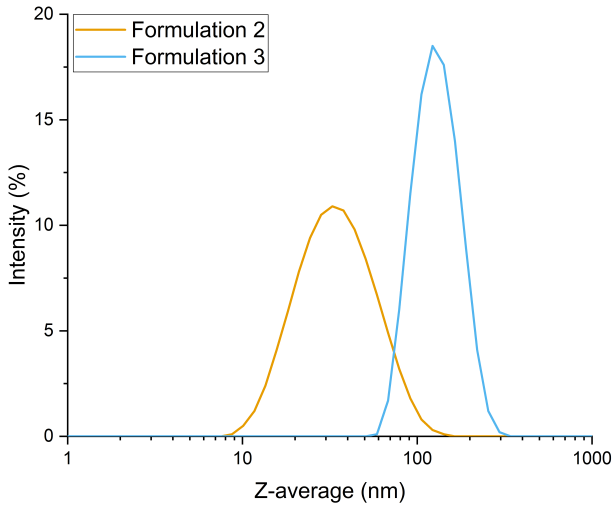

Figure 3.17: Intensity output from the DLS measurement for Formulations 2 and 3 shown in logarithmic scale (averages of all N elements).

Table 3.4: Statistical distribution values of Z-average (particle diameter) and PdI (polydispersity) of Formulations 2 and 3. The mean and standard deviation consider all instances equal, whereas the median and interquartile range concede less weight to outlying values.

(a) mean and standard deviation values

Formulation #	N	Z-average (me) ± stdev (nm)	PdI (me) ± stdev
2	81	30.8 ± 4.1	0.20 ± 0.03
3	108	123.2 ± 4.3	0.07 ± 0.02

(b) median and interquartile range values

Formulation #	N	Z-average (md) ± iqr (nm)	PdI (md) ± iqr
2	81	30.1 ± 6.5	0.20 ± 0.03
3	108	122.3 ± 4.9	0.07 ± 0.03

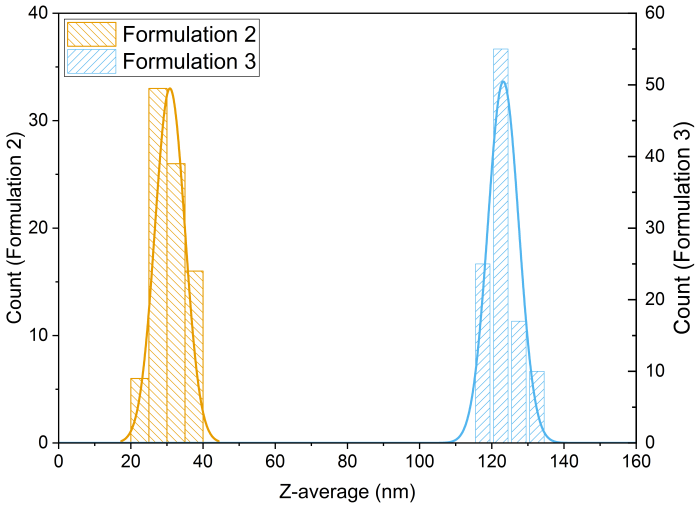

Figure 3.18: Global distribution of Formulations 2 and 3 according to the particle size (as measured by DLS method).

3.5 Summary

In this study, 17 formulations with increasing water contents were prepared for the synthesis of silica particles of various sizes via the Stöber method. The resultant particles were characterised to better understand the effect of varying the initial water content on their physical characteristics. The key findings are summarised below:

- By increasing the initial water content, the particle size increased until a maximum of 850 nm for 33 wt% of water.
- The particles reached their final size earlier than the consumption of all the volatile precursor.
- Changing the temperature of reaction seemed to reduce the induction period for the reactions to complete, decreased the particle size, and created a broader particle size distribution.
- At least stoichiometric amounts of water with respect to TEOS were necessary to produce discrete silica particles, until 48 wt% of water (according to the TEM

images c to g published by Bourebrab, Oben, et al. (2018) displayed in Figure 3.9).

- The particle size distribution could be measured via the DLS method for the formulations which water contents remained below 48 wt%. Above this threshold, a far more convoluted morphological profile was clearly present, and seen in the TEM images h to j by Bourebrab, Oben, et al. (2018) in Figure 3.9.

- The porosity and thermal degradation characterisations allowed to categorise the formulations regarding their structure and composition (according to the general formula of Assink and Kay (1984) $\mathrm{Si(OC_2H_5)}_x\mathrm{(OH)}_y\mathrm{(OSi)}_z$):

  - 1–2 produced by substoichiometric water contents (below 4.56 wt%), yielded disordered materials without well defined pore shape distribution, significant weight loss which suggests the presence of ethoxy groups (Formulation 1 only). They could most probably be described by $x > y$ and $z \simeq 0$.

  - 3–11, whose water contents were ranging between 8 wt% and 41 wt%, displayed defined pore shape (slit-shape or cylindrical) and size distributions, lower surface area, less residual weight on heating to 1000 °C, more dehydroxylation. Their compositions could be defined by $x \simeq 0$, $y > z$.

  - 12–17 with water contents above 48 wt% showed higher surface area (apart from Formulation 12 which was more of an intermediate) but disordered materials with less defined pore shape distribution, less dehydroxylation than the previous category. The groups attached to silicon could be determined by $x \simeq 0$, $y \geqslant z$ with $z_{(12-17)} \geqslant z_{(3-11)}$.

- A statistical analysis of various batches of Formulations 2 and 3 could be used for quality control to assess the consistency in terms of size as measured by DLS method and characteristics of the particles within one population in anticipation of an industrial application.

3.6 Recommendations

A thorough characterisation was carried out in this study, which focussed on the effect of water content on the resultant particle size. In the work published by Bourebrab, Oben, et al. (2018), a ternary diagram was introduced, although presenting a tie-line as the TEOS and ammonia contents remained constant throughout the set of formulations. Several other parameters can affect the shape, structure, composition, and behaviour of silica particles, especially the reagents concentration. Building up from this ternary diagram, by modifying the initial concentration of TEOS for example, could be a potential research lead. Additionally, changing the catalyst, or swapping the co-solvent for another alcohol would create similar systems with different characteristics (e.g. bigger particles when the alcohol possesses longer carbon chains). The end goal of continuing this work would be to create design rules to synthesise tailored-for-application materials.

Chapter 4

Functionalisation of silica Stöber spheres

4.1 Introduction

Silica particles are intrinsically hydrophilic, due to the presence of hydroxyl groups ($-OH$) on their surface (Zhuravlev 1993). Particles tend to agglomerate when their surface is not treated, which is why they are usually functionalised. It prevents the particles from agglomeration by reducing the number of available hydroxyl groups, therefore limiting the potential for hydrogen bonding which is the primary source of particle-particle interaction. Functionalisation also enables changes to the surface properties, such as providing a hydrophobic behaviour by grafting specific silanes on the surface of silica particles (Taylor et al. 2017).

Two sizes of silica Stöber spheres were functionalised, to compare if size could have an influence on functionalisation, biodegradation (see Chapter 5), and pyrolysis (see Chapter 6), whilst being small enough not to block the pores of the substrate. The impact of silane/Stöber silica ratio was investigated by using a simple gravimetric method, which was introduced by Posthumus et al. (2004). The hydrophobic silica particles were characterised by coating them on glass slides and measuring water and diiodomethane contact angles. Understanding the wetting behaviour of two probe liquids of different polarities allows a simple provisional assessment of the repellent

properties of two formulations of silica particles after deposition on glass slides, prior to application on other substrates, such as hemp shiv as described in Chapter 5. The coating process of glass slides and characterisation of repellence carried out is summarised in Figure 4.1, a follow-up of Figure 3.2.

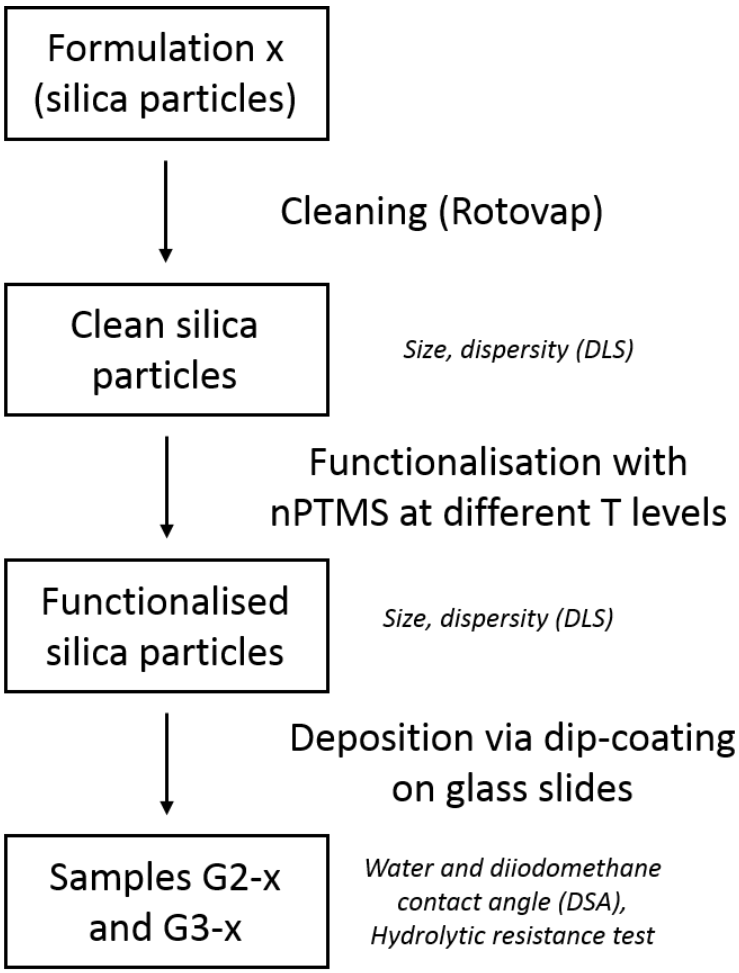

Figure 4.1: Flow chart representing the coating process of glass slides. The characterisation methods employed are shown in italic.

4.2 Process

4.2.1 Functionalising silica particles

In a first instance, silica particles were synthesised following the Stöber method as described in Chapter 3. Particles were made using Formulation 2 and 3 (see Table 3.1), corresponding to a diameter of 30 nm and 110 nm respectively. It is thought that particles of 30 nm diameter present more ethoxy groups than those of Formulation 3, according to results shown in Chapter 3. Their functionalisation was studied nonetheless in this chapter to see if their chemical structure could influence the functionalisation process and associated hydrophobicity.

Immediately after synthesis, the ammonia was removed by evaporating around 60 % of the supernatant liquid at 50 °C under vacuum, after which they were re-diluted with the same quantity of IMS. This process was repeated twice, to ensure no trace of ammonia was left in the solution. The non-volatile content (NVC) was measured after the cleaning process (see Section 3.2.2 for the method of calculation). The only non-volatile species present in the formulations are the hyrolysis/condensation products of TEOS. Empirically, for the formulations used in this study and under ideal conditions, the NVC is approximately 4.3 %, assuming that the exact same quantity of IMS was used for re-dilution. However, the emphasis is on knowing the NVC value, more than reaching this target concentration. In this experiment, the batch of cleaned silica particles made from Formulation 2 had a final NVC of 4.9 % after cleaning.

The particles were then functionalised with a hydrophobic silane, according to the theories mentioned in Section 2.3.3. After an experimental screening, the functionalising agent n-propyl trimethoxysilane (nPTMS) (Silanes & Silicones, Stockport, UK) was chosen over fluoroalkylsilanes due to their potential environmental hazards. The condensation catalyst used in this study was dibutyltin dilaurate (Sigma-Aldrich, Gillingham, UK), which was very compatible with this silane, despite its toxicity being known at the time of the study. Additional work in parallel demonstrated that alternative silanes, such as hexamethyldisilazane, could be used thanks to their propensity

for auto-catalysis, thus eliminating altogether the need for an external catalyst[1]. Using this silane required, however, an additional cleaning step after functionalisation to prevent condensation reactions between the silane chains themselves. As small quantities of dispersion were functionalised, this supplementary cleaning was not experimentally feasible under the current laboratory conditions. Further research for optimal silane–catalyst pairing will be carried out in subsequent work.

The silane was added to approximately 35 g (∼50 mL) (for most samples) of the same parent solution of silica particles under constant stirring. A small quantity, 0.2 % of the total weight of the suspension, of the catalyst was added (the process is sketched in Figure 4.2, and a schematic representation of functionalised particles is shown in Figure 2.7). This quantity of catalyst provided coated glass slides with the greatest repellent properties compared to lower quantities[2]. The formulations were then shaken for 10 min, and placed in the oven at 65 °C for 18 h so that hydrolysis-free condensation could occur between the alkoxy silane and the silanol groups of the surface of the silica.

Formulations 2 and 3 of functionalised silica particles were prepared with different ratios of the solution and silane, as is described in Table 4.1. Different levels of functionalisation were used: a T1.00 level corresponds to introducing the same weight of silane as silica solids in a given suspension. Similarly, T0.10 corresponds to a silane content of 10 % of the weight of non-volatile species.

4.2.2 Coating deposition

For each formulation, three soda-lime glass microscope slides were coated by immersion, and withdrawn at 100 mm/min. The glass slides were then dried at 150 °C for one hour. It is assumed that after this time all volatiles and excess unreacted silane have been removed.

[1] This study is part of another project work carried out in the FCR section at TWI Ltd.

[2] This study is also part of another project work carried out in the FCR section at TWI Ltd.

Table 4.1: Name of samples and quantities of silane used for each functionalisation level. G2 refers to the glass slides coated with silica particles synthesised from Formulation 2 (30 nm), and G3 from Formulation 3 (110 nm).

Formulation	Quantity of solution (g)	NVC (%) after cleaning	Quantity of silica (g)	Quantity of silane (g)	Functionalisation level T
G2-0-unf ∗	305.1	4.3	0.0	0.0	0
G2-0-nc §	303.6	4.3	13.1	13.1	0
G2-0.15	35.1	4.9	1.7	0.3	0.15
G2-0.20	37.8	4.9	1.9	0.4	0.20
G2-0.25	34.9	4.9	1.7	0.4	0.25
G2-0.30	36.4	4.9	1.8	0.5	0.30
G2-0.35	33.4	4.9	1.6	0.6	0.35
G2-0.40	35.9	4.9	1.8	0.7	0.40
G2-0.45	32.9	4.9	1.6	0.7	0.45
G2-0.50	36.5	4.9	1.8	0.9	0.50
G2-0.55	35.7	4.9	1.7	1.0	0.55
G2-0.60	35.0	4.9	1.7	1.0	0.60
G2-0.70	33.3	4.9	1.6	1.1	0.70
G2-0.80	35.4	4.9	1.7	1.4	0.80
G2-0.90	35.6	4.9	1.7	1.6	0.90
G2-1.00	31.6	4.9	1.5	1.5	1.00
G2-1.00′	303.2	4.3	13.0	13.0	1.00
G2-1.50	304.0	4.3	13.1	19.6	1.50
G2-2.00	313.1	4.3	13.5	26.9	2.00
G3-0-nc §	62.7	4.0	2.5	2.5	0
G3-0.50	278.5	4.0	11.1	5.5	0.50
G3-1.00	259.2	3.9	10.1	10.0	1.00

∗ unfunctionalised silica particles

§ no catalyst

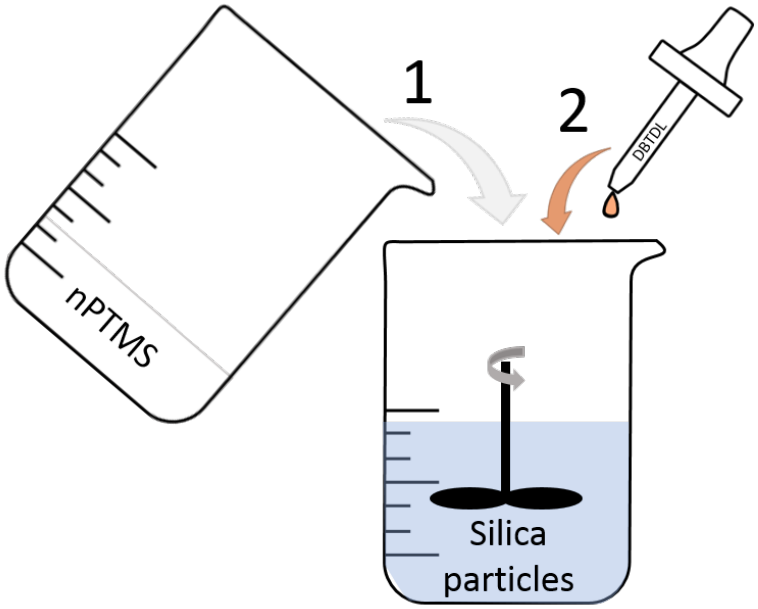

Figure 4.2: Schematic representation of the functionalisation process.

4.2.3 Analysis methods

Particle size distribution

The particle size distributions were analysed via Dynamic Light Scattering (DLS) to obtain their mean diameter (Z-average) and polydispersity index (PdI) values. This method is described in detail in Chapter 3, Section 3.2.2.

Contact angle (CA) measurements

The repellent behaviour was assessed by contact angle measurements on glass slides via the static sessile drop method. Two probe liquids were used: deionised water which is a polar protic liquid, and diiodomethane, a non-polar aprotic liquid. This choice is common practice to cover a good range of polarity, and therefore get a good estimation of the surface free energy (SFE) of a substrate so that the Fowkes' theory can be applied (Fowkes 1964).

In this study, the measurements were performed at room temperature ($24 \pm 1\,°C$) using the Drop Shape Analyser DSA-100 (Krüss GmbH, Hamburg, Germany, shown

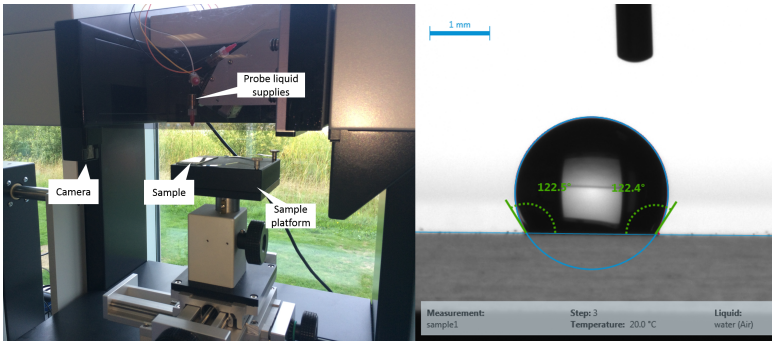

Figure 4.3: Drop Shape Analyser at TWI Ltd. and screenshot of the image produced by the Krüss Advance software.

in Figure 4.3). Three droplets of each probe liquid were deposited on each glass slide. The droplets each had a volume of 2 μL to minimise the impact of gravity and maintain their spherical shape (Marmur 2009), and thus their contact angle with the substrate. An image of each droplet was captured using Krüss Advance software to allow measurement of the key dimensions. The averaged values of water contact angle (WCA) and diiodomethane contact angle (DCA) were reported, along with the standard deviation between each droplet measured (a total of nine droplets of each probe liquid for each formulation). As explained in Section 2.3.1, the threshold value for demonstrated hydrophobicity corresponds to a WCA above 90°, with the greater the WCA the better. The WCA of nPTMS diluted in IMS deposited on glass slide is typically measured at approximately 80°[3], which is the lower threshold value to obtain when the silane is grafted on the silica particles. Similarly to WCA, the greater the DCA, the more repellent to diiodomethane the coated substrate is, and the lower its surface free energy (SFE) as well. Clean, uncoated glass slides typically exhibit a SFE of 55 mN/m, whereas a repellent surface should possess a much lower value, such as 20 mN/m obtained for polytetrafluoroethylene (Jańczuk and Białłopiotrowicz 1989).

Hydrolytic resistance test

In order to estimate the effect of water on the liquid repellence characteristics, the glass slides were immersed in a container filled with deionised water at room temperature

[3]This value was measured for another project work carried out in the FCR section at TWI Ltd.

for 24 h, without any stirring in place. The glass slides were then dried in the oven at 65 °C for 10 min to allow evaporation of the water film remaining on the surface. After that, the WCA and DCA were measured and compared to the values obtained before immersion. The whole experiment was carried out under ambient conditions (24 $\pm$ 1 °C) to be representative of a real-life scenario where a coated substrate could be in contact with water for prolonged period of time.

4.3 Effect of silane on the characteristics of the particles: particle size and repellence analysis

4.3.1 Hydrodynamic diameter and syneresis

The DLS method allows measurements of the hydrodynamic diameter of particles in Brownian motion, which measures the particle diameter including any grafted chains. Using this method can then help determine if the nPTMS chains are indeed grafted on the silica nanoparticles or not, and whether the particle size distribution has changed following functionalisation.

Firstly, the dispersion of silica particles was measured before being cleaned. The Z-average was found to be approximately 30 nm for Formulation 2, and 122 nm for Formulation 3 particles. The dispersions were cleaned at a higher temperature than the synthesis reaction, usually around 50 °C, under vacuum to evaporate the ammonia. After this step, the Z-average had dropped to approximately 26 nm and 108 nm respectively for each formulation (Table 4.2). The shift in measured diameter is similar to that recorded in Section 3.3.3, where particles synthesised at a higher temperature were smaller, which had also been observed by Tan et al. (1987), Bogush, Tracy, et al. (1988), and H.-C. Wang et al. (2006). This effect of temperature on the diameter of particles is thought to be caused by syneresis of the particles, a light densification with expulsion of excess liquid trapped in the pores of the material (Hench and West 1990). This is illustrated in Figure 4.4, by the slight shift of the particle size distribution before and after cleaning towards smaller sizes. The Z-average, specific surface area, and total pore volume values measured before and after cleaning are then likely to drop

(although the latter two were not studied here).

During the functionalisation process, the particles were also exposed to a higher temperature of 65 °C. Since the syneresis is a non-reversible phenomenon and shrinkage has already occurred, the Z-average is unlikely to change before and after functionalisation. This hypothesis was verified for particles of Formulation 3, whose particle size distribution is displayed in Figure 4.4. It remained fairly constant before and after functionalisation: the mean diameter of the two populations were measured at 108 nm and 106 nm respectively, however the distribution was slightly narrower for the latter, which was highlighted by the PdI value decreasing from 0.08 to 0.04 (Table 4.2). Particles of Formulation 2 after functionalisation demonstrated a slightly increased average diameter, from 26 nm to 31 nm. Knowing the particle diameter is important as quality control tool, which was introduced in Section 3.4, although a slight variation of its value should not be crucial on the repellent characteristics of the resultant coating.

4.3.2 Levels of functionalisation

When unfunctionalised silica particles were deposited as a single layer on the glass slides, the WCA remained very low, at 21° on average, which proved the hydrophilic character of the particles due to their numerous $-OH$ groups on their surface. Nevertheless, when the particles were functionalised with nPTMS, the WCA of all samples averaged 118.2°. This is graphically presented in Figure 4.5 and shown in Table 4.3. It appeared that as long as catalyst was present to promote the condensation reaction between the silane and the silica surface, grafting could occur, which led to the repellent behaviour to water which was observed. In the case that the catalyst was omitted (-nc samples), the WCA remained at 91.1° and 116.6° respectively for samples G2-0-nc and G3-0-nc, which suggests that some silane was still deposited on the glass slides – unreacted with the surface of the particles – and might not have been removed upon drying at 150 °C. The boiling point of this silane is 142 °C (Sigma-Aldrich 2016), thus just lower than the drying temperature of the coated glass slides. However, the drying process only lasted one hour which might not have been long enough to evaporate un-

Table 4.2: Characteristics of the particle size distribution for Formulations 2 and 3, before and after cleaning, and after functionalisation with nPTMS at a T1 level.

Formulation	Before cleaning		After cleaning		After funct. nPTMS T1	
	Z-average (nm)	PdI	Z-average (nm)	PdI	Z-average (nm)	PdI
2	29.7 ± 2.0	0.21 ± 0.01	26.0 ± 2.2	0.26 ± 0.02	30.6 ± 0.4	0.25 ± 0.01
3	122.4 ± 2.1	0.06 ± 0.02	108.0 ± 1.7	0.08 ± 0.02	106.2 ± 0.8	0.04 ± 0.02

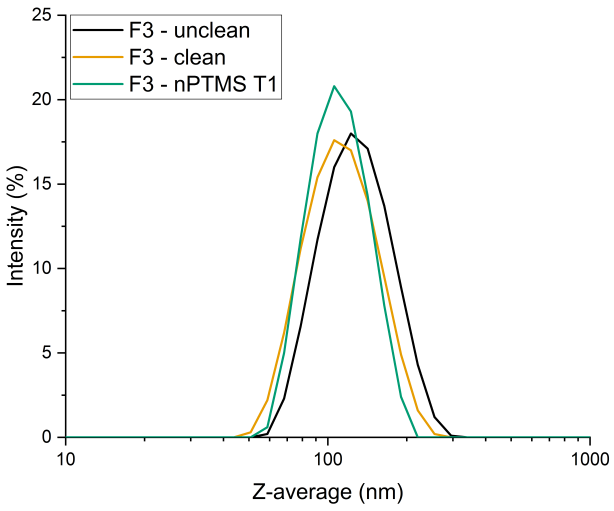

Figure 4.4: Particle size distribution of Formulation 3 particles, before and after cleaning, highlighting the syneresis phenomenon, and after functionalisation with nPTMS at a T1 level.

reacted silane. Future work will consider extending this drying time and then verify that no unreacted silane remain on the surface of glass slides.

Table 4.3: Water and diiodomethane contact angle values for each functionalisation level of particles of Formulations 2 and 3 coated on glass slides.

Sample	Functionalisation level T	Before hydrolytic resistance test	
		WCA (°)	DCA (°)
G2-0-unf	0.00	21.2 ± 1.2	31.4 ± 1.7
G2-0-nc	0.00	91.1 ± 6.3	42.4 ± 0.3
G2-0.15	0.15	116.1 ± 4.2	46.5 ± 1.9
G2-0.20	0.20	116.5 ± 2.4	49.5 ± 0.7
G2-0.25	0.25	118.1 ± 0.9	54.4 ± 2.8
G2-0.30	0.30	116.9 ± 0.5	57.9 ± 4.6
G2-0.35	0.35	119.6 ± 0.5	59.9 ± 8.5
G2-0.40	0.40	117.7 ± 1.6	63.6 ± 9.5
G2-0.45	0.45	121.8 ± 2.0	66.9 ± 11.4
G2-0.50	0.50	118.4 ± 3.0	71.7 ± 12.2
G2-0.55	0.55	118.4 ± 0.9	65.4 ± 10.3
G2-0.60	0.60	118.6 ± 1.4	69.2 ± 10.7
G2-0.70	0.70	118.1 ± 1.7	69.0 ± 12.2
G2-0.80	0.80	118.4 ± 2.0	69.2 ± 11.7
G2-0.90	0.90	118.7 ± 2.3	68.0 ± 9.1
G2-1.00	1.00	121.2 ± 1.4	58.7 ± 2.8
G2-1.00′	1.00	118.8 ± 1.3	61.1 ± 1.2
G2-1.50	1.50	118.5 ± 0.6	60.6 ± 4.9
G2-2.00	2.00	118.4 ± 0.5	58.7 ± 3.1
G3-0-nc	0.00	116.6 ± 1.3	49.9 ± 2.0
G3-0.50	0.50	122.6 ± 1.7	78.9 ± 3.0
G3-1.00	1.00	108.8 ± 4.6	64.3 ± 7.8

Diiodomethane is a non-polar aprotic liquid, and so has very different chemical character than water, therefore presents different wetting behaviour on a given substrate. The repellence to diiodomethane of all samples based on Formulations 2 and 3 particles is presented in Figure 4.6. Overall, the repellence increased then plateaued at 69.8° from a functionalisation level of T0.45, until a slight decrease for levels of func-

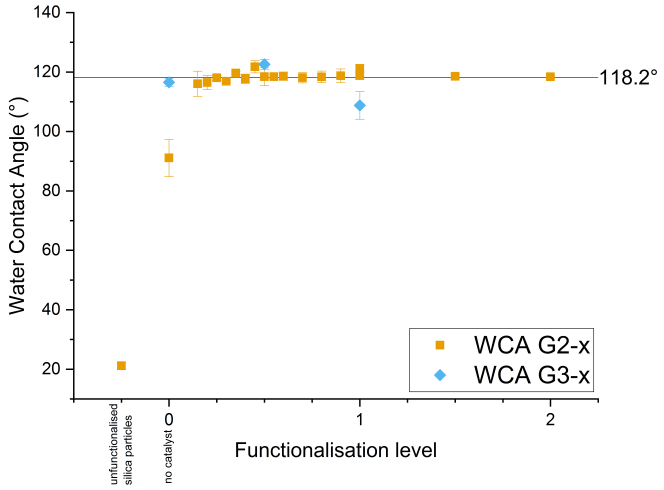

Figure 4.5: Water contact angle measurements on glass slides coated with Formulations 2 and 3 particles functionalised with nPTMS (samples G2-x and G3-x). The error bars represent the standard deviation between all measurements done per type of sample.

tionalisation greater than T1.00. Between T0.15 and T0.50 of functionalisation level, the linear relationship (Figure 4.7) suggests that the diiodomethane was more sensitive to slight changes in the functionalisation of the surface, which was not the case with water. The DCA measurements were a powerful tool to assess the functional performance of the coated surface in terms of repellence. Because diiodomethane is sensitive to $-OH$ groups too, the more silane in the formulation (increased T level), the fewer $-OH$ groups were available. The surface was therefore more repellent as there was less affinity between the probe liquid and the substrate, and this was proved to be by a linear relationship between T0.15 and T0.50. This feature, especially observed in Figure 4.7, gives indication on successful silane grafting and thus increased repellent behaviour.

Overall, the functionalisation of silica particles was successfully demonstrated by increased values of WCA (118.2° on average) and DCA (69.8° on average) compared to unfunctionalised systems. The quantity of silane seemed not to impact greatly the water repellence, as above a functionalisation level of T0.15, the WCA reached 116.1°, proof of hydrophobicity. On the other hand, diiodomethane exhibited more sensitiv-

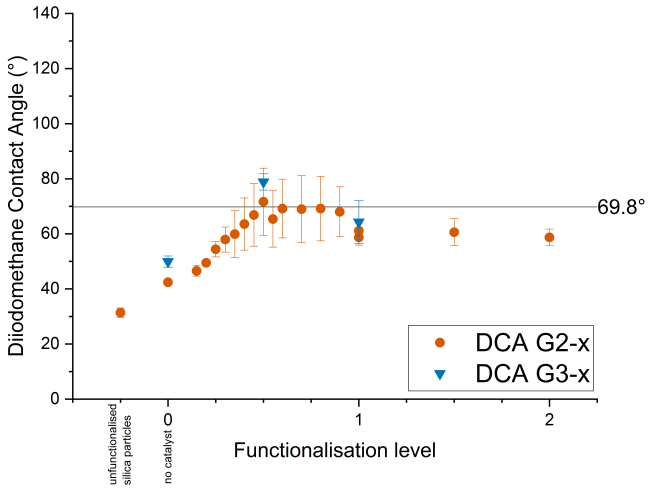

Figure 4.6: Diiodomethane contact angle measurements on samples G2-x and G3-x. The error bars represent the standard deviation between all measurements done per type of sample.

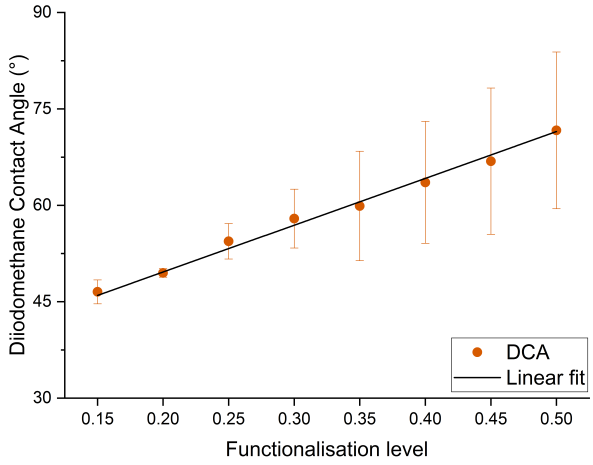

Figure 4.7: The linear fitting curve for the DCA measurements of Formulation 2 particles functionalised with nPTMS between T0.15 and T0.50 levels, which demonstrates a correlation coefficient r^2=0.98 and $DCA = 72.9 \times \text{T level} + 35.0$ for equation. The error bars represent the standard deviation between all measurements done (three glass slides per formulation, therefore nine droplets of the probe liquid were measured).

ity to available $-OH$ groups, as the DCA value increased linearly with the quantity of silane between T0.15 and T0.50 levels, before plateauing at approximately 69.8°. This different behaviour between water and diiodomethane demonstrated the importance of assessing repellence by two (or sometimes more) probe liquids to better understand the phenomenon occurring and thus the functional performance of the coated substrate. It can be more robust as the grafted silane protected the substrate from external elements (dirt, other liquids, etc.).

4.3.3 Hydrolytic resistance

Sometimes, unreacted silane can be deposited on the substrate during the dip-coating process and thus provide a certain repellence, although it is not fully grafted on the silica particles. Drying the glass slides at 150 °C upon coating should remedy this, but it is necessary to determine whether this is effective. One way of assessing if the silane has reacted and remains bound to the particles, and themselves being fully attached on the glass slides, was followed in this study. By immersing the coated glass slides in a bath of deionised water for 24 h, any decrease in the WCA and DCA measurements should indicate that the silane was not fully grafted onto the silica particles. The coating would not be resistant to liquid water, which could induce a loss of repellent properties. This was assessed in this experiment by measuring any decrease of WCA and DCA after immersion. As it was highlighted in Figure 4.5, the functionalisation level did not affect the WCA as long as catalyst was used in the process. For this reason, only seven samples amongst all were tested for hydrolytic resistance.

The results of this test are presented in Figure 4.8 and in Table 4.4. The overall behaviour reflects the hypothesis formulated: the repellent functionalised silica particles remained on the surface of the glass slides, even after having been immersed for 24 h in water.

Sample G2-0-nc presented a noticeable loss of water repellence after the test (Figure 4.8a), as the WCA dropped from 91.1° to 47.3°, which suggests that the silane was not fully grafted on the particles, and was removed by immersion in water. The WCA of the equivalent sample with bigger particles, G3-0-nc, did not change significantly

after the test (Figure 4.8b). This could be explained by the fact that for the condensation reaction to occur between the $-OH$ groups of the particles and the silane, a catalyst is needed. G3-0-nc was produced with a formulation in which more water was present than that of G2-0-nc, and this additional water might have helped to drive the condensation reaction forward, therefore acting as a secondary catalyst.

The remaining samples, G2-x and G3-x with a functionalisation level greater than zero, maintained their repellence to water and diiodomethane after immersion, with a slightly better repellence to the latter for the G2-x samples (Figure 4.8a). This slight increase in contact angle measurements was only monitored for diiodomethane, which seemed to be more sensitive to the presence of $-OH$ groups. One possible explanation for the behaviour observed could be that drying the glass slides after the HRT test, even for as little as 10 min, removed additional hydroxyl groups that were present on the outer surface of the particles. As for G3-x samples, the best formulation seemed to be using a functionalisation level of T0.50 (G3-0.50), as the WCA reached 122.6° (and 120.9° after the hydrolytic resistance test), with a moderate repellence to diiodomethane, equivalent to that of the other samples (Figure 4.8b).

The surface free energies (SFE) of each coating were estimated from the WCA and DCA measurements, and are reported in Table 4.4 as well. Expectedly, the greater values were obtained for G2-0-nc and G3-0-nc, especially following immersion in water. Samples which presented functionalised silica particles demonstrated a SFE smaller than 30 mN/m, characteristic of repellent surfaces, which was maintained after the hydrolytic resistance test. The lowest SFE was measured for the glass slides G3-0.50 before the HRT, at 18.3 mN/m, although it increased after test, due to a decreased DCA value.

The hydrolytic resistance test demonstrated being an important tool to assess whether the coatings would be affected by being immersed in water. Maintaining the WCA and DCA (and thus SFE) at their 'before' value after such test proved that the coatings were not degraded by liquid water and could perform equally before and after immersion in water in terms of repellence.

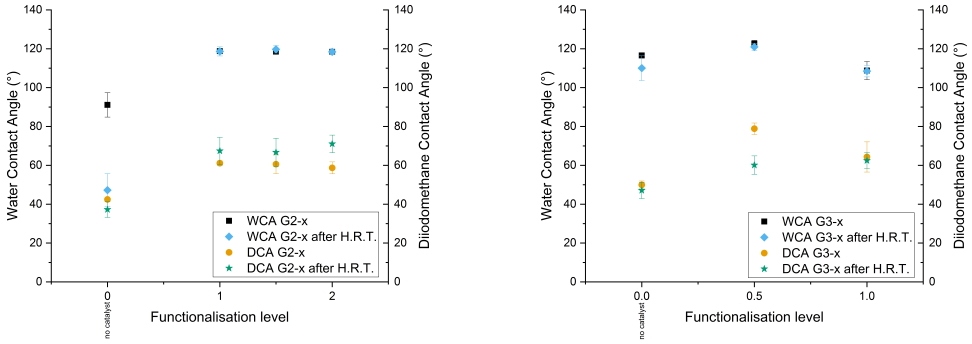

(a) G2-x samples **(b)** G3-x samples

Figure 4.8: Water and diiodomethane contact angle measurements before and after the hydrolytic resistance test. The error bars represent the standard deviation between all measurements done per type of sample.

Table 4.4: Water and diiodomethane contact angle and surface free energy values for each functionalisation level after hydrolytic resistance test (immersion in water bath for 24 h).

Sample	Functionalisation level T	Before hydrolytic resistance test			After hydrolytic resistance test		
		WCA (°)	DCA (°)	SFE (mN/m)	WCA (°)	DCA (°)	SFE (mN/m)
G2-0-nc	0.00	91.1 ± 6.3	42.4 ± 0.3	39.6 ± 1.1	47.3 ± 8.4	37.2 ± 4.0	59.9 ± 5.2
G2-1.00′	1.00	118.8 ± 1.3	61.1 ± 1.2	28.6 ± 0.8	118.7 ± 2.3	67.4 ± 6.9	24.8 ± 2.2
G2-1.50	1.50	118.5 ± 0.6	60.6 ± 4.9	28.9 ± 3.0	119.7 ± 1.9	66.7 ± 7.2	25.2 ± 4.1
G2-2.00	2.00	118.4 ± 0.5	58.7 ± 3.1	28.0 ± 1.1	118.4 ± 1.3	71.0 ± 4.5	22.4 ± 2.0
G3-0-nc	0.00	116.6 ± 1.3	49.9 ± 2.0	35.4 ± 1.4	110.0 ± 6.4	47.1 ± 4.2	36.2 ± 2.9
G3-0.50	0.50	122.6 ± 1.7	78.9 ± 3.0	18.3 ± 1.7	120.9 ± 1.8	60.1 ± 4.7	29.5 ± 2.9
G3-1.00	1.00	108.8 ± 4.6	64.3 ± 7.8	26.1 ± 4.6	108.5 ± 3.0	62.5 ± 4.0	27.2 ± 2.4

4.4 Concluding remarks

This study focussed on two types of particles, synthesised according to Formulations 2 and 3 (their characteristics were shown in Table 3.2), whose mean diameters were measured at 29.7 nm and 122.4 nm respectively. Upon cleaning the dispersions to remove all traces of ammonia, the particles underwent syneresis which was caused by the more elevated temperature they were exposed to. Therefore, the final hydrodynamic diameter of each formulation before being functionalised was measured at 26.0 nm and 108.0 nm respectively. The Z-averages after functionalisation were mea-

sured at 30.6 nm for Formulation 2 and 106.2 nm for Formulation 3. Other physical characteristics which would have been altered by syneresis and functionalisation were not examined in this study.

Functionalising the silica particles with a hydrophobic silane, here with n-propyl trimethoxysilane, was successfully carried out and validated by contact angle measurements. Assessing the repellence properties of different formulations deposited on glass slides gives insights on the performance of each formulation, which can then be applied on other substrates (on hemp shiv in Chapter 5). Here, sample G2-0-unf demonstrated a WCA of 21.2° (unfunctionalised silica particles), and once functionalised (G2-x and G3-x samples), this value increased to 118.2° on average, as long as catalyst was employed (for G2-x samples). After being immersed in water for 24 h, all samples with functionalised silica particles retained their repellence properties to both water and diiodomethane, with low surface free energy values typical of repellent surfaces.

Although not a crucial factor for the rest of the study (Chapter 5), the repellence to diiodomethane, a non-polar aprotic liquid, was still assessed to better understand the wetting behaviour provided by the coated surface. The DCA measurements were used as a tool to assess each level of functionalisation and their resultant repellence to the probe liquid. Indeed, this chemical compound seemed to be more sensitive to slight changes of availability of $-OH$ groups on the surface of the particles, which was exhibited by the linear increase of DCA between the functionalisation levels T0.15 and T0.50.

Other silanes could have been employed to reach greater water and diiodomethane contact angles, thus lower surface free energies, although such silanes are typically halogen-based – for instance presenting fluoroalkyl groups – which were avoided in this study due to their potential toxicity (see Chapter 2). Moreover, when sufficient water was present in the dispersion to act as a secondary catalyst for the condensation reaction between the silane chains and the surface of the silica particles, it seemed that the tin catalyst could be dismissed, thus reducing the toxicity concerns associated with its usage.

Chapter 5

Decay limitation of hemp shiv and derived composites

5.1 Introduction

Bio-materials present interesting properties to be used as insulation materials (Chapter 2). This study analyses hemp shiv, which 75 % of their composition is cellulose and hemi-cellulose, two polymers derived from glucose units. When they are subject to water, liquid or vapour by humidity exposure, these materials experience biodegradation. This phenomenon takes place especially when the environment is warm and humid, and leads to loss of integrity of the materials, as well as microbial growth. In order to prevent decay from occurring, bio-materials are usually protected with varnish, paint, and other coating systems. In this chapter, hemp shiv were coated by immersion, a simple process which does not require significant energy or specific equipment, whilst maintaining the integrity of the material. The protective treatment consisted of silica particles (Formulations 2, 3, and 5 of particles from Chapter 3, which were functionalised with n-propyl trimethoxysilane (nPTMS) as described in Chapter 4). The objectives of this study were:

- To uniformly cover the surface of hemp shiv with functionalised silica particles;

- To demonstrate that a simple silica-based treatment could change the water repellent behaviour of the substrate, from hydrophilic to hydrophobic;
- To estimate with a simple method the biodegradation extent of loose hemp shiv and derived composite structures when coated with the particles.

Such treatment is not used yet in this sector, therefore there are no standardised functional tests. Indicative assessment methods were thus developed in this study to allow a general appreciation of silica as a protective treatment against liquid water leading to biodegradation. The manufacturing and characterisation process followed in this chapter is illustrated in the flow chart in Figure 5.1.

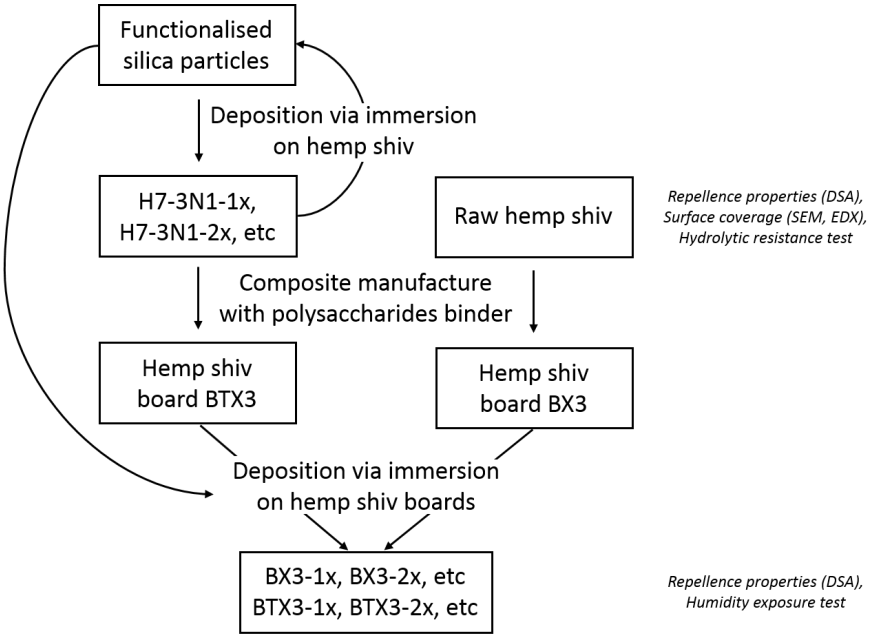

Figure 5.1: Flow chart representing the coating process of hemp shiv and composite manufacturing. The characterisation methods employed are shown in italic.

5.2 Materials and methods

5.2.1 Materials

Hemp shiv of different lengths were kindly provided by Cavac Biomatériaux (Sainte-Gemme-La-Plaine, France). The type Isofin (described here as HI) measured around

2 mm in length, grade 7 (H7) was of 7 mm, grade 8 (H8) of 8 mm, and Biofibat (HB) is the standard commercial product measuring around 10 mm (all types are displayed in Figure 5.2). The names and types of the samples and their characterisation procedures are described in Table 5.1. Three formulations of silica particles were used, Formulations 2 (approximately 30 nm in diameter after functionalisation), 3 (110 nm), and 5 (350 nm) from Chapter 3, which were functionalised with nPTMS at a T1 level (Chapter 4). Although Chapter 3 demonstrated that the hydrolysis-condensation reactions for Formulation 2 particles were not complete, hemp shiv were still coated with these particles in this chapter. The reason for this was to compare and contrast with results obtained in Chapter 4 on glass slides, and see if the chemical structure of these particles could actually affect the water repellence behaviour of hemp shiv when coated.

The hemp shiv were first dried in an oven at 90 °C for one hour, then were immersed in a beaker containing a suspension of functionalised silica particles, where they were vigorously stirred for two minutes to ensure silica particles were deposited on all aggregates. Previous experiments carried out prior to the work of Jiang, Bourebrab, et al. (2018) showed that the immersion time (between one and five minutes) did not modify the repellent behaviour of coated samples. Following immersion, the hemp shiv were strained to remove most of the liquid from the dispersions of silica particles, and placed in the oven to dry at 90 °C for one hour to evaporate the ethanol. This process, shown in Figure 5.3a for hemp shiv HB but valid for all types of hemp shiv, was repeated to coat the hemp shiv several times. For example, H7-3N1-1x samples were dried twice (before and after having been coated), whereas H7-3N1-5x were dried six times (before the first coat, between each coating step, and after the fifth one). The drying temperature of hemp shiv was purposefully chosen lower than that used to dry the glass slides in Chapter 4 in order to reduce their moisture content as much as possible (Hussain, Calabria-Holley, Schorr, et al. 2018) without degrading the shiv (see Section 6.3.1), as well as to remain consistent with the drying method followed by Jiang, Bourebrab, et al. (2018).

Composites of hemp shiv and polysaccharides-based binder were also manufactured. This crosslinker was kindly produced and provided by Cavac Biomatériaux,

Figure 5.2: Photographs of the different grades of hemp shiv

and is a mix of polysaccharides with around 10 % of commercially available oxirane-based glue. Two types of composites were made: with external coating only (BX3), and with coated hemp shiv and external coating (BTX3). Both types used Biofibat hemp shiv (HB); the shiv used for BTX3 samples were coated twice with Formulation 3 of silica particles which had been functionalised with nPTMS at a T1 level (process shown in Figure 5.3a and repeated twice, which corresponds to HB-3N1-2x hemp shiv). To make the composites, 155 g of hemp shiv (coated or not) were thoroughly mixed with 25 g of crosslinker in a food processor for 15 min. This mixture was then placed in a square steel mould of 10 cm x 10 cm, which had been covered with a non-stick film. The mould was placed on a Teflon slab, and a lid of steel was used to press the sample into the mould. This assembly was then placed for 15 min in a laboratory thermal press (Rotherwood Machinery Ltd., St Ives, UK) whose plates were heated at 180 °C, and 27 bar of pressure was applied by the top plate onto the mould (Figure 5.3b). Once cold, the sample was removed from the mould, and the external coating layers were applied by immersing it in a container filled with Formulation 3 - nPTMS T1 silica particles. The coated composites were then dried in the oven at 90 °C for one hour (Figure 5.3c). This last coating process was repeated to build up the external layers on the composites, twice to produce BX3-2x and BTX3-2x, and an additional third time for BX3-3x and BTX3-3x.

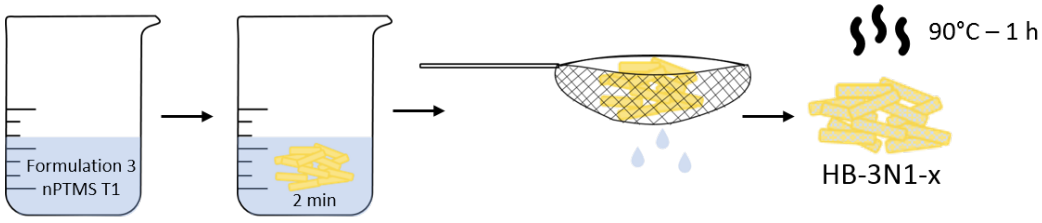

(a) Coating process of hemp shiv (by immersion)

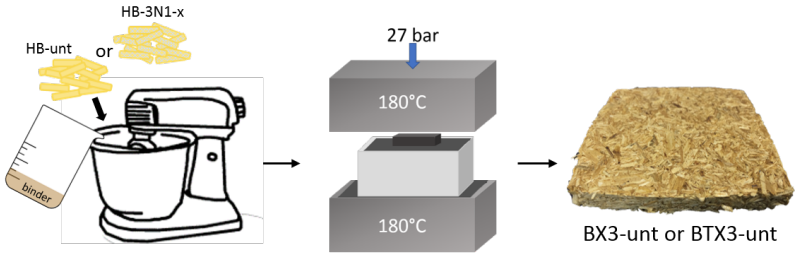

(b) Hemp shiv board manufacturing with thermal press (uncoated hemp shiv for BX3, coated for BTX3)

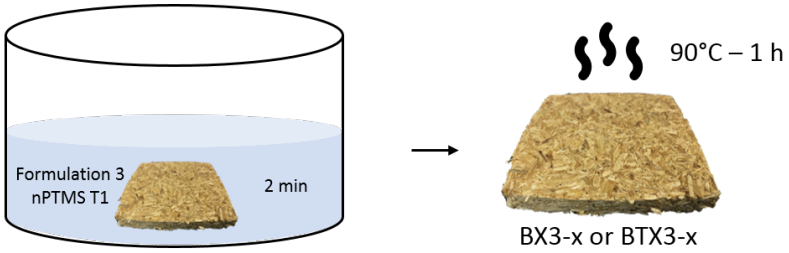

(c) Coating process of hemp shiv boards (by immersion)

Figure 5.3: Manufacturing process of coated hemp shiv boards: steps a, b, and c lead to samples BTX3, whereas BX3 samples are made following steps b and c only.

5.2.2 Test procedures

Imaging via Scanning Electron Microscopy (SEM)

In order to verify how the silica particles cover the surface of hemp shiv, the samples were imaged via SEM techniques, on a Zeiss Σigma FEGSEM (focussed electron gun SEM) (Zeiss, Germany) operating at 5 kV, which uses a secondary electron detector for topography analysis (Figure 5.4). Prior to imaging, the samples were gold coated via sputtering methods to prevent charging due to the accumulation of static electric fields from the instrument.

Figure 5.4: Image of the Zeiss Σigma FEGSEM equipment at TWI Ltd.

Energy-dispersive x-ray (EDX) spectroscopy

Elemental analysis of the surface of the samples was undertaken by obtaining EDX spectra of the selected areas of the samples during the SEM imaging, and by analysing them via the AZtec characterisation system (Oxford Instruments, UK).

Water repellence assessment over time

Similarly to the method described in Section 4.2.3, the hydrophobic properties of the coated hemp shiv were assessed by measuring static sessile drop characteristics of distilled water. Because hemp shiv are a natural material, they present rougher surfaces than glass slides, which means more variation in sessile drop measurements was expected per piece of hemp shiv. More images of different pieces of the bio-material from a same batch were thus taken for water contact angle (WCA) measurements (from 5 to 10 for each sample) to mitigate such fluctuation and obtain better statistical analysis. The consequent standard deviation of WCA values within one formulation of coating is displayed as the error bars on the graphs.

The time for which the hemp shiv presented a hydrophobic behaviour was assessed by measuring the WCA every minute, until this value dropped below 90°. Birdi

et al. (1989) estimated the evaporation of droplets of liquid water at 22 °C at a water/glass interface, for which diffusion in the solid substrate should not occur. They measured an evaporation rate of approximately 2×10^{-6} g/s for a 5 µL droplet. In contrast, Tavisto et al. (2003) measured that a 40 µL droplet of water was absorbed by a piece of untreated hemp shiv in three to five seconds, which would correspond to an absorption rate (or diffusion rate) of approximately 8×10^{-3} g/s. Although the evaporation and diffusion behaviours might not be linear with the volume of the droplet, this simple comparison indicates that the kinetics of water evaporation should not be significant compared to the absorption rate of water by the hemp shiv. Evaporation of water was therefore not taken into account when designing this test method, which was carried out in a non-confined environment.

Hydrolytic resistance test (HRT)

Immersing hemp shiv in a water bath for 24 h can affect their water repellent characteristics, especially if a thin water film forms on the surface of the shiv. This was estimated by a hydrolytic resistance test, similar to that described in Section 4.2.3.

Humidity exposure test (HET)

Loose hemp shiv, untreated and treated with different formulations of functionalised silica particles (as described in Table 5.1), and the composites were placed in a humid environment to determine its effect on the repellent properties of the bio-materials. The parameters of the humidity chamber (Vötsch VC 0020, Weiss Technik, Germany) were set at 35 °C and 90 % of relative humidity (RH). There are currently no benchmark test to measure the effect of humidity exposure on the coating of bio-materials different from wood, which is why the set-up was chosen to follow recommendations from the ISOBIO project. The WCA was measured on each sample every 24 h without any drying step. The test was terminated when traces of mould were visible on at least one piece in a sample of loose hemp shiv. Thereupon the undamaged samples were dried at room temperature for five days, and a final WCA measurement was taken. As regards the composite samples (BX3 and BTX3), they remained in the humidity

chamber until more than 5 % of the surface of each sample was covered by mould (assessed by a semi-quantitative study, see Section 5.5.3), after which the samples were discarded.

Summary

All the samples of loose hemp shiv analysed in this chapter are collated in Table 5.1, along with the characterisation procedures they underwent. The name of each sample corresponds to the grade of hemp shiv, the formulation of particles and functionalisation level with nPTMS, and the number of times it has been coated with said treatment. For example, sample H7-3N1-2x represents a hemp shiv of grade 7, coated with Formulation 3 particles (110 nm), which were functionalised with nPTMS at a T1 level. The sample was coated twice with this formulation.

Table 5.1: Testing procedures on loose hemp shiv.

Sample			Characterisation methods					
Hemp shiv	Treatment	Coated x times	SEM	EDX	WCA	HRT	time when WCA>90°	HET
H7	untreated		✓	✓	✓	✓	✓	✓
H7	2N1	1x	✓	✓	✓	✓	✓	
H7	2N1	2x	✓	✓	✓		✓	
H7	2N1	3x	✓∗	✓	✓		✓	
H7	2N1	5x	✓∗	✓	✓		✓	
H7	2N1.5	1x			✓	✓		
H7	2N2	1x			✓	✓		
H7	3N1	1x	✓	✓	✓	✓	✓	
H7	3N1	2x	✓	✓	✓		✓	
H7	3N1	3x	✓	✓	✓		✓	
H7	3N1	5x	✓∗	✓	✓		✓	
H7	5N1	1x			✓	✓	✓	
H7	5N1	2x			✓		✓	
H7	5N1	3x			✓		✓	
H7	5N1	5x			✓		✓	
H8	3N1	2x			✓			✓
HB	3N1	2x			✓			✓
HI	3N1	2x			✓			✓

∗ SEM imaging was carried out, but the samples were damaged by the vacuum they were exposed to, therefore no images were exploitable.

5.3 Surface coverage

Verifying that silica particles were indeed deposited onto the hemp shiv is essential to understand how silica can protect the aggregates beneath from the external environment. For this reason, nine samples of hemp shiv were examined by SEM (Figure 5.5). Two formulations of silica particles were used, which meant two types of samples were analysed: series H7-2N1 and series H7-3N1, coated once to five times with the same formulation, as well as one untreated hemp shiv to compare (H7-unt).

Generally, the difference between the untreated sample (Figure 5.5a) and the treated ones was evident, which showed that silica was successfully deposited. When the samples were coated only once or twice, which corresponds to H7-2N1-1x, H7-2N1-2x, H7-3N1-1x, and H7-3N1-2x (Figures 5.5b, 5.5c, 5.5d, and 5.5e respectively), partial coverage was already attained. It also seemed that the smaller particles provided a slightly better coverage when comparing H7-2N1-1x and H7-3N1-1x. Increasing the times the samples were coated also led to a more complete and uniform coverage of the surface, as demonstrated for sample H7-3N1-3x in Figure 5.5f (the cracks seen in this figure are due to the vacuum which the hemp shiv were exposed to). It was also possible to confirm the size of the particles deposited on sample H7-3N1-2x by using a greater magnification (Figure 5.5e). The image analysis indicated a size distribution of particles measured at 107.9 ± 18.1 nm (mean and standard deviation values), which fits well with the result of the DLS analysis for this formulation of functionalised particles (106.2 nm, as shown in Table 4.2).

Characterisation of the samples by EDX is a semi-quantitative method, which allows the identification of which chemical elements are present on the surface under examination (i.e. hemp shiv). The analysis was carried out on all the samples analysed by SEM (from the magnified micrographs of Figure 5.5), of which the spectra of the untreated sample, H7-2N1-1x, H7-2N1-5x, H7-3N1-1x, and H7-3N1-5x are shown in Figure 5.6.

Similarly to the SEM images, there was a clear difference between all treated samples and H7-unt, for which no peak for silicon was displayed (Figure 5.6a). Carbon and oxygen were however the most abundant species, originating from the cellulose

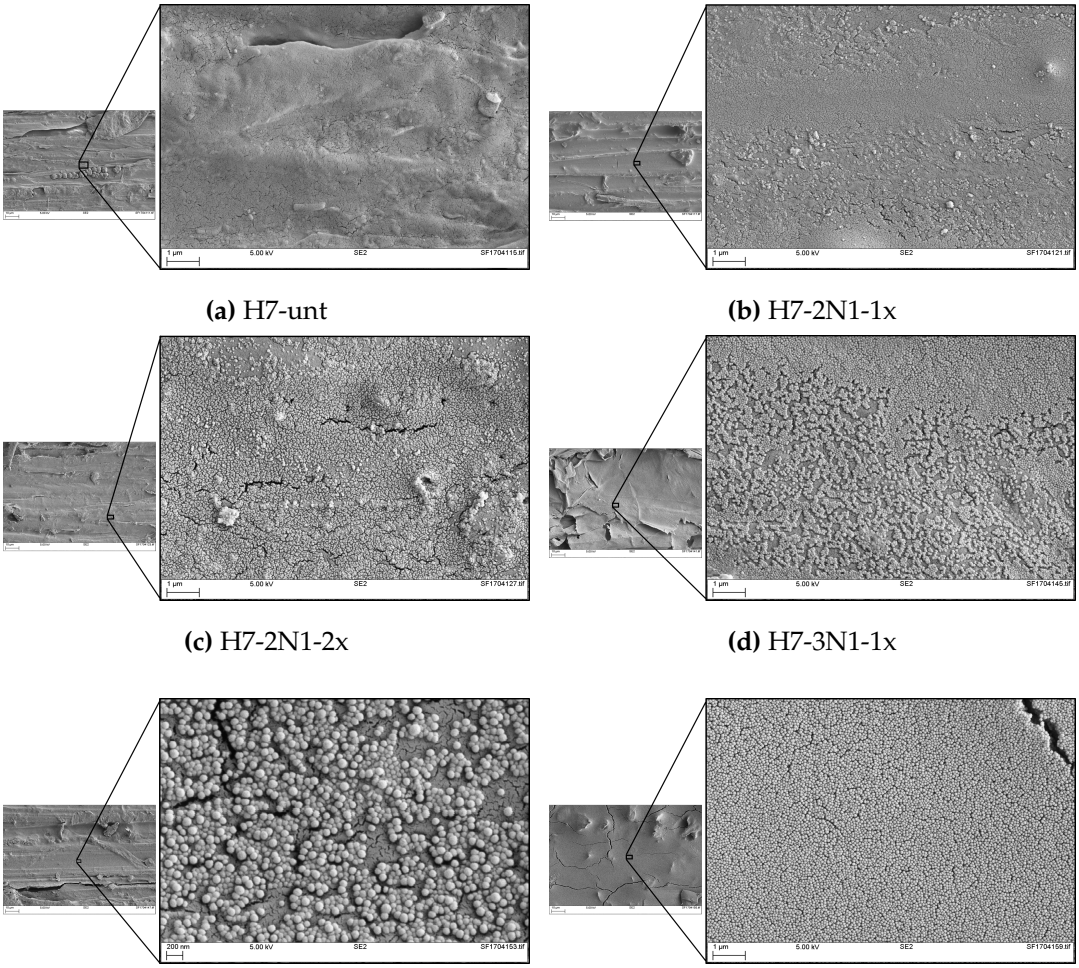

(a) H7-unt

(b) H7-2N1-1x

(c) H7-2N1-2x

(d) H7-3N1-1x

(e) H7-3N1-2x

(f) H7-3N1-3x

Figure 5.5: SEM images of different hemp shiv samples. The visible cracks are due to the vacuum the shiv were exposed to.

and its derived units which make up the shiv. Those elements were also present on the treated samples, but not as much as silicon which produced the highest peak for all of them (Figures 5.6b, 5.6c, 5.6d, and 5.6e). Samples coated only once with silica particles demonstrated peaks of carbon and oxygen of fairly the same height (Figures 5.6b and 5.6d). When more silica was present on the surface of the samples (H7-2N1-5x and H7-3N1-5x, Figures 5.6c and 5.6e), the peak for carbon was reduced. Indeed, less carbon was directly present on the exposed surface as it was covered by the particles, which is in accordance with the SEM images demonstrating a more complete coverage by silica for samples coated multiple times (Figure 5.5). The peak for oxygen remained fairly equivalent for all samples, and is likely to be explained by the presence of oxygen forming the silica particles and originating from the silane. Finally, all spectra showed the presence of the gold element, which was used during the sample preparation for SEM analysis.

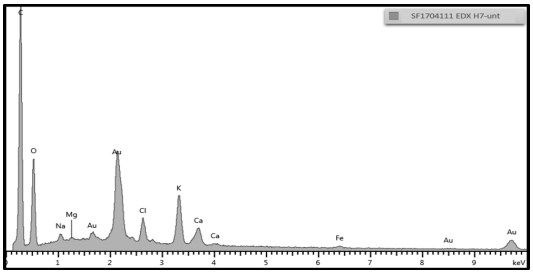

(a) H7-unt

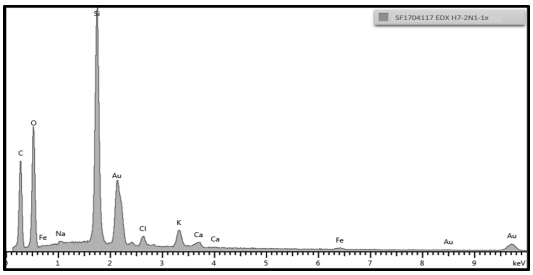

(b) H7-2N1-1x

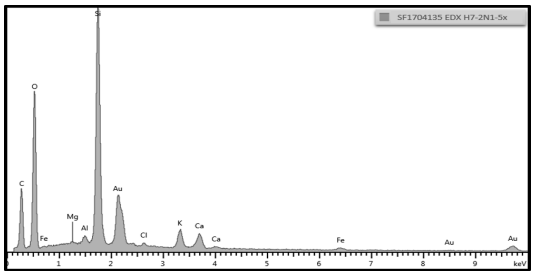

(c) H7-2N1-5x

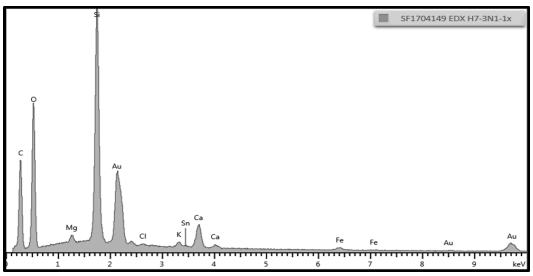

(d) H7-3N1-1x

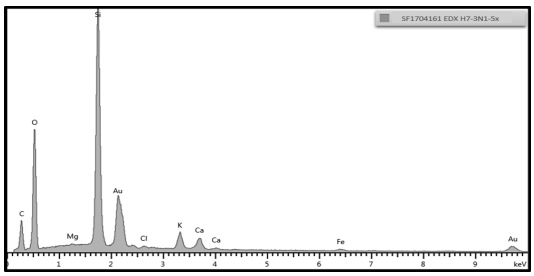

(e) H7-3N1-5x

Figure 5.6: EDX analysis of different hemp shiv samples

5.4 Hydrophobic treatment on loose hemp shiv

5.4.1 Initial assessment and hydrolytic resistance test

The effect of the hydrophobic coating was demonstrated by comparing H7-unt with different treated hemp shiv, by measuring the sessile drop behaviour of 2 μL of distilled water deposited on each sample. The hydrophobic properties of H7-2N1-1x, H7-2N1.5-1x, H7-2N2-1x, H7-3N1-1x, and H7-5N1-1x were determined by measuring the static water contact angle (WCA) of the sessile drop. Some of those samples were chosen to be made from similar formulations to those tested on glass slides (whose sessile drop response after hydrolytic resistance test were shown in Figure 4.8) to indicate how the surface roughness and nature might affect the water repellence.

The values of WCA can be found in Table 5.2 and these are plotted in Figure 5.7. Firstly, the hydrophobic character provided by the silane grafted on the particles was clearly demonstrated since the WCA was greater than 90° for all samples, whereas it was only of 56.0° for the untreated sample. This value is close to the findings of Mantanis and Young (1997) who measured a WCA of distilled water of 60° on wood, which indicates that the chemical nature of the substrate can influence its repellent properties to distilled water, as a non-coated glass slide present a WCA of around 20°. Similarly to the results on glass slides, increasing the quantity of silane did not induce a significant change in WCA for the hemp shiv H7-2N1-1x, H7-2N1.5-1x, and H7-2N2-1x, averaging 113.4° for these three samples. This behaviour was also observed for silica particles functionalised at different T levels and deposited on glass slides (with a WCA averaging 118.2°, as described in Table 4.3). Whilst H7-3N1-1x also demonstrated a WCA of a close value (116.4°), the WCA of H7-5N1-1x was considerably lower, at 93.1°. Because the particles from Formulation 5 were bigger, and the hemp shiv were coated only once, it is likely that the coverage was not complete, in the same way that the smaller particles on H7-2N1-1x provided a better coverage to the shiv than on H7-3N1-1x (Figures 5.5b and 5.5d).

The data presented here then suggests that the level of functionalisation does not matter as much as the size of the particles for equivalent water repellence, as WCA

greater than 110° were achieved for all functionalisation levels of particles of 31 nm and 108 nm, even for hemp shiv coated only once.

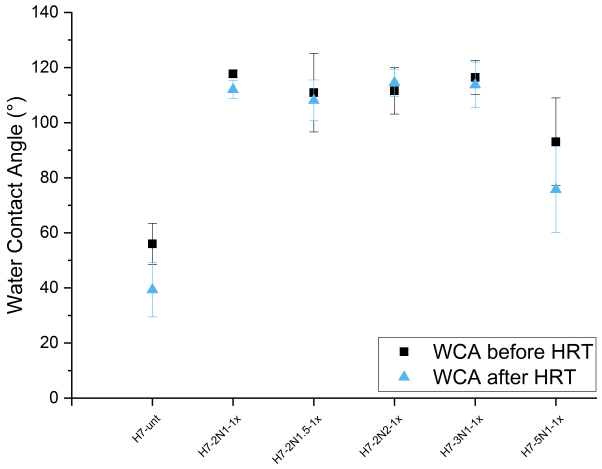

Figure 5.7: Water contact angle measurements of coated hemp shiv before and after immersion in water for 24 h to assess the durability of the coatings. The standard deviation was calculated from the variation of WCA within one type of sample and is shown as the error bars.

The hydrolytic resistance test was then carried out on these samples by immersing them in a water bath for a period of 24 h, and drying any water remaining on their surface by placing the samples in the oven at 65 °C for 10 min. The WCA was measured at this point, in order to verify whether the functionalised particles remained on the hemp shiv, and that they retained their repellent properties. The values obtained are also displayed in Table 5.2 and can be seen as the blue triangle symbols in Figure 5.7. In line with expectation, the WCA for H7-unt dropped to 39.3°, which suggests that some the affinity of the shiv with water has increased, whether water was still entrapped inside the pores of hemp shiv, or a thin water film was still present on the surface despite the quick drying. Sample H7-5N1-1x also demonstrated a decrease of its WCA value after the test, which confirms the aforementioned supposition that its coverage by silica particles was only partial. The remaining of the samples maintained equivalent WCA values after immersion in water, which were similar to those obtained for the same treatment on glass slides. This suggests that the water repel-

lence provided by the functionalised silica particles was not adversely affected by this water immersion test. Having obtained similar values of WCA before and after the hydrolytic resistance test also proves the effectiveness of the hydrophobic treatment as a protection of hemp shiv against liquid water.

Table 5.2: Water contact angle values for each sample of loose hemp shiv before and after hydrolytic resistance test (immersion in water bath for 24 h).

Sample	WCA±stdev (°) before HRT	WCA±stdev (°) after HRT
H7-unt	56.0 ± 7.5	39.3 ± 9.8
H7-2N1-1x	117.7 ± 1.3	112.0 ± 3.3
H7-2N1.5-1x	110.9 ± 14.3	108.1 ± 7.4
H7-2N2-1x	111.6 ± 8.4	114.5 ± 4.9
H7-3N1-1x	116.4 ± 6.2	113.7 ± 8.3
H7-5N1-1x	93.1 ± 15.9	75.7 ± 15.5

5.4.2 Loose hemp shiv coated several times

The SEM imaging (Figure 5.5) demonstrated that in order to completely cover the surface of the hemp shiv with silica, the aggregates should be coated more than once. The WCA was measured for the series of samples H7-2N1, H7-3N1, H7-5N1, and H7-unt, with several layers of coating applied on the shiv. The results are displayed in the bar graph in Figure 5.8 and in Table 5.3.

Increasing the quantity of functionalised silica particles deposited on hemp shiv led to an increment of 10° in WCA value, for the series H7-2N1 and H7-3N1, from when the shiv were coated once (114.4° and 115.5° respectively) to five times (124.2° and 125.9° respectively). H7-5N1-1x presented a lower WCA than H7-2N1-1x and H7-3N1-1x (as it was hypothesised for the hydrolytic resistance test that bigger particles might not cover as well the surface of the shiv), however once the aggregates were coated twice or more, their water repellence improved as measured by the WCA increasing significantly from 93.1° to 128.0°.

As a result of their composition, hemp shiv are naturally hydrophilic, and a droplet

of liquid water can penetrate its structure in three to five seconds, as it was demonstrated by Tavisto et al. (2003). This feature was indeed verified, with the measurement of WCA possible only for no more than 10 s after the droplet was deposited, at which point it was absorbed entirely. By coating the hemp shiv and thus delaying water absorption in their structure, the time it took for the WCA to drop below 90° (threshold of hydrophobicity) increased with the number of times the shiv were coated. These results are also represented in Figure 5.8 with the black symbols for each sample. Expectedly, the more silica present on the surface of the aggregates, the longer the WCA was maintained at a greater angle than 90°, which was more than 20 min for all three samples coated five times (H7-2N1-5x, H7-3N1-5x, and H7-5N1-5x). Said values of maintained hydrophobicity are detailed in Table 5.3 as well.

These results relating to delayed absorption of water support the conjecture that in order to limit liquid water from penetrating within the hemp shiv, they require being coated twice or more to ensure complete surface coverage. The possibility of having coated parts of the pores of hemp shiv, as can be seen in Figure 2.2 with another coating formulation, might have played a part in delaying the absorption of water in the structure of the shiv.

Although the measurements of water contact angles gave indication on the hydrophobic behaviour of coated hemp shiv, they were not significantly different from one treatment to another, considering the measure incertitudes. The time for maintained hydrophobicity really provided more understanding in how the functionalised silica particles limited the ingress of liquid water, as it drastically increased from untreated hemp shiv (10 s), to one layer of coating (just below 10 min), and to five (over 23 min).

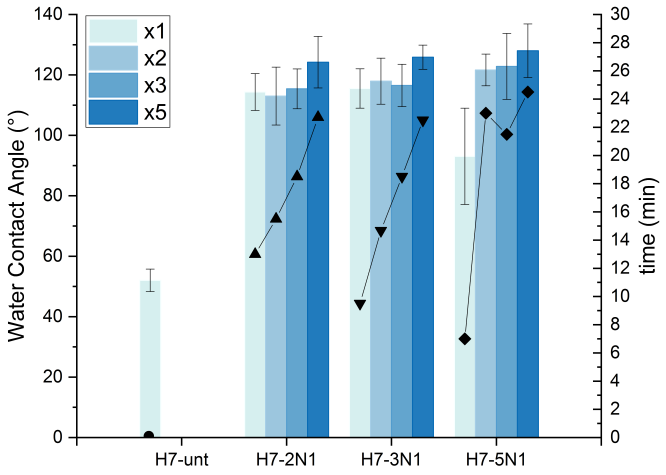

Figure 5.8: Increasing the layers of silica particles coated on hemp shiv substrates allowed to maintain hydrophobic behaviour (measured by the WCA, left hand y-axis) for longer periods of time (right hand y-axis).

Table 5.3: Water contact angle and standard deviation values for each type of loose hemp shiv coated several times, as well as the time for which the water contact angle was greater than 90°.

Sample	H7-unt		H7-2N1		H7-3N1		H7-5N1	
	WCA± stdev(°)	time (min)	WCA± stdev(°)	time (min)	WCA± stdev(°)	time (min)	WCA± stdev(°)	time (min)
unt	52.0 ± 3.7	0.1	–	–	–	–	–	–
1x	–	–	114.4 ± 6.1	13.0	115.5 ± 6.5	9.5	93.1 ± 15.9	7.0
2x	–	–	113.0 ± 9.6	15.5	117.9 ± 7.6	14.7	121.6 ± 5.2	23.0
3x	–	–	115.4 ± 6.6	18.5	116.5 ± 7.0	18.5	122.8 ± 10.9	21.5
5x	–	–	124.2 ± 8.5	22.7	125.9 ± 4.0	22.5	128.0 ± 8.9	24.5

5.5 Effect of humidity: maintained hydrophobicity and mould growth delay

5.5.1 Water repellence and moisture buffering

The importance of coating hemp shiv several times to ensure complete coverage of their surface and hydrophobicity was demonstrated in Sections 5.3 and 5.4. It was deduced that the bio-aggregates should be coated at least twice to ensure extensive repellence to liquid water owing to the barrier effect provided by functionalised silica. This study focussed on exposing hemp shiv to humid conditions, and measuring how it could affect the repellence to liquid water. Because the three formulations examined previously proved fairly similar results in terms of WCA as long as two or more coats were applied, it was decided to keep this parameter constant, but to change the substrate type. Therefore, different grades of hemp shiv were coated twice with Formulation 3 of silica particles, which had been functionalised with nPTMS at a T1 level: H8-3N1-2x, HB-3N1-2x, and HI-3N1-2x. They were compared with a sample of H8-unt, knowing that the two types H7 (studied extensively in this Chapter) and H8 were very similar and could be substituted.

The test can generally be appreciated by the fairly steady WCA values obtained throughout, which is shown in Figure 5.9. All coated samples demonstrated hydrophobic properties even after three days of exposure to 35 °C and 90 % RH. The lack of data at this point for the untreated sample is due to mould growth, at which point the sample was discarded. In fact, humidity clearly affected the untreated hemp shiv, which was likely to have absorbed water from its environment (due to its moisture buffering properties), as the WCA dropped from 68.4° before the test to 39.3° after two days. In addition, water vapour would have condensed within its pores, which led to microbial development.

Another study carried out within the ISOBIO project on hemp shiv coated with functionalised silica particles (but a different silane as functionalising agent) exhibited excellent moisture buffering properties (reported by Jiang, Bourebrab, et al. (2018)). This study proved that silica could not only provide an effective barrier to liquid wa-

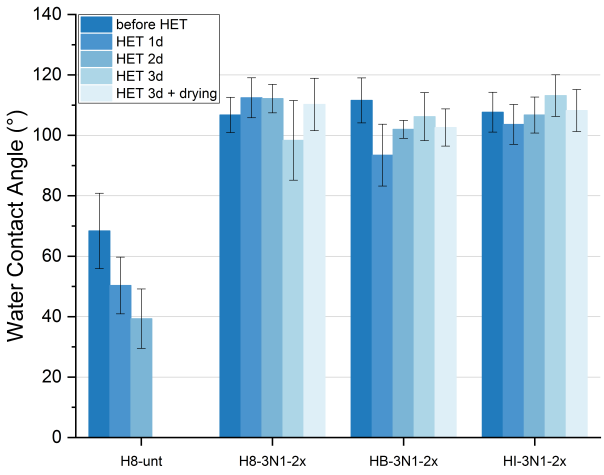

Figure 5.9: The treated hemp shiv being placed in humidity chamber still demonstrated hydrophobic properties after three days, and no sign of mould growth.

ter, but also did not block the pores of hemp shiv, therefore still allowed water vapour to permeate through its micropores. Moreover, Table 5.4 gathers the averaged WCA values measured during the humidity exposure test (HET), which were all above the hydrophobicity threshold, whether the treated hemp shiv were humid (during the test) or dried (following HET). Such results mean that irrespective of the grade of hemp shiv, the silica treatment could still repel liquid water from their pores and surface; even though water vapour was absorbed in the micropores of the shiv, which therefore would lead to mould growth prevention.

Table 5.4: Water contact angle and standard deviation values (°) for loose hemp shiv during the humidity exposure test (35 °C and 90% RH).

Sample	before HET	after 24 h	after 48 h	after 72 h	after 72 h + drying
H8-unt	68.4 ± 12.5	50.3 ± 9.4	39.3 ± 9.8	sample discarded	
H8-3N1-2x	106.8 ± 5.8	112.4 ± 6.6	112.2 ± 4.7	98.3 ± 13.2	110.2 ± 8.7
HB-3N1-2x	111.6 ± 7.5	93.4 ± 10.2	102.0 ± 3.0	106.2 ± 8.0	102.6 ± 6.2
HI-3N1-2x	107.7 ± 6.6	103.6 ± 6.6	106.7 ± 6.0	113.2 ± 6.9	108.2 ± 7.0

5.5.2 Hydrophobic bio-composite structures

A similar experiment was carried out, this time with the composite structures made from hemp shiv and polysaccharides-based binder (BX3 and BTX3 series). The test was terminated and the samples were removed from the humidity chamber when more than 5 % of the surface of the sample was covered by mould (this analysis is described in Section 5.5.3).

In general, the samples treated externally demonstrated a greater WCA value than BX3-unt and BTX3-unt (Figure 5.10). The WCA was more influenced by the number of times the composites were coated (i.e. from none to three), than by the coating applied on the hemp shiv in the first place (difference between BX3 and BTX3). Before the experiment, both BX3-unt and BTX3-unt displayed a WCA at the limit of hydrophobicity, at 89.7° and 91.4° respectively. The WCA of the BX3 series are shown in Table 5.5a, which increased to 112.2°, then 114.4°, and 122.7° when the samples were externally coated once, twice, and three times respectively. The WCA of the equivalent samples of the BTX3 series increased to 112.6°, 114.4°, and 124.7° (Table 5.5b). Such change proved greater hydrophobicity the more silica was present on the external surface of each sample.

The breakdown of most WCA measurements per series of samples throughout the humidity exposure test is shown in Table 5.5 and all are plotted in Figure 5.10. The WCA remained very consistent with its initial value for each sample, despite the fact that it was measured whilst the composites were still humid. Such results emphasised the resistance to liquid water provided by the silica particle coating. Finally, the main difference between the two series of samples was the mould growth: whilst both BX3-unt and BTX3-unt presented enough mould to be discarded after seven days, the coated BX3 samples were in the humidity chamber for eight days and were discarded on the ninth, whereas the coated BTX3 remained for 15 days.

5.5.3 Mould coverage of bio-composites

The series BX3 and BTX3 were photographed throughout the humidity exposure test. This visual assessment allowed to carry out a semi-quantitative study of mould cov-

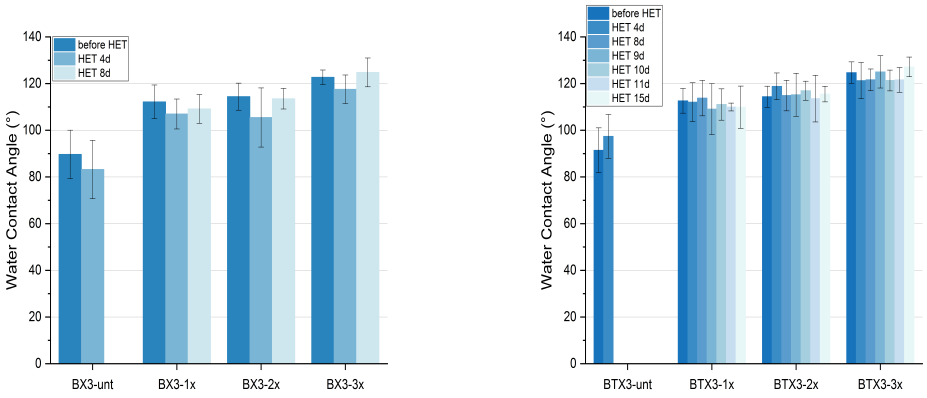

(a) BX3 samples **(b)** BTX3 samples

Figure 5.10: Water repellence assessment of BX3 and BTX3 series in humidity chamber.

erage of the surface of each sample. A quadrat was applied on each photograph to estimate the total surface of the sample, as is illustrated in Figure 5.12, similarly to a method used in ecology studies (Weaver 1918). Each entity or part of square where mould developed was measured. The ratio of the two thus gave an approximation of the surface area covered by mould. It was arbitrarily decided to put a threshold at 5 % of the upper surface of a sample to be covered by mould to terminate the test for this sample.

The estimated values of mould coverage for the series of samples BX3 and BTX3 are shown in Table 5.6. Both untreated samples, BX3-unt and BTX3-unt, displayed larger traces of mould than any other after only seven days (Figure 5.12a). It is interesting to mention that the mould had a white-foamy appearance (see close-up photograph in Figure 5.11). Because the estimation was greater than 5 %, the samples were discarded, whilst all other samples remained in the humid environment. After nine days, all BX3 samples showed more mould growth, and reached the 5 % threshold (Figure 5.12b). As for the BTX3 samples, the mould appeared to cover only around 1.5 % of the surface after the same time, which is why the experiment was carried on for these (Figure 5.12c). Both series however demonstrated a black kind of mould, which was much different that for the untreated sample. This suggests that the treat-

Table 5.5: Averages of water contact angle measurements on BX3 and BTX3 series throughout the humidity exposure test. The standard deviations were calculated based on the average value of WCA for each type of sample at each time of measurement.

(a) WCA (°) of BX3 samples

Sample	Days in humidity chamber		
	0	4	8
BX3-unt	89.7 ± 10.4	83.2 ± 12.5	–
BX3-1x	112.2 ± 7.2	107.0 ± 6.4	109.1 ± 6.2
BX3-2x	114.4 ± 5.8	105.5 ± 12.7	113.5 ± 4.4
BX3-3x	122.7 ± 3.1	117.6 ± 6.1	124.8 ± 6.2

(b) WCA (°) of BTX3 samples.

Sample	Days in humidity chamber				
	0	4	8	11	15
BTX3-unt	91.4 ± 9.6	97.4 ± 9.4	–	–	–
BTX3-1x	112.6 ± 5.3	112.1 ± 8.3	113.8 ± 7.6	110.0 ± 1.7	109.9 ± 9.1
BTX3-2x	114.4 ± 4.5	118.8 ± 5.7	114.9 ± 6.5	113.6 ± 10.0	115.5 ± 3.3
BTX3-3x	124.7 ± 4.6	121.3 ± 7.8	121.6 ± 4.7	121.6 ± 5.3	127.1 ± 4.2

ment also affected the type of fungi which could develop on the hemp substrates. Eventually, the BTX3 samples demonstrated enough mould on their upper surface (results shown in Table 5.6) to terminate the experiment after 15 days of exposure to humidity (Figure 5.12d).

Generally, the more external layers of coating the samples presented, the less degradation occurred, for a similar time of exposure. Between being non-coated, just externally coated (BX3 series), and both internally and externally coated (BTX3), the factor which appeared to influence the most the biodegradation prevention was the internal coating, i.e. when silica particles were deposited on the hemp shiv before the composite manufacture, and after as an external layer. The external coating prevented water which condensed from the humid environment to remain on the sample which would induce mould growth, whilst the internal coating (directly on the hemp shiv) provided protection against the spread of fungal growth within the composites.

Table 5.6: Estimation of mould coverage on the series of samples BX3 and BTX3 placed in humidity chamber.

Sample	Days in HC	BX3	BTX3
untreated	7	30.06 %	6.58 %
1x	9	19.37 %	1.48 %
2x	9	6.54 %	1.64 %
3x	9	5.93 %	1.23 %
1x	15	-	18.57 %
2x	15	-	10.93 %
3x	15	-	7.52 %

Figure 5.11: Appearance of mould on samples BX3-unt after seven days in humidity chamber

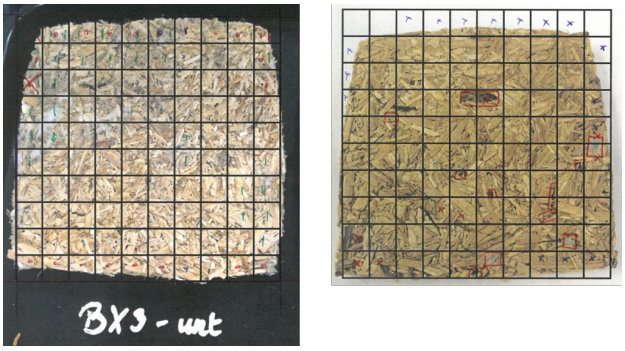

(a) BX3-unt (left) and BTX3-unt (right) after 7 days

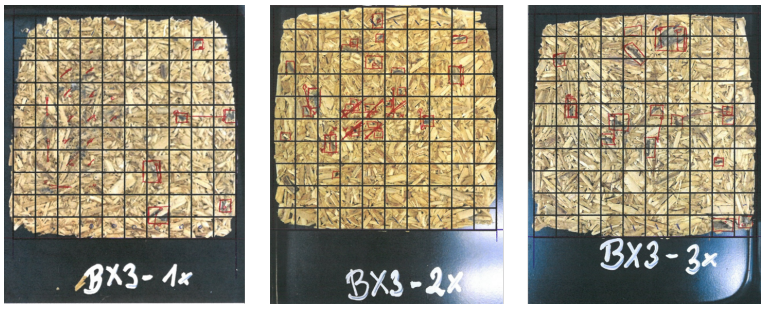

(b) BX3-1x,-2x, -3x after 9 days

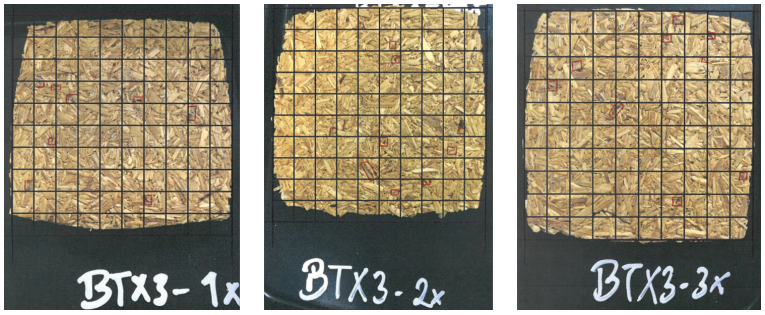

(c) BTX3-1x,-2x, -3x after 9 days

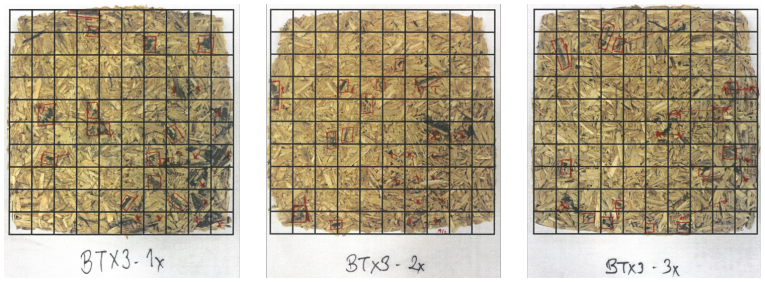

(d) BTX3-1x,-2x, -3x after 15 days

Figure 5.12: Semi-quantitative analysis of mould coverage on hemp shiv boards BX3 and BTX3 after several days in humidity chamber. The red areas represent parts of squares where mould was visible, and a full square was counted where a cross was marked.

5.6 Validation of experiments and recommendations

Measuring the water contact angle for various samples of hemp shiv, and then monitoring this measure over time allowed to demonstrate the extensive hydrophobic property of the treatments used. It was clear that depositing functionalised silica particles on the surface of the hemp shiv benefited in several ways:

- better surface coverage the more silica was coated, which was verified by the SEM images, as was displayed in Figure 5.5;
- resistance of the coatings to liquid water, on the surface of the samples and when they were immersed in water (Figure 5.7);
- prolonged hydrophobic behaviour (over 20 min when the loose samples were coated five times, which was shown in Figure 5.8);
- delayed biodegradation of the samples when exposed to a humid environment, especially as the hydrophobicity was maintained, as seen in Figures 5.9 and 5.10.

Although this study successfully presented how silica could be used as a protective layer on bio-materials, the assessment methods only proved the concept and feasibility. More thorough analyses could be undertaken to represent in-service conditions: testing both loose hemp shiv and derived composites in an environmental chamber with climatic simulations, such as rain and drying times associated with temperature changes, which could be representative of the conditions the materials would be exposed if used in a typical bathroom or other living environment. In addition, the estimation of mould coverage was only a subjective, semi-quantitative method, based on visual assessment and appreciation. A more accurate software-based image analysis could have been performed, but some issues arose due to the nature of the material: the aspect and characteristics of each piece of hemp shiv is different from one another (length, thickness, roughness, colour, etc), and some shiv can present a similar colour to mould which only a human eye could determine the difference. Finally, the testing procedures were not based on standard tests, as those are mainly developed for wood-based materials. An actualisation of building codes should take

into account hemp shiv and other bio-materials, so that their utilisation could be implemented more widely as an insulation material for building envelopes.

Chapter 6

Thermal degradation of hemp shiv and effect of silica

6.1 Introduction

This chapter presents an analysis of the thermal degradation of loose hemp shiv, which characterisation process is summarised in the flow chart in Figure 6.1. Thermogravimetric analysis (TGA) and differential scanning calorimetry (DSC) are used to understand the pyrolysis phenomenon of each main polymeric compound (cellulose, hemicellulose, and lignin), and how the silica particle treatment could reduce the final mass loss and the mass loss rate, and the mechanism of this operation. The combined TGA-DSC methods are commonly used to determine the temperatures, mass losses, and heat released associated with the pyrolysis process of small samples. Operating under inert atmosphere such as N_2 corresponds to ideal conditions to observe pyrolysis only, as this phenomenon is characteristic of thermal degradation under very limited (or no) oxygen supply. As the hemp shiv studied in this chapter are intended to be used in building, understanding their thermal degradation in air is also important, to visualise both pyrolysis and the oxidation reactions during combustion.

To identify the flammability of samples, the cone calorimeter was used, which monitors both the mass loss under exposure to radiant heat and the gases released during combustion (Babrauskas 1984). The flammability of polymers is typically evalu-

ated by exposing to a radiant heat flux between 10 kW/m^2 and 100 kW/m^2 (Witkowski et al. 2016). However, in this study both the flaming and smouldering phenomena of hemp shiv were analysed, the latter being especially visible at lower heat fluxes (below 20 kW/m^2) (McLaggan 2016). The flammability experiments were therefore carried out at a 11.5 kW/m^2 exposure. This heat flux is sufficient for with piloted ignition, which is the case here, but still low not to have a thermally driven process. Mass loss, ignition, the different modes of combustion, and the heat released upon burning were evaluated. The aim of this study was to build an understanding of the behaviour of hemp shiv under elevated temperature conditions. Specifically, an understanding of how the silica particle treatments developed (Chapter 4) can affect the thermal degradation of hemp shiv (Chapter 6), as it had also proven previously to limit the effects of moisture (Chapter 5), before using these bio-materials in composite structures (Chapter 7).

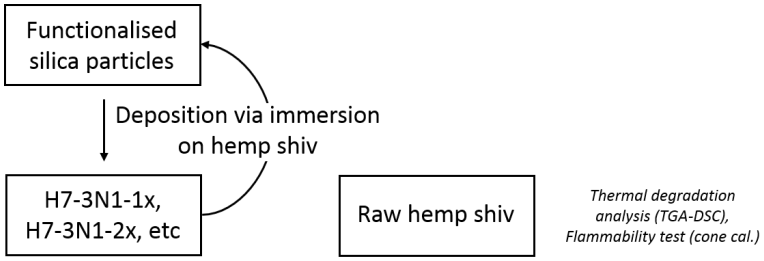

Figure 6.1: Flow chart representing the characterisation of the pyrolysis phenomenon of loose hemp shiv. The methods employed are shown in italic.

6.2 Materials and testing overview

6.2.1 Materials

The hemp shiv used in this study were the same as presented in Chapter 5, especially hemp shiv of grade 7 (H7). Three formulations of silica particles (2,3, and 5), described in Chapter 3, were deposited once having been functionalised with the hydrophobic silane nPTMS at a T1 functionalisation level according to the processes (and nomenclature) described in Chapter 4. The samples are reported in Table 6.1, along with the

characterisation methods they underwent.

Table 6.1: Description of the loose hemp shiv samples characterised by TGA and cone calorimetry.

Sample			Characterisation methods	
Hemp shiv	Treatment	Coated x times	TGA-DSC	Cone calorimetry
H7	untreated		✓	✓
H7	2N1	1x	✓	✓
H7	2N1	3x	✓	
H7	2N1	5x	✓	
H7	3N1	1x	✓∗	✓
H7	3N1	3x	✓∗	✓
H7	3N1	5x	✓∗	
H7	5N1	1x	✓∗	✓
H7	5N1	3x	✓∗	
H7	5N1	5x	✓∗	

∗ The DSC analysis was carried out for all samples at the same time as the TGA, however only the curves for H7-unt and the H7-2N1 series are displayed in this chapter to limit redundancy.

6.2.2 Thermogravimetric analysis and differential scanning calorimetry

Several samples of hemp shiv, with silica particle treatments and without, were analysed by thermogravimetric analysis (TGA) and differential scanning calorimetry (DSC) (Netzsch STA 449 F3 Jupiter equipped with silicon carbide furnace, Netzsch, Germany, shown in Figure 3.6). Approximately 6.5 mg of hemp shiv were cut to fit in the Pt-Rh crucible, as is shown in Figure 6.2a. In the same way that the silica particles were analysed previously by TGA (Section 3.3.5), all the tests of this section were also carried out from room temperature to 1000 °C at a rate of 10 °C/min, in air, unless stated otherwise. A high heating rate (around 80 °C/min) tends to be more representative of a real fire, however for small samples (less than 10 mg), the selected heating rate is sufficient to assume that the sample and the apparatus are in thermal equilibrium (Witkowski et al. 2016). The results show the thermogravimetric (TG) curves and their derivatives (DTG), and the DSC curves for selected samples (all samples were analysed but only the curves of the H7-2N1 series are displayed to limit redundancy).

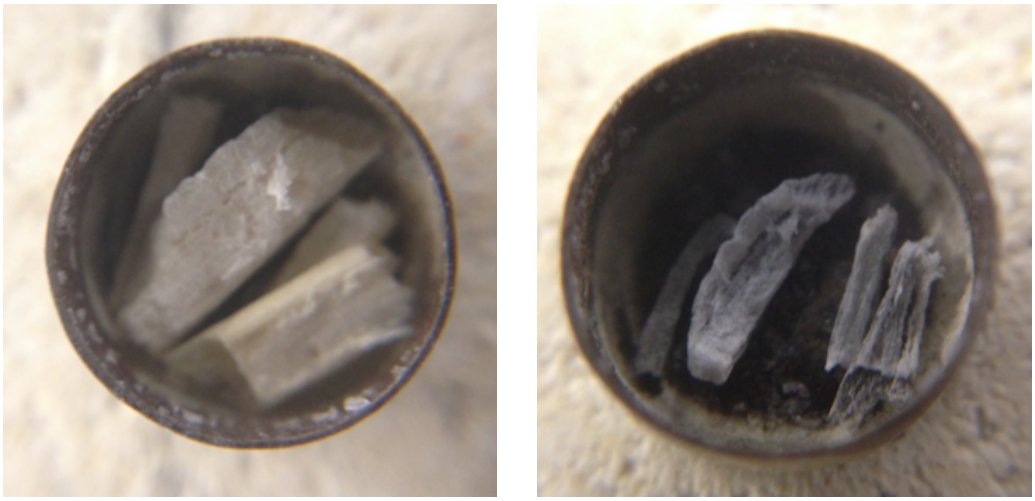

(a) before TGA **(b)** after TGA

Figure 6.2: Sample H7-3N1-5x in crucible before and after TGA (from room temperature to 1000 °C).

6.2.3 Flammability test in cone calorimeter

Description

The flammability of loose hemp shiv was assessed by cone calorimetry, according to the principles described in ISO 5660-1 (International Organization for Standardization 2015) and ASTM E1354 (ASTM 2017b). The apparatus is shown in Figure 6.3. The cone calorimeter allows measurement of the sample mass as a function of time, and the composition of the gaseous species produced during combustion. This allows the calculation of the heat release rate (HRR, also noted $\dot{q}$ as described in Table 6.2) using the oxygen consumption (OC) method of Janssens (1991). The cone calorimeter typically enables the visualisation of both flaming and smouldering combustion. The latter differs in the sense that oxidation of the material occurs at the solid phase of the fuel, instead of the gaseous phase for flaming combustion (Rein 2009).

The sample preparation method is shown in Figure 6.4 where hemp shiv were placed in a stainless steel mould of 100 mm $\times$ 100 mm, previously insulated with one layer of ceramic paper and aluminium foil in order to limit heating by radiation from the sides (ASTM 2017b). This mould was then placed inside a sample holder (sample

pan and retainer), which was mounted onto the weighing scale to monitor the mass loss. The height of the cone calorimeter was adjusted so that the top of the sample was situated 25 mm under the base of the cone heater. The temperature of the cone heater was then adjusted to obtain the desired heat flux. After this period of preheating, the sample holder could be placed on the scale in the combustion chamber.

The experiment started when the electrodes producing a spark of 10000 V were positioned above the sample. This spark ignited the flammable gases released upon exposing the sample to the heat. This type of set-up with a spark is called piloted ignition (ASTM 2017b), which represents the most realistic scenario to occur as it assumed that construction materials become involved after a fire has already established, compared to spontaneous ignition which is only reached at much higher heat fluxes for this type of material.

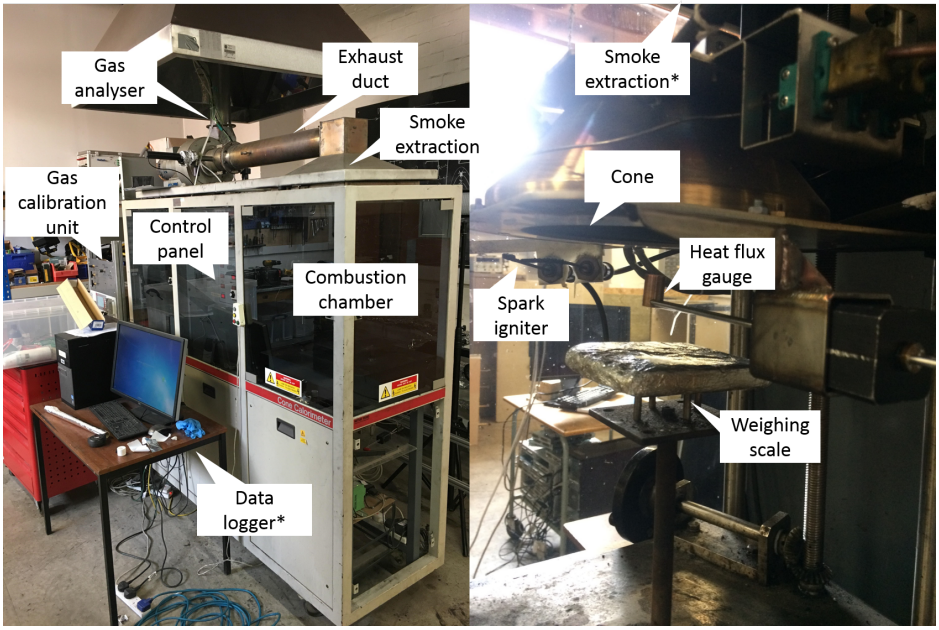

Figure 6.3: Cone calorimeter at the University of Edinburgh, and the combustion chamber, shown in the set up used for calibration, according to ISO 5660-1 (International Organization for Standardization 2015) and ASTM E1354 (ASTM 2017b). The instruments with an asterisk are not visible in the picture.

Approximately 25 g of loose hemp shiv, enough to completely fill the cell holder, with different silica particles treatments were studied (each treatment is described in

Table 6.1). Three samples of each type of hemp shiv/treatment were analysed. The values reported are therefore the averages of the three measurements. It was then possible to reliably estimate the influence of the silica particle treatments.

Should the hemp shiv be exposed to a high heat flux such as 50 kW/m^2 as is common with the cone calorimeter method, the surface temperature of the samples would be greater than the pyrolysis temperature. This means that the combustion process becomes more thermally driven and transition between different modes of combustion is more challenging to observe. The loose hemp shiv were then exposed to a relatively low heat flux, set at 11.5 kW/m^2 for all the experiments. This was selected after preliminary testing as it was sufficient to result in piloted ignition of the hemp shiv but also low enough to observe smouldering combustion after flame out.

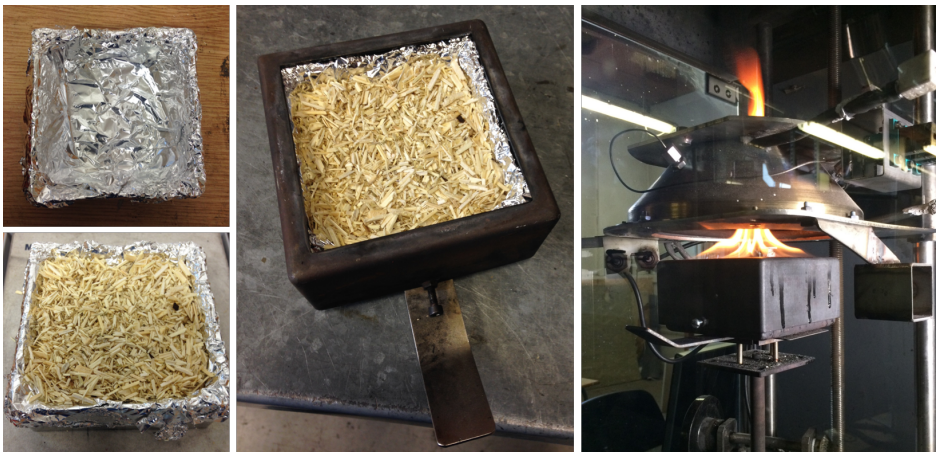

Figure 6.4: Sampling method for cone calorimetry of loose hemp shiv. Top left photograph represents the insulated mould, which contain the hemp shiv (bottom left photograph). Middle photograph shows the cell holder to be placed under the cone. Right photograph shows the sample just after ignition, placed on the weighing scale 25 mm under the base of the cone.

Nomenclature

In this chapter and Chapter 7, a specific nomenclature was adopted to describe the fire tests in the cone calorimeter according to ASTM (2017b), which is described in the following Table 6.2:

Table 6.2: Nomenclature for fire tests in cone calorimeter.

Symbol	Definition and units
TTI	time to ignition (s)
m_0	initial mass of the sample, normalised (wt%)
$m_{t=x}$	mass of the sample at t=x s, normalised (wt%)
$\dot{m} = \frac{-dm}{dt}$	normalised mass loss rate (wt%/s)
$\dot{m}_{max}$	maximum mass loss rate (wt%/s), also peak of MLR in text
$\dot{q}$	heat release rate (kW)$*$
$\dot{q}''$	heat release rate per unit area (kW/m^2)
$q''_{tot,t=x}$	total heat released between $t = 0$ and $t = x$ s (MJ/m^2)
$\dot{q}''_{max}$	maximum heat release rate per unit area (kW/m^2), also peak of HRR
$\Delta h_{\text{c,eff}}$	average effective heat of combustion (kJ/wt%)
	$*$ kW=kJ/s

6.3 Thermal decomposition of hemp shiv

As a cellulose-based material, hemp shiv decomposes when heated to elevated temperatures. Here, the results from TGA-DSC are used to compare samples of hemp shiv coated with silica particles to untreated ones. Quantification of the thermal degradation processes of hemp shiv allows the mechanism of operation of the silica, i.e. whether there is a chemical effect or a thermal effect, to be established.

6.3.1 Thermogravimetric analysis

The thermal analyses were carried out primarily in air to be able to capture the pyrolysis and oxidation processes. These processes are respectively thermally driven and oxygen dependent, therefore understanding the effect that the silica particles have on each of these phases of decomposition will allow the mechanism by which it operates to be elucidated. One sample of untreated hemp shiv, H7-unt, was also run under inert atmosphere (nitrogen) to estimate the contribution of the pyrolysis only (occur-

ring in N_2) and the combination of pyrolysis followed by oxidation (occurring in air). It also allows to compare with the descriptions of thermal degradation found in the literature.

The thermal analyses of H7-unt in air and N_2 are shown in Figure 6.5. The first period of mass loss (up to 120 °C) is attributed to the evaporation of moisture present in the hemp shiv (the untreated materials were not dried prior to testing). The thermal degradation of cellulose and hemi-cellulose corresponds to the mass loss that occurs 215 °C and 370 °C both in air and N_2, which matches the local minima of the greatest peak of mass loss rate in Figure 6.5b. In fact Yang et al. (2007) observed a significant mass loss rate from 315 °C to 400 °C, peaking at 355 °C, corresponding to the pyrolysis of cellulose. This assumption seems correct as in this temperature range, there are close to no distinction between results obtained in air and N_2. However, above 370 °C the data diverge, showing a dissimilar behaviour.

The values of the DTG curve in N_2 between 370 °C and 1000 °C are close to zero (Figure 6.5b), demonstrating that no further reaction occurred. This is even clearer from the difference between the two TG curves in Figure 6.5a as the sample in air oxidised. Approximately 20 wt% of the initial mass of the untreated sample tested in N_2 remained at the end of the analysis. It was therefore anticipated to observe a much smaller residue at 1000 °C for H7-unt tested in air (3.1 wt%, see Table 6.3) as the remaining compounds of hemp shiv (principally lignin) decomposed further from a consequence of the oxidation reactions which occurred in the presence of oxygen. The char produced by the pyrolysis reaction oxidised and yielded mostly CO_2, leaving very little residue. These two processes – pyrolysis and oxidation – are key to the decomposition of hemp shiv in air.

All the mass loss (TG) curves for each type of treated sample and their derivatives (DTG) are displayed in Figure 6.6, with key values presented in Table 6.3. Overall, the thermal degradation in air appears very similar, irrespective of the treatment deposited on the hemp shiv.

There was a first period of mass loss occurring at temperatures below 120 °C, followed by a much more significant one, between 215 °C and 370 °C, which is similar

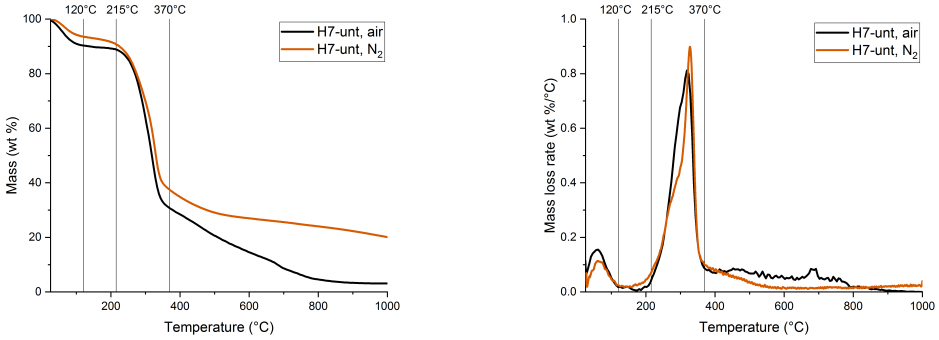

(a) Mass loss of H7-unt (TG curves)

(b) Mass loss rate of H7-unt (DTG curves)

Figure 6.5: Thermogravimetric analyses of H7-unt in air and under inert atmosphere between 25 °C and 1000 °C at a 10 °C/min rate. The absolute values of the derivative curves (DTG) represent the mass loss rates.

to the results of H7-unt (Figure 6.5). All the treated samples, however, displayed a smaller first mass loss than that of H7-unt, which is more evident to discern from the derivative curves in Figures 6.6b, 6.6d, and 6.6f), which was attributed to the evaporation of intrinsic moisture. The reason for this is likely to be that the untreated hemp shiv were not dried prior to the thermal analysis, unlike the treated samples which were dried at 90 °C for one hour after having been coated (to evaporate solvent, as illustrated in Figure 5.3a). The treated samples lost on average 5.5 wt% of their initial mass during this period, whereas H7-unt lost 9.7 wt%.

The second mass loss period, as discussed earlier, can be attributed to the depolymerisation by pyrolysis of cellulose and hemi-cellulose, which occurred between 215 °C and 370 °C. On average, the treated hemp shiv lost 52.8 wt% during this stage, a little less than H7-unt with 58.1 wt%. Although the difference in final residual mass between each treatment was very small, and might not be significant, there still seems to be a general pattern for which the three series of samples experienced lower mass loss the more silica they were coated with (apart from sample H7-5N1-5x). A possible explanation for this would be that the mass of silica was greater for those samples, and as it did not react nor transform in the studied temperature range, a greater residue was expected. Quantifying the mass of silica on each piece of hemp shiv remained

Table 6.3: Mass loss values at different stages of thermal degradation, and peak of mass loss rate (MLR) and associated temperature for the loose hemp shiv samples, tested in air.

Sample		mass loss (wt%) at T=120 °C	mass loss (wt%) at 215<T<370 °C	residue (wt%) at T=1000 °C	peak MLR (wt%/°C)	T peak MLR (°C)
H7-unt		9.7	58.1	3.1	0.81	319
H7-2N1	1x	5.5	54.2	8.5	0.64	338
	3x	4.2	53.3	13.2	0.79	333
	5x	4.5	46.7	20.5	0.66	334
H7-3N1	1x	7.1	55.1	6.0	0.79	324
	3x	5.3	51.9	11.0	0.76	324
	5x	5.3	48.2	15.0	0.64	329
H7-5N1	1x	5.6	57.7	4.3	0.77	324
	3x	6.9	53.3	7.9	0.74	339
	5x	5.2	54.7	9.3	0.69	334

challenging due to the precision required from the weighing scale, which could not be achieved here. The change in emissivity of the coated hemp shiv could also influence the reduced thermal degradation of samples with the most silica present. Figure 6.2b shows that after TGA, H7-3N1-5x presented a grey-white colour, which means that their emissivity was greater than H7-unt (which remained dark grey, not pictured here). Heat had more potential to dissipate externally compared to being absorbed by the hemp shiv to elevate their internal temperature and contribute to their degradation.

The peaks of mass loss rate (MLR), reported in Table 6.3, occurred during the greatest mass losses, between 215 °C and 370 °C (seen in the DTG curves in Figures 6.6b, 6.6d, and 6.6f). The untreated sample reached the highest value of peak of MLR at 0.81 wt%/°C. Samples H7-3N1-1x and H7-5N1-1x demonstrated a very close behaviour (Figures 6.6d and 6.6f), with a peak at 0.77 wt%/°C and 0.79 wt%/°C respectively. Although these values are close and the difference between them could be just minimally significant, it is worth noting that this behaviour was exhibited for all three types of treatment, thus showing that silica might affect pyrolysis.

When the hemp shiv coated only once were examined using an electron microscope (in Chapter 5, Figure 5.5d), it was clear that the surface was not entirely cov-

ered by the silica particles. It seems that the more silica present on the surface of the shiv, the smaller the peaks of MLR, which were all reached by the samples -5x, at 0.67 wt%/°C on average for the three series. The fact that this phenomenon was not verified for H7-2N1-1x might be due to the presence of smaller particles (31 nm of diameter once functionalised), which provided more coverage to the surface for a same number of coats (Figure 5.5b). A possible explanation could be that when silica effectively covered the surface of the shiv, the release of volatiles produced from pyrolysis was limited.

The peak of mass loss rate was reached at a lower temperature for the untreated sample (319 °C) compared to the treated ones (331 °C on average). Considering that the heating rate was set at 10 °C/min, this only corresponds to just over a minute difference in the observed phenomenon between the two types of sample. In order to observe a clearer distinction, a slower heating rate could be chosen. In these conditions, the effect of the presence of inorganic particles increasing the thermal mass of the whole sample could be better assessed. A greater thermal mass means that more energy would be necessary for the hemp shiv to pyrolyse, thus this phenomenon would start at slightly greater temperatures the more silica coated. Such hypothesis could be confirmed by quantifying the effective silica mass present on the surface of each piece of hemp shiv, although it could not be carried out due to the limitations of weighing such small quantities of silica.

The residual mass at 1000 °C was the most affected by the presence of silica. Only 3.1 wt% of the initial mass of H7-unt remained at the end of the analysis, and this value was greater for all treated samples (Table 6.3). It increased with the number of times the hemp shiv were coated, up to 20.5 wt% for H7-2N1-5x. This suggests that for a more uniformly covered hemp shiv surface, the smaller silica particles might have impeded the release of pyrolysis gases, and limited the oxygen access to the bio-materials, which in turn delayed and limited the oxidation reactions. The greatest residual masses per size of particles were obtained in the following order: $\text{residue}_{H7-2N1-5x} > \text{residue}_{H7-3N1-5x} > \text{residue}_{H7-5N1-5x}$. It is likely that the smaller particles covered more uniformly and completely the surface of hemp shiv,

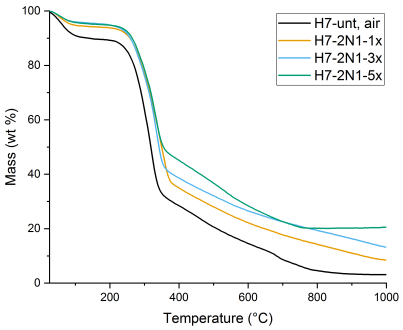

(a) TG curve of H7-2N1

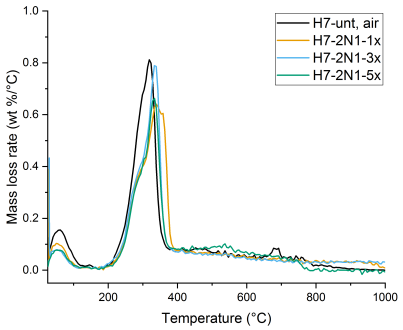

(b) DTG curve of H7-2N1

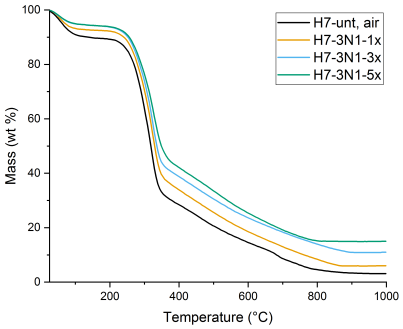

(c) TG curve of H7-3N1

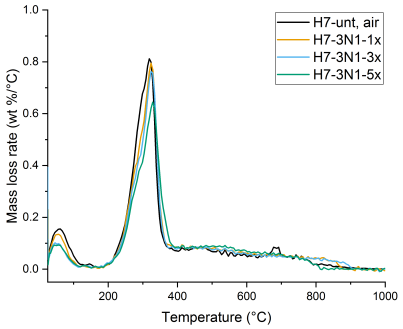

(d) DTG curve of H7-3N1

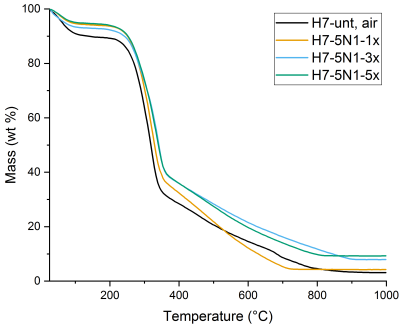

(e) TG curve of H7-5N1

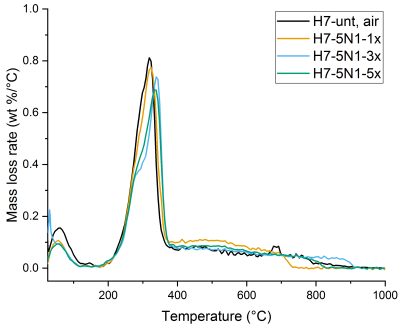

(f) DTG curve of H7-5N1

Figure 6.6: TGA on loose hemp shiv samples, and comparison with untreated shiv. The left column shows the mass loss of each type of sample (TG curves), and the right column the absolute values of their associated derivatives (DTG curves).

thus leaving less space between each particle for gases egress or oxygen ingress. Such hypothesis could be verified by imaging via SEM all these types of samples, although this method proved challenging for small particles which would require greater magnification, and damaged the samples due to the vacuum (see Section 5.3).

This increased residual mass from samples -1x to -5x could reflect either the greater emissivity of the coated samples the more silica was present, or the increased silica mass on the hemp shiv, although this statement cannot be validated without a thorough chemical analysis of the residual materials, nor knowing the exact initial mass of silica deposited. It is however likely that the mass of coated silica was far lower than the residual mass of the samples at 1000 °C. If particles of 110 nm are considered to uniformly and completely coat as a single layer one piece of hemp shiv of 7 mm^2 in surface (H7-3N1-3x), there would be approximately 10^9 particles on both sides of the piece of hemp shiv. On the hypothesis that one silica particle has a density of approximately 3×10^{-3} g/cm^3 and a volume of approximately 10^{-22} m^{-3}, the total mass of silica particles coating one piece of hemp shiv would be approximately 10^{-9} g. Compared to the residual mass of hemp shiv after TGA (11.0 wt%, so 0.66 mg for a 6.0 mg sample), the residue outweighs by 10^7 the mass of silica present initially.

6.3.2 Differential scanning calorimetry

The DSC method allows the evaluation of the quantity of energy absorbed by a material when heated. The DSC curve of sample H7-unt in air is shown in Figure 6.7. An endothermic peak occurred between 330 °C and 360 °C, which would most likely represent the pyrolysis phenomenon. According to Yang et al. (2007), mostly cellulose and hemi-cellulose decomposed endothermically in this range of temperatures. When the hemp shiv were treated, as is observed for the H7-2N1 series of samples in Figure 6.7, the endothermic peaks were shifted to greater temperatures the more silica was present on the hemp shiv, until almost no peak was visible for H7-2N1-5x, which could demonstrate the effect of silica protecting the bio-material against pyrolysis. Three (possibly connected) mechanisms could explain these observations:

- The silica particles fully covered the surface of the hemp shiv, therefore volatiles produced during pyrolysis could not be released at the pyrolysis temperature of untreated hemp shiv, but only when the temperature increased;
- Silica acted as a "heat sink": a specific quantity of energy is required to bring the hemp shiv to their pyrolysis temperature, however as silica was present on their surface, some of this energy was absorbed by the inorganic particles. More energy would therefore be required to start and sustain pyrolysis.
- The emissivity of the samples increased the more silica was present, thus more heat was dissipated externally compared to within the hemp shiv.

From 700 °C onwards, the thermal degradation became exothermic, which is then characteristic of the oxidation reactions occurring in the remaining of the hemp shiv. This finding confirms the supposition that only oxidation reactions took place beyond 500 °C as it was demonstrated by the TG and DTG curves produced in N_2 in Figure 6.5, for which the lack of oxygen supply limited further thermal degradation of the shiv. Indeed, the curves associated with the coated samples could demonstrate that less char oxidation occurred at these greater temperatures, compared to untreated hemp shiv. The DSC method thus allowed to better understand the thermal degradation processes of hemp shiv in air, especially the shift from endothermic pyrolysis to exothermic oxidation.

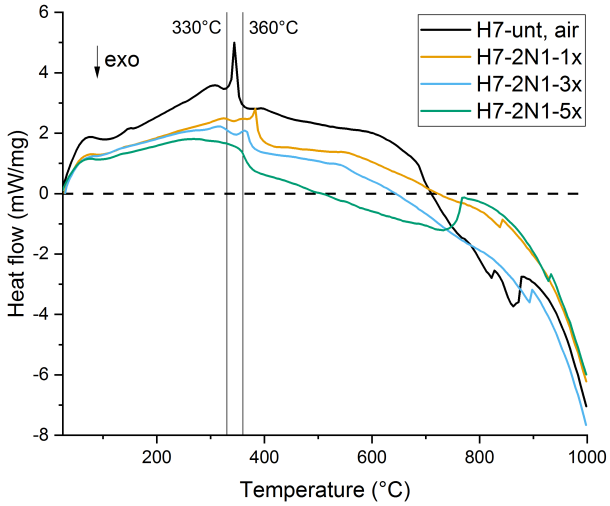

Figure 6.7: Differential scanning calorimetry curves for samples H7-unt and H7-2N1 series, from 25 °C to 1000 °C at a 10 °C/min rate. Positive values of the y-axis correspond to endothermic reactions, whilst negative values to exothermic ones.

6.3.3 Reaction to fire – cone calorimeter

Ignition and mass loss rate

Since the TGA-DSC data demonstrated that there is an effect due to the thermal mass of the silica, a series of flammability tests were carried out on the samples stated in Table 6.1. The results aim to determine whether this effect was apparent under more realistic conditions of heating, and which reaction to fire parameters were affected by the silica treatments, particularly the time to ignition (TTI), mass loss rate (MLR, $\dot{m}$), and heat release rate (HRR, $\dot{q}$).

Ignition is defined as the time at which sustained flaming (at least four seconds) of a material is observed (ASTM 2017b). The recorded times to ignition are reported in Table 6.4 and Figure 6.8 shows the mass measurement during the cone calorimetry experiment, capped at 600 s. The time to ignition by flaming (represented by the lighter orange rectangle) was slightly greater for the treated hemp shiv, reported at 67 s on average, whereas H7-unt ignited after 63 s. The mass suddenly decreased as

a result of the release of flammable gases, which appears more clearly in the focussed graph, displayed in Figure 6.8b. At the end of the flaming period, represented by the grey (H7-unt) and darker orange rectangles (-1x samples), the hemp shiv continued to lose mass as smouldering became the primary mode of combustion.

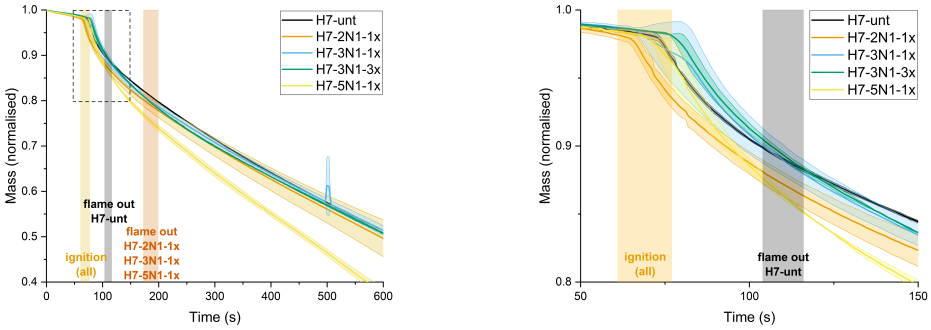

(a) Mass loss of loose hemp shiv

(b) Focus on the flaming period

Figure 6.8: Mass loss of loose hemp shiv by cone calorimetry. The shaded areas around each curve represent the standard deviation amongst a sampling population. The shaded rectangles correspond respectively to the time to ignition (average from all types of samples), flame out time of H7-unt, and flame out time of the -1x samples (sample H7-3N1-3x was omitted from the average calculation as it occurred much later). Part 6.8b is a close-up of the dashed area in part 6.8a.

The following analyses show the mass loss rates as the opposite of the derivative of the mass ($\frac{-dm}{dt}$). These derivative data have been smoothed using a Savitzky-Golay filter, with a polynomial order of 5 and 15 points of window. This filter was applied to reduce the noise, and its parameters were chosen to preserve the information contained in the peak of mass loss rate (height and width notably).

Figure 6.9 shows the difference of MLR between samples H7-unt and H7-3N1-3x, before ignition to the end of the flaming period of H7-3N1-3x. The untreated hemp shiv flamed for 47 s, whereas the flaming period for H7-3N1-3x lasted approximately 204 s. The peak of MLR was just slightly lower for H7-3N1-3x than for the H7-unt, which can be visualised in Figure 6.9b. As the H7-3N1-3x samples weighed on average 26.7 g, the value of $\dot{m}_{max}$ corresponds actually to a loss of 114 mg/s, compared to

128 mg/s for H7-unt. Out of all samples tested here, the lowest $\dot{m}_{max}$ was attributed to the samples H7-3N1-3x (represented in Figure 6.9), whilst all other samples demonstrated similar values to the untreated type (H7-3N1-1x), or even worse values (H7-2N1-1x, H7-5N1-1x).

The right side of the peak of the $\dot{m}$ curve for H7-3N1-3x presented a smaller gradient, indicating a slower mass loss than for H7-unt. This phenomenon is likely to be induced by a reduction of pyrolysis rate as the thermal mass of the sample increased with the presence of silica, coated three times on the hemp shiv. This observation correlates with the TGA results (Figure 6.5b), where silica also reduced the pyrolysis rate of hemp shiv by blocking egress of volatiles, as it was demonstrated by the values of residual mass of treated hemp shiv in Table 6.3. Nevertheless, the sampling size between these analytical methods was significantly different, and the influence of silica particles was clearer on a small specimen. The mechanism by which silica could absorb some of the heat and thus more energy was required to bring the coated hemp shiv to their pyrolysis temperature was more clearly demonstrated on a small sample analysed by TGA-DSC methods. The quantity of silica present on a 25 g sample of coated hemp shiv was not enough to significantly increase the thermal mass of the whole sample and thus to limit the thermal degradation caused by the radiant heat flux of 11.5 kW/m^2.

Should a material show significantly better fire performance in terms of reduced mass loss, its $\dot{m}_{max}$ would be as low as possible, and occurring with as much delay as possible. This corresponds to the bottom right quadrant formed by the dashed lines in Figure 6.10. These are associated to the median value of $\dot{m}_{max}$ (between lowest $\dot{m}_{max} - stdev$ and highest $\dot{m}_{max} + stdev$) and the median value of time to $\dot{m}_{max}$ obtained with a similar calculation. This analysis allows the comparison of each type of treatment between one another in terms of $\dot{m}_{max}$ values. Following this method, samples H7-3N1-1x and H7-3N1-3x belonged to said quadrant, although only H7-3N1-3x is entirely contained with its error bars.

These analyses and visualisation suggest that some improvement in a slightly delayed time to ignition and lower peak of MLR for hemp shiv coated with silica parti-

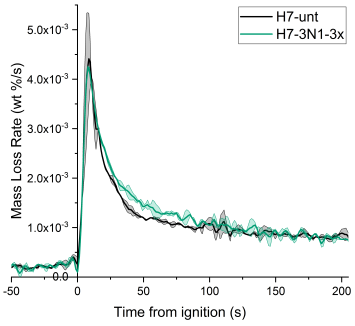

(a) Mass loss rate during the flaming period

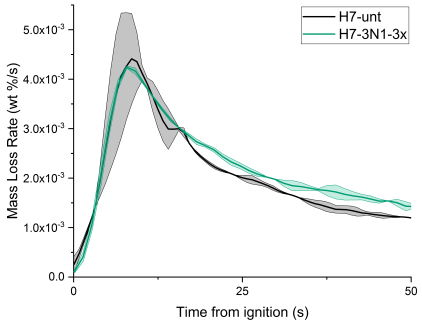

(b) Focus on the peak of MLR

Figure 6.9: Mass loss rate ($\dot{m}$) of samples H7-unt and H7-3N1-3x plotted from the time to ignition. The shaded areas around each curve represent the standard deviation amongst a sampling population.

cles could be measured. However, the thermal mass of coated samples appeared not to have significantly changed which was not sufficient to demonstrate the potential of silica to limit the thermal degradation processes provoked by a radiant heat flux of this value.

Table 6.4: Key mass loss rate values obtained during combustion of hemp shiv by cone calorimetry: time to ignition, peaks of mass loss rate and their associated times, and time of flame out. The values are given with their standard deviation calculated from each sample of the same population. Due to the slight variations, the $\dot{m}_{max}$ values are given with more significant figures.

Sample	TTI (s)	Mass Loss Rate		Flame out (s)	Flaming period (s)
		$\dot{m}_{max}$ ($\times 10^{-3}$ wt%/s)	time (s)		
H7-unt	63 ± 1	4.56 ± 0.73	78 ± 1	110 ± 6	47 ± 8
H7-2N1-1x	62 ± 1	4.99 ± 0.70	70 ± 1	181 ± 8	119 ± 12
H7-3N1-1x	65 ± 9	4.48 ± 0.32	80 ± 9	185 ± 6	119 ± 20
H7-3N1-3x	69 ± 3	4.28 ± 0.05	82 ± 3	274 ± 18	204 ± 29
H7-5N1-1x	71 ± 6	5.33 ± 0.58	78 ± 5	190 ± 9	119 ± 22

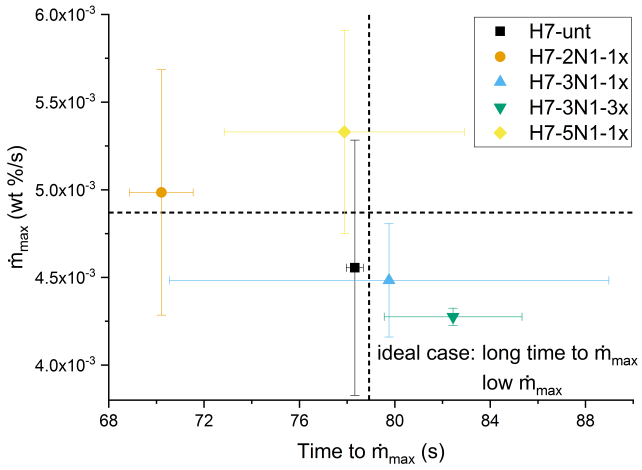

Figure 6.10: Summary of $\dot{m}_{max}$ and their times for loose hemp shiv, as seen in Table 6.4. The dashed lines correspond to $t = 79$ s and $\dot{m}_{max} = 4.87 \times 10^{-3}$ wt%/s.

Heat release rate and heat of combustion

The heat release rate can be calculated from the analysis of the exhaust gases from the cone calorimeter. In addition, concentrations of O_2, CO, and CO_2 are measured. The combustion process of hydrocarbon materials involves consumption of O_2, as well as production of CO_2, and of CO in the case of incomplete combustion (which occurs especially during smouldering combustion). The energy released during a fire can be evalated by calculation from the gas concentration, as hydrocarbon materials typically release 13.1 kJ/g of O_2 consumed (Huggett 1980) during flaming combustion. These gas phase measurements then allow investigation of various combustion phenomena:

- The type of combustion: the ideal case of flaming combustion consumes O_2 and produces CO_2 mainly, whereas incomplete combustion mainly yields CO, which is typical of smouldering combustion involving bio-based materials;
- The heat released upon burning ($\dot{q}''$, q''_{tot} based on the oxygen consumption (OC) according to Janssens (1991);
- The effective heat of combustion ($\Delta h_{c,eff}$), which indicates the amount of energy produced upon burning therefore allows the comparison of different fuels.

As the gas analyser is placed after the exhaust duct of the instrument (see Figure 6.3), the gas concentration data has a delay compared to the time such gases were released by the sample. The following curves which are based on gas concentrations take into account this delay, which has been calculated as the difference between the sudden drop in oxygen concentration and a sudden mass loss. Similar to the MLR curves, the HRR ones have also been smoothed out with a Savitzky-Golay filter, which polynomial order was set at 5 to keep the information in the peaks, but the points of window were increased to 50, as the analyser was more sensitive to small changes in concentration, which means the signal produced was noisier.

The gas analyses shown in Figure 6.11 demonstrate how the combustion of a sample of H7-3N1-1x occurred. Typically, hemp shiv pyrolysed when exposed to radiant heat (which was observed by TGA-DSC and discussed in Sections 6.3.1 and 6.3.2).

Shortly after more oxygen was supplied to the fuel which started flaming combustion, marked by the ignition of the samples and characterised by the greater consumption of O_2. This event was associated with the generation of CO_2, peaking around the time of ignition. Towards the end of the flaming period, CO was mostly released, whilst the levels of O_2 and CO_2 plateaued. Thereafter, the combustion of hemp shiv yielded mostly CO, which is characteristic of smouldering. When the maximum of CO was released marked the transition from flaming to smouldering combustion, at which point the chemical processes change from releasing mainly CO_2 (which is promoted in the flaming type of combustion) to mainly CO (promoted during smouldering) (Hadden 2011).

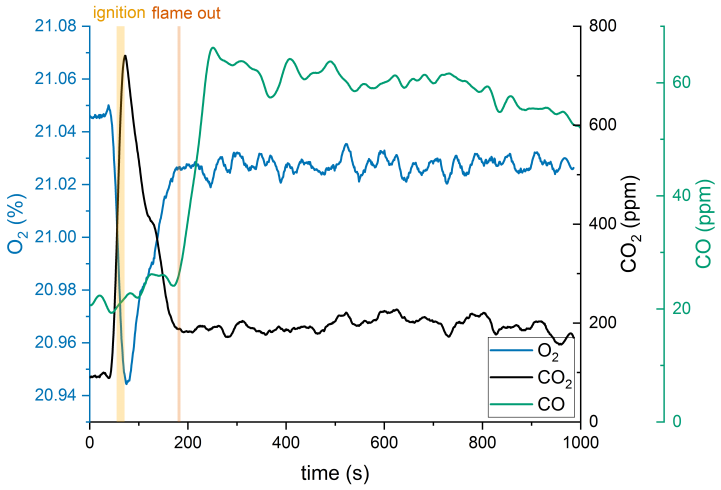

Figure 6.11: Gas analysis of a sample of H7-3N1-1x by cone calorimetry. The shaded rectangles correspond to the average time to ignition according to the measure of MLR, and to the average flame out time as it was observed visually.

Table 6.5 presents the values of heat release for the different samples. The heat released upon combustion of the samples, both during flaming and smouldering, was evaluated based on oxygen consumption. Following the calculation described in ASTM (2017b), the value of heat released at a certain time can be obtained knowing the concentration of O_2. This approach was followed to compare flaming and smouldering combustion, although this method described by Janssens (1991) might

not be relevant after flame out. The HRR can also be calculated using the CO_2 and CO concentrations (Brohez et al. 1999), although not carried out here for consistency.

Table 6.5: Heat release analysis of combustion of hemp shiv by cone calorimetry, calculated from the oxygen consumption method (Janssens 1991): peaks of heat release rate and their associated times, total heat released and effective heat of combustion during flaming and after flame out for the smouldering one, total heat released over 600 s. The values of $\dot{q}''_{max}$ are given with their standard deviation calculated from each sample of the same population, whereas the other values were calculated directly from the averages.

Sample	Heat Release Rate		$q''_{\text{tot,period}}$ (MJ/m^2)			$\Delta h_{\text{c,eff,period}}$ (MJ/wt%)	
	$\dot{q}''_{max}$ (kW/m^2)	time (s)	flaming	smouldering	total	flaming	smouldering
H7-unt	68.7 ± 3.6	69 ± 2	2.9	5.7	8.6	26.1	15.1
H7-2N1-1x	73.7 ± 5.2	66 ± 4	5.6	4.9	10.5	27.3	16.4
H7-3N1-1x	54.1 ± 6.1	72 ± 8	4.3	4.2	8.5	21.4	14.7
H7-3N1-3x	60.1 ± 1.3	74 ± 4	6.3	2.5	8.8	22.5	11.8
H7-5N1-1x	78.6 ± 4.1	75 ± 5	6.5	6.2	12.6	25.9	16.5

The curves obtained for the heat release rate of the untreated hemp shiv and the treated ones are displayed in Figure 6.12. The HRR curves obtained are typical of a charring solid, with an initial peak followed by a decrease leading to a relatively steady state of burning (Lyon 2000). Here, the HRR peaked shortly after ignition of the shiv, which can be visualised more clearly in Figure 6.12b. It corresponds to the decreasing O_2 concentration and increasing CO_2 concentration shown in Figure 6.11. Similarly to the MLR and $\dot{m}_{max}$, the lowest values of $\dot{q}''_{max}$ were obtained for the hemp shiv coated with 110 nm particles, H7-3N1-1x and H7-3N1-3x, at 54.1 kW/m^2 and 60.1 kW/m^2 respectively. The samples H7-5N1-1x exhibited the fastest mass loss, as seen from their $\dot{m}_{max}$ values, and also the most energy released (12.6 MJ/m^2), peaking at $\dot{q}''_{max}$=78.6 kW/m^2. This emphasises the difference of protective behaviour the silica can provide on hemp shiv when their surface does not present a complete coverage, probably due to the size of the particles coated.

The peak of HRR for each type of hemp shiv, noted $\dot{q}''_{max}$, is shown in Table 6.5, and represented in Figure 6.13 to compare each treatment in a similar way to $\dot{m}_{max}$ in Figure 6.10. Again, both H7-3N1-1x and H7-3N1-3x belonged to the ideal case quadrant

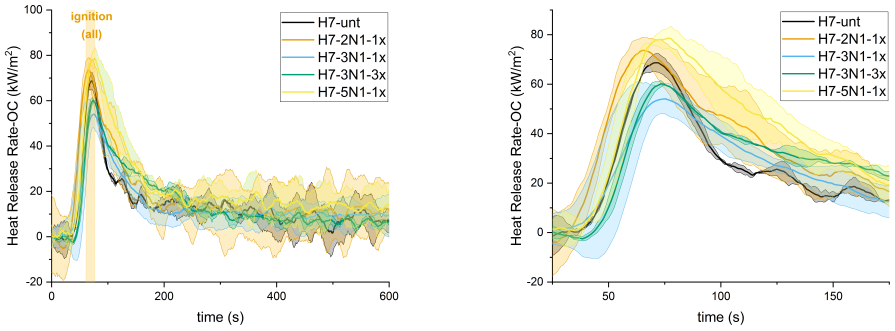

(a) Heat release rate

(b) Focus on the peak of HRR

Figure 6.12: Heat release rate Mass loss rate ($\dot{q}''$) of the untreated and treated hemp shiv (capped at 600 s of test). Part 6.12b specifically focusses on the peak of HRR per type of treatment. The shaded areas around each curve represent the standard deviation amongst a sampling population. The delay due to the gas analyser has been taken into account, and the shaded rectangle indicates the average time to ignition of all samples.

with their relatively lower $\dot{q}''_{max}$ and longer times for the HRR to peak than those of the other samples of hemp shiv. Greater distinctions between each type of samples and their associated $\dot{q}''_{max}$ could have been observed had the mass of silica been significant with regards to the mass of the hemp shiv. As a result, a definite conclusion could not be drawn on the silica effect to decrease the peak of HRR with this test method.

The total heat released over the first 600 s of test was calculated according to Equation 6.1, and the effective heat of combustion for flaming and smouldering were obtained from Equation 6.2.

$$q''_{tot,600} = \int_0^{600} \dot{q}''(t)dt \tag{6.1}$$

$$\Delta h_{c,eff}(t) = \frac{\dot{q}''(t)}{\dot{m}(t)}$$

$$\Rightarrow \Delta h_{\text{c,eff,flaming}} = \frac{q''_{\text{tot,flaming}}}{m_0 - m_{\text{flame out}}} \text{ and } \Delta h_{\text{c,eff,smouldering}} = \frac{q''_{\text{tot,smouldering}}}{m_{\text{flame out}} - m_{600}} \tag{6.2}$$

The total heat released during the first 600 s of test ($q''_{\text{tot,600}}$) is shown for each type of sample in Table 6.5 and corresponds to the area under the curve of $\dot{q}''(t)$ displayed in Figure 6.12. Samples H7-5N1-1x produced the most heat, four units more than the untreated hemp shiv, which themselves released 8.6 MJ/m^2. This value was very close

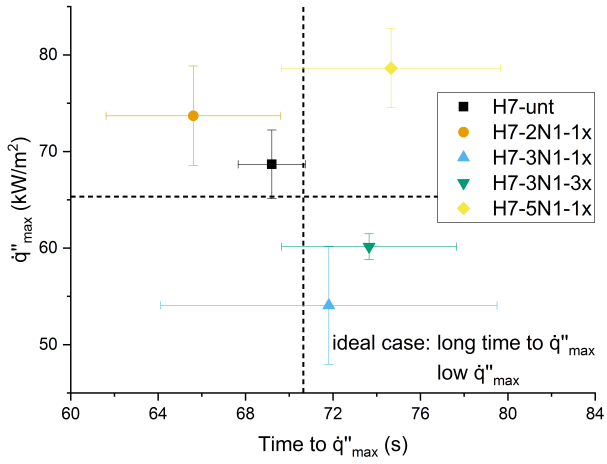

Figure 6.13: Summary of $\dot{q}''_{max}$ and their times for loose hemp shiv, as seen in Table 6.5. The dashed lines correspond to $t = 71$ s and $\dot{q}''_{max} = 65.3$ kW/m^2.

to those obtained for H7-3N1-1x and H7-3N1-3x. This suggests that the presence of silica helped to decrease the peak of HRR, although overall, even with lower $\dot{q}''_{max}$ values, the heat released throughout the experiment (capped here at 600 s) was roughly equivalent.

In fact, the calculation of q''_{tot} during the flaming and smouldering rely on the length of each period. The untreated hemp shiv thus released the least heat during flaming of all the samples because their flaming period was the shortest (47 s on average, Table 6.4). Similarly, $q''_{\text{tot,fl}}$ was greater for H7-3N1-3x than for H7-3N1-1x, despite their $q''_{\text{tot,600}}$ being equivalent, because samples H7-3N1-3x flamed longer than the hemp shiv coated once with the 110 nm particles (204 s and 119 s respectively). Such behaviour could be due to residual ethanol from the coating process still present in the hemp shiv at the time of the test even though they had been dried between each coating step. It is however unlikely as the mass loss measured by TGA below 120 °C was smaller for H7-3N1-3x than H7-3N1-1x (Table 6.3), thus indicating less water and/or ethanol evaporated at lower temperatures.

All three types of sample with particles coated once on hemp shiv (samples -1x) flamed for 119 s, with H7-3N1-1x releasing the least heat, and H7-5N1-1x the most

during flaming. The latter also yielded the most heat upon burning by smouldering ($q''_{tot,sm}$= 6.2 MJ/m^2), but when reported to the mass consumed in that period, it equates that of hemp shiv H7-2N1-1x ($\Delta h_{c,eff,sm}$= 16.5 MJ/wt%). The lowest $\Delta h_{c,eff,sm}$ was obtained for H7-3N1-3x, but its smouldering period was also the shortest owing to its longest flaming time. By comparing samples with equivalent flaming and smouldering periods (H7-2N1-1x, H7-3N1-1x, and H7-5N1-1x), H7-3N1-1x exhibited the lowest $\Delta h_{c,eff,sm}$ at 14.7 MJ/wt%. Even though H7-3N1-3x flamed the longest, its $\Delta h_{c,eff,fl}$ was of the lowest values, and close to that of H7-3N1-1x. Such result could support the hypothesis of good surface coverage by the silica particles, thus preventing volatiles produced from the thermal degradation of hemp shiv to be released during flaming and smouldering combustion.

6.4 Conclusion and remarks

The thermogravimetric analysis and differential scanning calorimetry methods demonstrated that coating loose hemp shiv with silica particles affect the pyrolysis of the material when small samples (∼6.5 mg) were considered. Greater residues were obtained the more silica was present on the hemp shiv even though it is thought that the mass of silica was nearly negligible compared to the mass of the residues. Several potentially dependent hypotheses were proposed to explain this behaviour:

- Increased loading of silica particles provided a better and more complete coverage thus limiting both the release of volatiles and oxygen ingress, which led to reduced thermal degradation. This was evidenced by the greater residues for the -5x samples which performed better than those with fewer coating layers. The decreased exothermicity of the char oxidation process with increased quantities of silica corroborates this hypothesis.

- Heat was absorbed first by the particles before it was transferred to the hemp shiv, which delayed reaching pyrolysis temperature. This supposition is in agreement with Branda et al. (2016) and Hussain, Calabria-Holley, Jiang, et al. (2018) for which sodium silicate or a sol-gel network of silica respectively protected

hemp and led to increased residual mass at 800 °C via TGA. Moreover, the DSC experiment showed that no chemical actions were attributed to the silica and it was observed to operate by acting as a heat sink and thereby reducing the rate of pyrolysis.

- Modification of emissivity of the samples when they were coated with silica, which helped dissipating heat outwards.

The time to ignition of loose coated hemp shiv, their mass loss rate, heat release rate and other characteristics of combustion were recorded and compared for different sizes of particles by cone calorimetry. At larger scale (samples weighed approximately 25 g), the fire retardant effect of silica was more intricate to discern. When coated, hemp shiv performed just slightly better than untreated samples in terms of increased time to ignition and reduced mass loss rate. The heat released upon combustion and associated characteristics, such as HRR and its peak, were calculated via the concentration of oxygen (Janssens' method). It was supposed that this calculation was not adequate during smouldering combustion. Moreover, the gas analyses were not precise enough to observe clear differences between untreated hemp shiv and coated ones. Significantly greater quantities of silica could lead to more distinctive results. Finally, because of the sampling method, oxygen was also very likely to be present between the loose hemp shiv, which would have contributed to their combustion. Better packing to ensure less air is present within the samples could address this issue, such as the method followed in Chapter 7 with binders.

This study suggests that silica can help reduce pyrolysis at a small scale, e.g. a couple of hemp shiv in a crucible for a TGA-DSC analysis, but greater loadings of silica (or any other inorganic material) are required to truly make a significant difference on the fire performance of coated samples at larger scale.

Chapter 7

Improved fire performance of hemp shiv composites

7.1 Introduction

Before introducing bio-materials within building envelopes, it is necessary to understand the fire risks that are associated with their nature, and seek treatments or methods to reduce them. In this chapter, hemp shiv boards were manufactured with the same treated hemp shiv as those tested in Chapters 5 and 6.

One goal was to demonstrate the effect of several commercially available fire retardants, such as magnesium sulfate combined or not with boron- or phosphorus-based compounds (categorised as chemical action fire retardants) and to compare the results with silica particles (which provide a physical action, as was explained in Chapter 2). Additionally, some samples were manufactured so that a mineral binder (inorganic) would also act as a heat sink and delay the onset of pyrolysis. This was explored to follow on from the remarks in Chapter 6 which suggested that greater quantities of inorganic materials were required to exhibit demonstrable effect as fire retardant.

Typically, the flammability of wood-based products is studied at fairly low heat flux exposure (Gratkowski et al. 2006). McLaggan (2016) sought the critical heat flux for hemp-lime composites, which could compare to the HSB-M samples studied here, and determined that (non-piloted) ignition by smouldering would occur under an

exposure of at least 8.0 $\pm$ 2.5 kW/m^2. Additionally, Hidalgo-Medina (2015) tested common insulation materials, such as isocyanurate foams, and confirmed their critical heat flux being between 12 kW/m^2 and 15 kW/m^2. Both flaming and smouldering phenomena are of interest in this study, which is why the hemp shiv boards were exposed to 15 kW/m^2. Under such conditions, it is expected to visualise the action of the different fire retardant additives, both the chemically active and inorganic ones, on the combustion process of hemp shiv composites.

7.2 Modes of operation of fire retardants

Most common fire retardant additives act chemically, which means that upon burning, gases are released which influence the progression and sustainability of combustion. This process cools down and dilutes the gaseous phase by the release of water vapour, e.g. phosphorus- and boron-based fire retardants (Equations 7.1 and 7.2 according to Balci et al. (2012)). Moreover, using hydrate compounds magnifies this effect, which is the case of $MgSO_4, 7\,H_2O$ studied here, as it dehydrates when heated, producing anhydrous magnesium sulfate ($MgSO_4$) and water vapour (Scheidema and Taskinen 2011). The flame can also be poisoned by recombination of radicals which are less reactive that $H^\bullet$ and $HO^\bullet$, e.g. halogen- and phosphorus-based fire retardants (recombination of $HO^\bullet$, $PO^\bullet$, and $HPO_2{}^\bullet$ for the latter according to Schartel (2010)), as was discussed in Chapter 2.

$$2\,H_3PO_4 \xrightarrow{\Delta} H_4P_2O_7 + H_2O \tag{7.1}$$

$$H_3BO_3 \xrightarrow{\Delta} HBO_2 + H_2O$$

$$4\,HBO_2 \xrightarrow{\Delta} H_2B_4O_7 + H_2O \tag{7.2}$$

$$H_2B_4O_7 \xrightarrow{\Delta} 2\,B_2O_3 + H_2O$$

Owing to their inorganic nature, silica, magnesium oxide, and silicates (clay) insulate the substrate by absorbing some of the radiant heat, which means than more energy is required for the onset of pyrolysis of the treated material. An inorganic layer also prevents egress of the volatiles produced during pyrolysis and oxygen ingress, thereby reducing the combustion rate of the treated material, which was seen for silica

in Chapter 6. This occurs in the solid phase (substrate), which is why such inorganic material are said to have a physical action on the combustion process (Hshieh 1998). In this study, different commercially available fire retardant solutions were used in the manufacture of hemp shiv boards (which compositions are described in Table 7.1) and used as benchmarks to compare the combustion processes of samples incorporating silica particles, although the fundamental mechanisms of action might differ.

7.3 Manufacturing process

7.3.1 Hemp shiv boards

In order to be introduced as insulation materials within building envelopes, hemp shiv need to be made into panels, which are composite structures. In this chapter, those composites were designed and produced by Cavac Biomatériaux. Their compositions, manufacture, and their thermal performance assessment are summarised in the flow chart presented in Figure 7.1.

The hemp shiv boards tested in this study were entirely formulated, designed, and produced by Cavac Biomatériaux in their facilities (Colson, Bourebrab, et al. 2019). The manufacturing process was similar to that described in Section 5.2.1 to produce samples BX3 and BTX3, but of greater thickness. The complete description of the samples is given in Table 7.1. The different types of samples are shown in Figure 7.2, and described thereafter. Three specimens of each type were analysed, unless time and testing constraints limited this to two (which is stated in Table 7.1 by the symbol $*$).

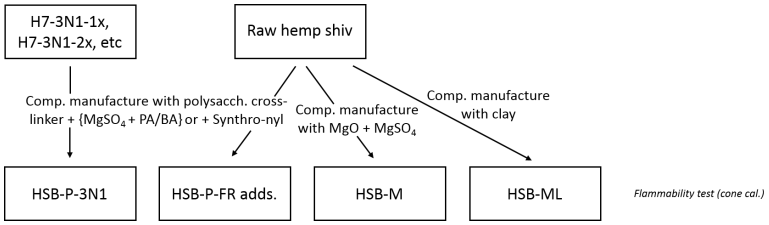

Figure 7.1: Flow chart representing the characterisation of the pyrolysis phenomenon of hemp shiv–derived composites. The method employed is shown in italic.

Table 7.1: Description of the hemp shiv boards composition tested by cone calorimetry.

Sample	Quantities (wt%)				Weight (g)	Dimensions (mm^3)	Bulk density (g/dm^3)
	Hemp shiv	Binder	FR adds.	Mineral			
HSB1-P-control ∗	92.0	8.0	–	–	72.0 ± 3.8	95×95×50	159.6 ± 8.5
HSB1-P-BA	87.0	8.0	BA: 5.0	–	69.9 ± 6.8	95×95×50	154.8 ± 15.0
HSB1-P-MKP	87.0	8.0	MKP: 5.0	–	73.0 ± 3.5	95×95×50	161.7 ± 7.9
HSB1-P-3N1	87.0	8.0	3N1: 5.0	–	72.8 ± 6.1	95×95×50	161.4 ± 13.4
HSB2-P-control ∗	89.6	10.4	–	–	113.7 ± 3.3	100×100×51	227.4 ± 6.5
HSB2-P-10MgS ∗	80.6	9.4	$MgSO_4$: 10.0	–	111.3 ± 1.3	100×100×54	202.3 ± 2.3
HSB2-P-20MgS	71.7	8.3	$MgSO_4$: 20.0	–	125.9 ± 4.6	100×100×56	220.9 ± 8.1
HSB2-P-BA	77.9	9.1	$MgSO_4$: 10.0 H_3BO_3: 3.0	–	118.0 ± 1.4	100×100×58	203.4 ± 2.4
HSB2-P-PA	77.9	9.1	$MgSO_4$: 10.0 H_3PO_4: 3.0	–	119.8 ± 1.6	100×100×55	217.8 ± 2.8
HSB2-P-3N1	77.9	9.1	$MgSO_4$: 10.0 3N1: 3.0	–	112.3 ± 5.0	100×100×59	187.1 ± 8.3
HSB2-P-Syn	77.9	9.1	Syn.: 13.0	–	119.2 ± 2.3	100×100×55	205.5 ± 4.0
HSB-M-1	33.3	–	$MgSO_4$: 33.3	MgO: 33.3	261.4 ± 0.2	96×96×60	463.1 ± 0.3
HSB-M-2 ∗	40.0	–	$MgSO_4$: 30.0	MgO: 30.0	210.7 ± 1.8	97×97×58	407.2 ± 3.5
HSB-M-3 ∗	50.0	–	$MgSO_4$: 25.0	MgO: 25.0	162.3 ± 1.4	93×93×57	313.6 ± 2.7
HSB-ML-2:1 ∗	80.3	6.4	–	clay: 13.3	124.8 ± 5.8	100×100×50	249.6 ± 11.7
HSB-ML-4:1 ∗	77.6	6.4	–	clay: 16.0	159.3 ± 3.1	100×100×50	318.6 ± 6.3

∗ Only two specimens instead of three could be analysed due to time and testing constraints.

With polysaccharides-based binder: HSB1-P and HSB2-P

Biofibat hemp shiv (HB type), binder, and fire retardant additives were used to make samples of the HSB-P type. The thermosetting binder was a mixture of polysaccharides and a cross-linker, identical to the one used for samples BX3 and BTX3, and developed by Colson, Le Cunff, et al. (2017).

Two kinds of HSB-P samples were manufactured: HSB1-P and HSB2-P. The first type (HSB1-P) had the fire retardant additives blended with the binder for three minutes, which were then mixed with the hemp shiv also for four minutes, as illustrated in Figure 7.3. The fire retardant additives were:

- Monopotassium phosphate, abbreviated MKP and of formulation KH_2PO_4 (readily available due to its use as a fertiliser), expected to release water vapour upon burning which dilutes the gaseous phase;
- Boric acid, abbreviated BA and of formulation H_3BO_3, which also decomposes with heat to produce water vapour;
- Silica particles of Formulation 3, functionalised with nPTMS at a T1 level (3N1

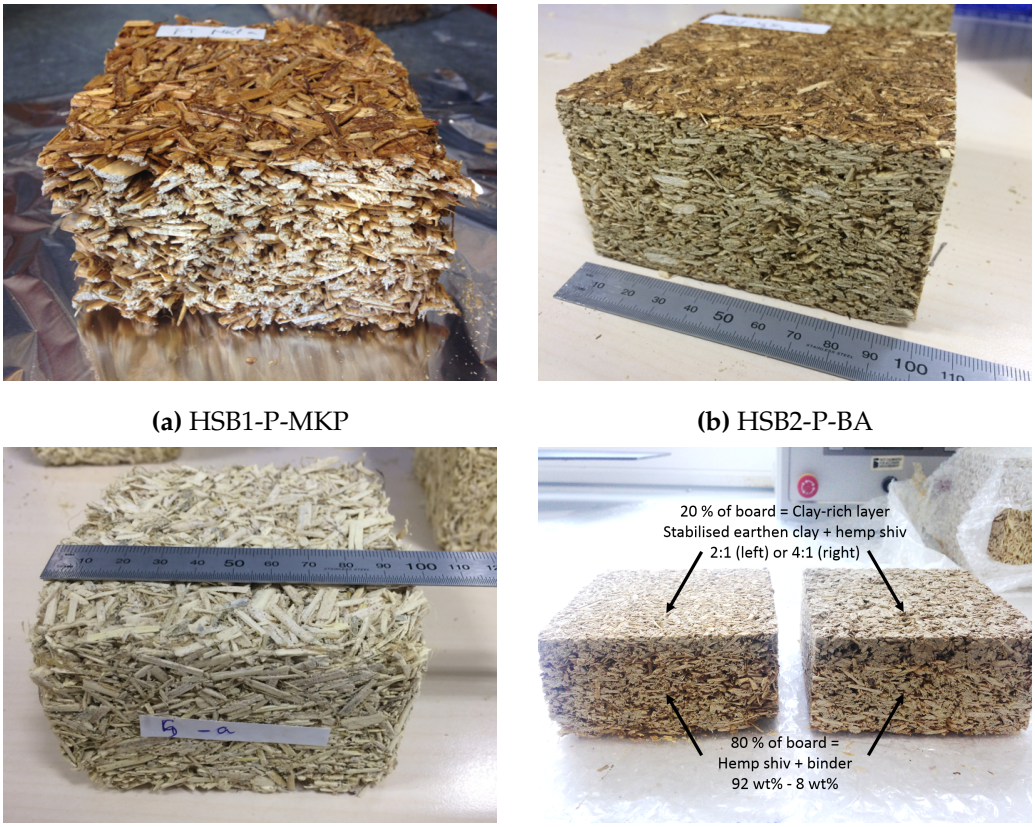

(a) HSB1-P-MKP

(b) HSB2-P-BA

(c) HSB-M-2

(d) HSB-ML-2:1 and HSB-ML-4:1

Figure 7.2: The different types of hemp shiv boards tested by cone calorimetry. One sample of each type is shown owing to their resemblance.

particles as described in Chapter 4), acting as a heat sink in the condensed phase, as seen in Chapter 6.

The fire retardant additives were added so that their final solid content constituted 3 wt% of the final weight of the sample, which was approximately of 71.9 $\pm$ 4.7 g, with the binder accounting for 8 wt%, and the remaining (87 wt% or 92 wt% for the untreated type) of hemp shiv. The example of HSB1-P-MKP is shown in Figure 7.2a.

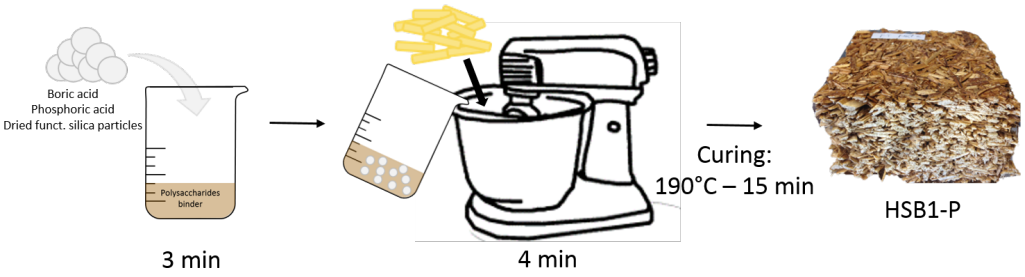

Figure 7.3: Manufacture of HSB1-P

As regards HSB2-P, the fire retardants additives were either a combination of magnesium sulfate with other chemicals as described below, or a commercially available compound (which is illustrated in Figure 7.4):

- Magnesium sulfate (abbreviated here MgS, of formulation $MgSO_4$) was present in each of the following formulations. The additives used are sold under the name Epsom salts, EPSO Top® $MgSO_4, 7\,H_2O$. They were dissolved in water to 20 wt% solid content. When heated, this compound dehydrates, thus water vapour dilutes the gaseous phase (similarly to the MKP in the HSB1-P-MKP samples). It was used as follows:
  - Two different contents of magnesium sulfate (10 wt% and 20 wt%), not combined with other additives (the first step in Figure 7.4 was then omitted).
  - Combined with boric acid (BA, H_3BO_3, commercial grade TG Granular Optibor®)), which also degrades to produce water vapour when heated past its boiling point (gas diluent type). It was solubilised in water to achieve 4 wt% solid content, in which the hemp shiv were immersed before being mixed with the magnesium sulfate solution.
  - Combined with phosphoric acid (PA, H_3PO_4, concentrated at 85 %) also a gas diluent when degraded. It was diluted to 10 wt% concentration, in which the hemp shiv were immersed before being mixed with the magnesium sulfate solution.

  - Combined with silica particles (3N1) which act as heat sink, originally at 7 wt% concentration in IMS. In the HSB2-P-3N1 case, silica particles were coated twice on the hemp shiv to ensure good coverage of their surface, followed by drying, which corresponds to hemp shiv HB-3N1-2x (which were used in the manufacture of BTX3 in Chapter 5). The coated hemp shiv were then immersed in the magnesium sulfate solution.

- Ammonium polyphosphate flame retardant (commonly used in intumescent fire retardant coatings and known as APP, of formulation $[NH_4PO_3]_n(OH)_2$), Synthro®-nyl SNP 1813 S supplied as a 50 wt% solution, was used in the manufacture of samples HSB2-P-Syn after having been diluted to 25 wt% in which the hemp shiv were then immersed (the addition took place at the first step represented in Figure 7.4 but the second step was omitted).

All the additives were applied on raw hemp shiv and mixed for three minutes, before the addition of magnesium sulfate, and the binder, thoroughly mixed in a food processor for three and four minutes respectively. The formulations were made so that the final solid content of the fire retardant additives represented 13 wt% of the final weight of each sample (3 wt% for the chemical additives similarly to HSB1-P type, and magnesium sulfate accounting for 10 wt%). HSB2-P-20MgS contained more $MgSO_4$ for comparative purposes. The HSB2-P samples weighed approximately 117.2 ± 5.5 g. The example of HSB2-P-BA is shown in Figure 7.2b.

Figure 7.4: Manufacture of HSB2-P

Both HSB1-P and HSB2-P were fabricated by pouring the mixture into a steel mould, and by being pressed to reach a final thickness of approximately 50 mm. They were then cured for 15 min under the thermopress which plates were heated to 190 °C

to allow cross-linking with the hemp shiv. Each sample was then cut to a final size of approximately 100 mm $\times$ 100 mm $\times$ 50 mm.

Both boric and phosphoric acids start to dehydrate at temperatures below that of the curing temperature, which might cause some of their loss already during the manufacturing process. However, TGA results by Colson, Bourebrab, et al. (2019) of hemp shiv treated with the mixture of magnesium sulfate and boric or phosphoric acid demonstrated no significant mass loss which could be attributed to the treatment below 200 °C. It might be due to either the action of magnesium sulfate protecting the coated hemp shiv with the acids, or the dehydration reaction of these acids not occurring fast enough within the time necessary to reach pyrolysis temperature of the treated shiv, under the given TGA conditions for the experiment.

With a mineral binder: HSB-M

The samples with a mineral binder HSB-M were produced so that equal quantities of hemp shiv were mixed with different magnesium oxide and magnesium sulfate contents, with the latter two decreasing from type 1 to type 3. The manufacturing procedure was similar to the other samples in the sense that Biofibat hemp shiv were thoroughly mixed with $MgSO_4$ in a food processor for three minutes, to which MgO was added and thoroughly blended for another three minutes, as illustrated in Figure 7.5. The mixture was then poured into the steel mould, pressed for a final thickness of approximately 55 mm, and placed in the thermopress at the same conditions as the HSB-P samples, 190 °C for 15 min. The example of HSB-M-2 is shown in Figure 7.2c.

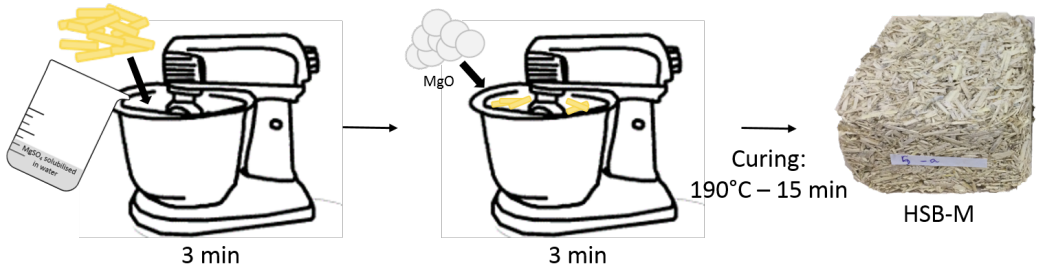

Figure 7.5: Manufacture of HSB-M

Multi-layered boards: HSB-ML

The multi-layered hemp shiv boards HSB-ML were manufactured so that 80 % in height of each sample were made of 92 wt% hemp shiv and 8 wt% polysaccharides binder (similar to HSB1-P-control), which thickness was 40 mm. The other 20 % were made of hemp shiv and stabilised earthen clay (commercially available earthen clay made from a magnesite cement formulation, which exact compositions cannot be disclosed). This clay-rich layer was 10 mm thick. The manufacturing process is illustrated in Figure 7.6. In the case of samples HSB-ML-2:1, the clay-rich layer was made of twice the solid quantity of clay to hemp shiv, and there were four times more clay than shiv in samples HSB-ML-4:1. The two parts were only thermally pressed to bind, at 190 °C for 15 min. These two types of hemp shiv boards can be seen in Figure 7.2d.

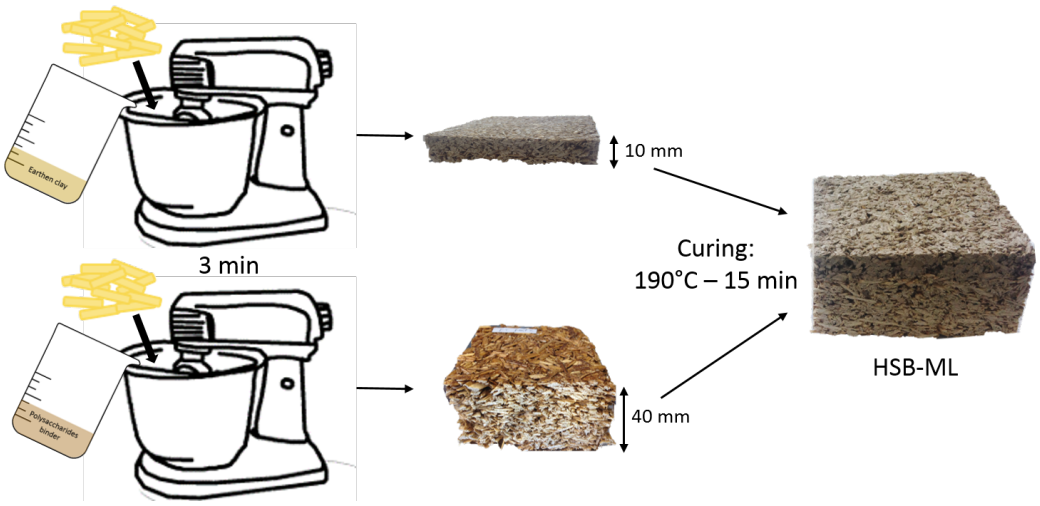

Figure 7.6: Manufacture of HSB-ML

7.3.2 Testing method

Several methods exist to assess the different characteristics of thermal decomposition of materials, which were summarised by Witkowski et al. (2016). The UL-94 test (IEC 60695-11-10) gives indication on ignitability and rate of flame spread, which is commonly used for polymeric materials to analyse their contribution in flaming combustion. The Limiting Oxygen Index test (ISO 4589-2) focusses on the ease of extinction

of materials. Flammability of construction materials is often analysed via the Single Burning Item test (EN 13823), which determines the fire growth rate and total heat released, but usually utilises two walls in a corner disposition without ceiling, therefore can be considered a pilot- to real-scale testing.

Bench-scale assessment of flammability of materials can be performed via cone calorimetry, as demonstrated in Section 6.2.3 for loose hemp shiv, following the procedure described in ISO 5660-1 (International Organization for Standardization 2015) and ASTM E1354 (ASTM 2017b). Such method only requires small samples (100 mm $\times$ 100 mm $\times$ t mm with 50 mm $<$t$<$ 100 mm), which makes the procedure simpler whilst providing enough information to understand ignitability and heat release rate of both flaming and smouldering combustions. Additionally, ignition can be piloted (as is the case in this study) or not if heat exposure is sufficient to ignite the materials, which is the case for high heat fluxes. For the composite materials analysed in this chapter, both flaming and smouldering phenomena were of interest. An exposure to a heat flux greater than the critical heat flux for smouldering ignition was then desired, therefore greater than 8.0$\pm$2.5 kW/m^2 as McLaggan (2016) measured for hemp-lime, and 12 kW/m^2 for wood (Drysdale 2011). It was therefore decided to expose the samples to a heat flux of 15 kW/m^2 after preliminary results. This chosen heat flux was high enough for flaming combustion to occur, but deliberately low compared to usual cone calorimeter tests at 50 kW/m^2 to prevent the combustion process being only thermally driven.

For this study, the sampling is shown in Figure 7.7. In a similar manner to the test method used for the loose hemp shiv samples in Section 6.2.3, each hemp shiv board was insulated with one layer of aluminium foil, then placed on the sample holder. Samples of the HSB1-P type were fitted in the stainless steel mould which was lined with ceramic paper insulation and aluminium foil to overcome the slightly smaller dimensions of the samples and ensure a close fit in the sample holder. The retainer was installed over the sample, and the complete assembly put on the scale in the combustion chamber for testing.

Figure 7.7: Sampling method of hemp shiv boards for cone calorimeter testing. Top left photograph shows a sample of the HSB-P type, which has been insulated with aluminium foil and placed onto the sample holder (bottom left). The retainer was then adapted on the cell holder (bottom middle), which was then mounted onto the scale in the combustion chamber (right photograph).

7.4 Flammability of hemp shiv boards

All the tests carried out in this chapter were done with the cone calorimeter, therefore the results are expressed according to the nomenclature introduced in Table 6.2. The purpose of this section is to understand the combustion process of the hemp shiv boards (HSB), and how this was affected by the presence of fire retardant additives including silica. The approach followed was similar to that presented in Section 6.3.3, and using key parameters described in Table 6.2.

7.4.1 Silica effect on pyrolysis, ignition, and flaming

The effect of silica particles within the hemp shiv board was analysed, whether they were introduced in the binder (HSB1-P-3N1), or on the hemp shiv (HSB2-P-3N1). The flammability of the hemp shiv board was only slightly affected when silica particles were mixed with the polysaccharides binder, with a delayed ignition of 11 s between

the control and HSB1-P-3N1 type (see values in Table 7.2a). Figure 7.8a shows that the peak of mass loss rate ($\dot{m}_{max}$) was similar for both types, but the flaming was much longer for the samples with silica.

For the second type of HSB-P board, the effect was the fire retardant additives was more notable. The time to ignition (TTI), flaming duration, and mass loss rate (MLR) were all affected (Table 7.2b). In all cases, the time to ignition was longer, 123 s on average, compared to 80 s for the control samples and 112 s for the sample treated with magnesium sulfate only (HSB2-P-10MgS). The flaming period was also shorter than those two types of samples, by on average 30 s for the control and by 15 s for HSB2-P-10MgS. The peak in MLR was delayed and the magnitude was slightly reduced. The pyrolysis of hemp shiv boards was altered by the combined presence of silica and $MgSO_4$, which is highlighted by having smaller values of $\dot{m}$ for HSB2-P-3N1 than for HSB2-P-control, and a MLR curve much below that of the control samples. Additionally, the pyrolysis rate of HSB2-P-3N1 seemed slower than that of HSB2-P-10MgS, since the MLR returned quicker to lower values after its peak, therefore highlighting how silica could enhance the already improved properties of a fire retardant treated material. These factors indicate that the addition of magnesium sulfate had a positive impact on the fire performance of these products under the conditions tested, and even more so when combined with silica, which highlights their synergistic effect.

These results suggest that the combination of magnesium sulfate and silica can influence the ignition time of the samples by delaying the onset of pyrolysis and hence the release of flammable gases upon heat exposure. Moreover, the $\dot{m}_{max}$ for all the HSB2-P samples averaged $10{\times}10^{-4}$ wt%/s, whereas it reached twice as much for all the HSB1-P type of samples. This difference is likely to be due to the presence of $MgSO_4$ in the second type, but also to a lesser extent to the greater density of those samples, since $\dot{m}_{max} = 21{\times}10^{-4}$ wt%/s for HSB1-P-control, and was halved for HSB2-P-control.

The gas analyses for the first 500 s of combustion of HSB2-P-control, HSB2-P-10MgS, and HSB2-P-3N1 are shown in Figure 7.9. Because the gas analyser is positioned after the exhaust duct, the gas concentration data has a delay compared to the

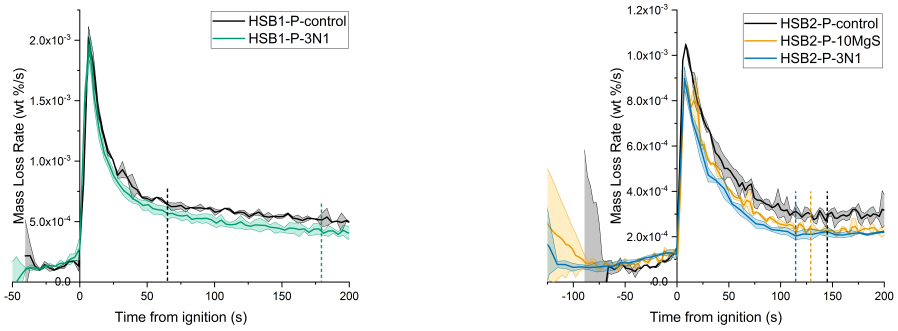

(a) HSB1-P: silica in the binder

(b) HSB2-P: silica on the hemp shiv

Figure 7.8: Effect of silica demonstrated by the Mass Loss Rate curves of HSBx-P-control and HSBx-P-3N1, plotted from the time to ignition until 200 s. The shaded areas represent the standard deviation amongst one type of sample, and the dashed lines correspond to the end of the flaming periods of HSBx-P-control (black), HSBx-P-3N1 (green or blue respectively), as well as HSB2-P-10MgS (orange).

time of occurrence. This delay was introduced to plot the concentration curves and in the calculations of time to $\dot{q}''_{max}$ so that the time to ignition (TTI) and time at which the concentration of oxygen diminished would correspond (the TTI of these samples are shown in the comparative bar graph in Figure 7.11). Consequently, it was expected to observe the $\dot{q}''$ increasing significantly, and peaking around the same time than when the concentration of O_2 reached their lowest values. Besides the notable delay of TTI between the control and 3N1 samples, the mix of $MgSO_4$ and silica induced reduced yields of CO_2 and CO during the smouldering part of combustion.

7.4.2 The smouldering problem

Towards the end of the flaming period, smouldering became the dominant combustion process. Smouldering of samples HSB2-P-control, HSB2-P-10MgS, and HSB2-P-3N1 were determined as a sudden increased concentration of CO, which is illustrated in Figure 7.9 by the green shaded areas. It remains difficult to be certain of the timings of such occurrences and to quantify the effects of smouldering alone, as its ignition overlapped with flaming combustion.

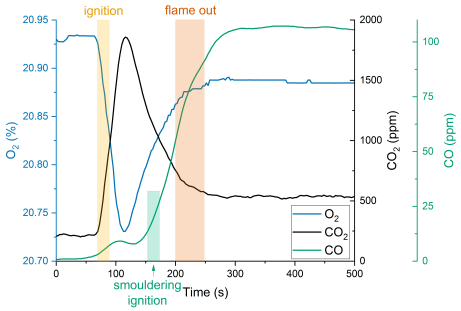

(a) HSB2-P-control

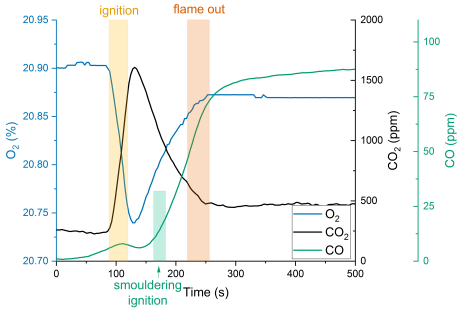

(b) HSB2-P-10MgS

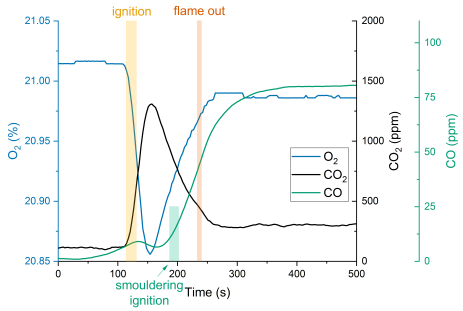

(c) HSB2-P-3N1

Figure 7.9: Gas analyses of samples HSB2-P-control, HSB2-P-10MgS, and HSB2-P-3N1 by cone calorimetry. The shaded areas correspond to ignition (flaming) and time of flame out as observed visually (and described in Table 7.2b), as well as the smouldering ignition determined from the CO yield. The average values of concentrations are shown, but the standard deviations are omitted for clarity.

The smouldering phase is characterised by a much higher ratio of CO/CO_2 compared to the flaming combustion phase (Hadden 2011). Smouldering typically occurs at lower temperatures than flaming, which means that upon exposure to a relatively low heat flux (around 10 kW/m^2), materials can ignite by smouldering only, with no flaming (Hadden 2011; McLaggan 2016). Traditionally, standard test methods do not take into account smouldering for the performance assessment of a material under heat exposure, which can lead to usage of combustible materials without proper understanding of their combustion behaviour.

All the hemp shiv board composites studied in this chapter experienced smouldering, which was expected due to the nature of hemp shiv and the structure of the

material. The CO concentration data presented in Figure 7.9 show an increase during the flaming period, which was attributed to the beginning of smouldering combustion. Figure 7.10 demonstrates a sample of HSB2-P-3N1 before and after exposure to 15 kW/m^2. The board in Figure 7.10b was photographed over an hour after having been removed from the combustion chamber and it is evident that smouldering continued beyond the end of the experiment. Rein (2009) described the energy balance at the smouldering front, which demonstrated that the heat released by the reaction and the heat losses to the environment were the two major terms influencing the velocity of propagation of the smouldering front. This means that once the samples were removed from the combustion chamber and thus the external heating system stopped, smouldering was sustained until the sample lost sufficient heat externally, which was observed over an hour after the end of the experiments.

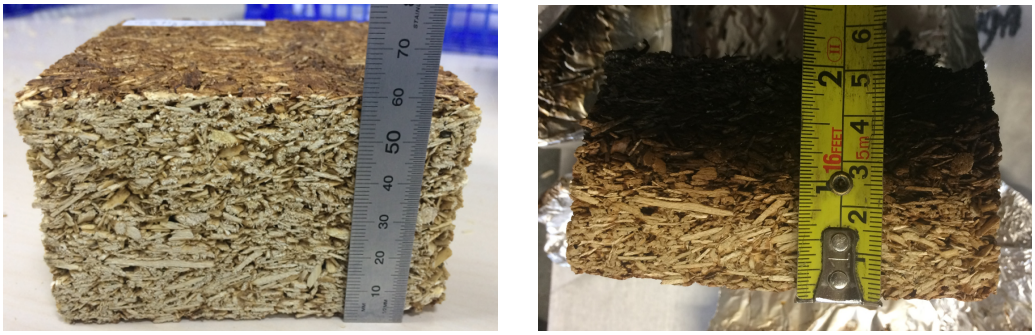

(a) before testing **(b)** after testing

Figure 7.10: Sample of HSB2-P-3N1 before and after testing with the cone calorimeter. The sample was photographed over an hour after having been removed from the combustion chamber, during which period smouldering combustion continued despite the absence of external radiant heat flux.

7.5 Comparative study with commercially available fire retardants

In order to assess the comparative effectiveness of silica as a fire retardant, a series of studies using commonly available fire retardants is presented. The criteria of interest

are: time to ignition (TTI), mass loss rate (MLR, $\dot{m}$), heat release rate (HRR, $\dot{q}$), and heat of combustion ($\Delta h_{c,eff}$). An overview of all results is given first, followed by a more in-depth analysis per type of fire retardant additive.

7.5.1 Overview results of all treatments

Time to ignition and mass loss rate

As means of comparing the different treatments in a first instance, the time to ignition of each type of HSB-P sample is shown in Figure 7.11. The samples in which minerals were added (mineral binder for the HSB-M series and multi-layered samples with a clay-rich layer HSB-ML) did not flame, therefore their ignition occurred during smouldering. Hence they are not shown in Figure 7.11, but their case is discussed in Section 7.5.5. A clear difference can be observed between the HSB1-P and HSB2-P series, as the first generally ignited less than 60 s after having being exposed to the radiant heat flux of 15 kW/m^2.

The mass loss analyses are reported in Table 7.2a. Overall, the samples ignited by flaming, reached the peak of MLR shortly after (around 6 s) and flamed for a period of time. Once the flame went out, the combustion process changed from flaming to sustained smouldering. Plotting the $\dot{m}_{max}$ values against the times they were reached for each type of HSB1-P boards allowed the assessment of each fire retardant additive performance (Figure 7.12a). Similarly to Figure 6.10, the dashed lines correspond to the median value between the lowest $\dot{m}_{max} - stdev$ and highest $\dot{m}_{max} + stdev$, and likewise for the time to $\dot{m}_{max}$. Only one sample of HSB2-P-Syn out of three flamed, whose results are shown in Table 7.2b and its $\dot{m}_{max}$ plotted in Figure 7.12b. Because of this, its values of $\dot{m}_{max}$ and associated time were not taken into account in the calculation of the median values represented by the dashed lines of Figure 7.12b.

The HSB2-P types ignited later than HSB1-P, up to 165 s after the spark was switched on in their gas phase (this value was obtained for one sample of HSB2-P-20MgS). This phenomenon could be explained by the presence of magnesium sulfate in the HSB2-P type, and to a lesser extent their denser structures (highlighted by the difference in time to ignition between HSB1-P-control and HSB2-P-control). Typically, their

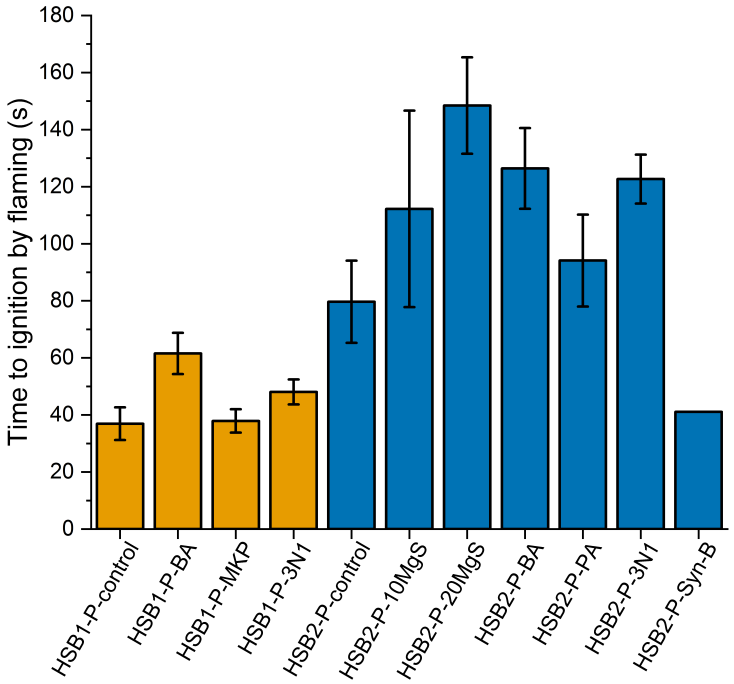

Figure 7.11: Comparison of the time to ignition of all samples that flamed (HSB-P types). The error bars represent the standard deviation within one type of sample.

$\dot{m}_{max}$ was about half of what was obtained for the HSB1-P samples. Such behaviour was probably observed as the HSB2-P samples were denser, therefore the hemp shiv boards could limit oxygen ingress into their structure. Indeed, Figures 7.2a and 7.2b showed a significant difference in the stacking of the hemp shiv pieces.

Apart from HSB2-P-control, all the HSB2-P types yielded $\dot{m}_{max}$ values in the bottom half part of the plot shown in Figure 7.12b (which are reported in Table 7.2b), although HSB2-P-3N1 was just at the limit. Considering the relatively low loading levels of additives in the formulations of each type of sample, their fire performance could still be positively affected by the presence of fire retardant additives, especially that of $MgSO_4$.

Heat release rate and heat of combustion

The heat released upon burning the hemp shiv boards was monitored via the oxygen concentration, according to the method described by Janssens (1991). The values

Table 7.2: Mass loss rate values obtained during combustion of HSB1-P and HSB2-P by cone calorimetry: times to ignition and flame out, peaks of mass loss rate and their associated times, residual mass loss after flaming and after 2400 s. The values are given with their standard deviation calculated from each sample of the same population. Due to the slight variations, the $\dot{m}_{max}$ values are given with more significant figures.

(a) HSB1-P samples

Sample	Flaming times (s)			Mass Loss Rate		Residual mass (wt%)	
	Ignition	Flame out	period	$\dot{m}_{max}$ ($\times 10^{-4}$wt%/s)	time (s)	at flame out	2400 s
HSB1-P-control	37 ± 6	102 ± 1	65 ± 5	21.15 ± 0.12	44 ± 6	93.2 ± 0.2	23.2 ± 2.0
HSB1-P-BA	62 ± 7	129 ± 9	68 ± 4	19.00 ± 0.05	68 ± 7	94.0 ± 0.5	37.9 ± 8.5
HSB1-P-MKP	38 ± 4	185 ± 21	147 ± 18	21.20 ± 0.10	44 ± 4	89.4 ± 1.3	31.0 ± 3.7
HSB1-P-3N1	48 ± 4	227 ± 19	179 ± 22	20.17 ± 0.09	54 ± 4	87.9 ± 1.6	34.4 ± 6.5

(b) HSB2-P samples

Sample	Flaming times (s)			Mass Loss Rate		Residual mass (wt%)	
	Ignition	Flame out	period	$\dot{m}_{max}$ ($\times 10^{-4}$wt%/s)	time (s)	at flame out	2400 s
HSB2-P-control	80 ± 14	225 ± 33	145 ± 48	10.70 ± 0.14	87 ± 14	92.6 ± 0.3	40.9 ± 2.5
HSB2-P-10MgS	112 ± 34	241 ± 31	129 ± 3	9.08 ± 0.16	120 ± 34	93.8 ± 0.3	51.9 ± 0.6
HSB2-P-20MgS	148 ± 17	249 ± 10	101 ± 7	7.63 ± 0.11	157 ± 17	95.2 ± 0.1	62.8 ± 0.4
HSB2-P-BA	126 ± 14	213 ± 14	87 ± 2	8.89 ± 0.18	135 ± 14	95.3 ± 0.1	59.6 ± 0.8
HSB2-P-PA	94 ± 16	213 ± 20	119 ± 6	8.50 ± 0.27	101 ± 16	94.8 ± 0.2	58.3 ± 0.9
HSB2-P-3N1	123 ± 9	237 ± 4	115 ± 5	9.21 ± 0.43	130 ± 9	94.5 ± 0.2	59.7 ± 1.3
HSB2-P-Syn-B †	41	77	36	8.41	49	98.1	55.9

† Only one sample out of three of HSB-P-Syn flamed, whose results are reported here.

Table 7.3: Mass loss rate analysis of combustion of HSB-M and HSB-ML by cone calorimetry. The averages of $\dot{m}$ were calculated over the 2400 s of test. The values are given with their standard deviation calculated from each sample of the same population.

Sample	Residue at 2400 s (wt%)	Mass Loss Rate ($\times 10^{-5}$ wt%/s)		
		$\dot{m}_{avg,2400}$	$\dot{m}_{max}$	time (s) of $\dot{m}_{max}$
HSB-M-1	87.5 ± 0.7	5.23 ± 1.46	7.14 ± 0.21	717 ± 157
HSB-M-2	82.9 ± 0.1	7.17 ± 2.51	10.47 ± 0.50	482 ± 14
HSB-M-3	76.8 ± 0.6	9.74 ± 2.65	13.87 ± 0.36	425 ± 93
HSB-ML-2:1	59.2 ± 7.4	17.2 ± 5.8	28.9 ± 7.1	167 ± 4
HSB-ML-4:1	73.8 ± 1.6	11.0 ± 3.0	1st peak: 12.4 ± 0.3 2nd peak: 15.1 ± 1.4	272 ± 14 725 ± 70

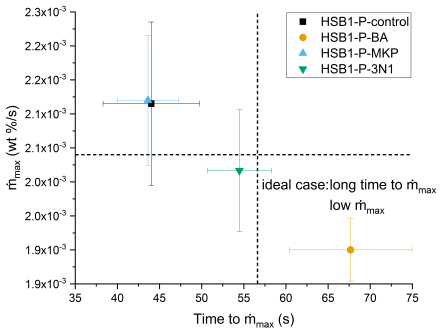

(a) Results for HSB1-P, as seen in Table 7.2a. The dashed lines correspond to $t = 57$ s and $\dot{m}_{max} = 20.45 \times 10^{-4}$ wt%/s.

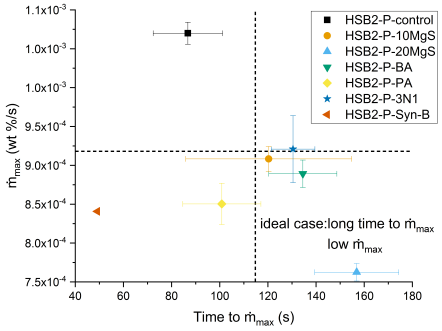

(b) Results for HSB2-P, as seen in Table 7.2b. The dashed lines correspond to $t = 115$ s and $\dot{m}_{max} = 9.18 \times 10^{-4}$ wt%/s (sample HSB2-P-Syn was not taken into account in the calculation of these median values).

Figure 7.12: Summary of $\dot{m}_{max}$ and their times for hemp shiv shiv boards with polysaccharides binder HSB1-P and HSB2-P.

reported in Table 7.13 were obtained via similar calculations to those explained and made in Section 6.3.3. Figure 7.13 shows the values of peak of HRR, $\dot{q}''_{max}$, and their associated times for the HSB1-P and HSB2-P series of hemp shiv boards. There was a clear difference between HSB1-P and HSB2-P types in terms of $\dot{m}_{max}$ values, being halved for the samples HSB2-P containing magnesium sulfate (or the commercial flame retardant in the case of HSB2-P-Syn). This was however not so much the case for the $\dot{q}''_{max}$ values, which were more clustered around a value of 80–90 kW/m^2. The heat release analysis of HSB1-P series is described by its key values in Table 7.4a, and that of HSB2-P series in Table 7.4b. The neat difference between the values of $\dot{q}''_{max}$, $q''_{tot,2400}$, and $\Delta h_{c,eff,fl}$ obtained for the HSB2-P-control and the other HSB2-P samples suggests the positive effect on either type of fire retardant treatment used on the hemp shiv.

Table 7.4: Heat release analysis of combustion of hemp shiv boards HSB1-P and HSB2-P by cone calorimetry, calculated from the oxygen consumption method (Janssens 1991): total heat released over 2400 s, peaks of heat release rate and their associated times, and effective heat of combustion (during flaming and after flame out for the smouldering one). The values are given with their standard deviation calculated from each sample of the same population.

(a) HSB1-P samples

Sample	Heat Release Rate		$q''_{tot,2400}$ (MJ/m^2)	$\Delta h_{c,eff,period}$ (kJ/wt%)	
	$\dot{q}''_{max}$ (kW/m^2)	time (s)		flaming	smouldering
HSB1-P-control	92.6 ± 13.1	64 ± 7	28.8 ± 15.9	35.2 ± 6.3	36.4 ± 22.7 ×10^3
HSB1-P-BA	60.1 ± 4.0	86 ± 8	15.6 ± 5.6	21.0 ± 4.5	24.4 ± 0.9 ×10^3
HSB1-P-MKP	93.7 ± 2.2	57 ± 2	42.4 ± 14.5	75.3 ± 4.5	60.6 ± 26.8 ×10^3
HSB1-P-3N1	83.1 ± 1.5	67 ± 5	27.9 ± 1.0	69.4 ± 2.5	38.1 ± 0.2 ×10^3

(b) HSB2-P samples

Sample	Heat Release Rate		$q''_{tot,2400}$ (MJ/m^2)	$\Delta h_{c,eff,period}$ (kJ/wt%)	
	$\dot{q}''_{max}$ (kW/m^2)	time (s)		flaming	smouldering
HSB2-P-control	106.0 ± 2.8	76 ± 13	63.7 ± 0.5	99.0 ± 6.2	104.2 ± 5.4 ×10^3
HSB2-P-10MgS	87.3 ± 2.2	103 ± 33	43.1 ± 6.9	74.2 ± 3.1	85.1 ± 13.9 ×10^3
HSB2-P-20MgS	80.2 ± 2.8	142 ± 19	39.8 ± 5.9	62.1 ± 2.8	103.8 ± 18.2 ×10^3
HSB2-P-BA	82.9 ± 1.6	121 ± 15	46.5 ± 1.6	59.4 ± 0.8	114.0 ± 7.1 ×10^3
HSB2-P-PA	79.1 ± 5.2	87 ± 12	30.4 ± 15.1	63.3 ± 4.9	65.5 ± 38.7 ×10^3
HSB2-P-3N1	85.0 ± 1.3	116 ± 10	34.2 ± 1.3	66.2 ± 1.7	79.2 ± 2.2 ×10^3
HSB2-P-Syn-B †	40.9	27	30.8	14.9	69.5 ×10^3

† Only one sample out of three of HSB-P-Syn flamed, whose results are reported here.

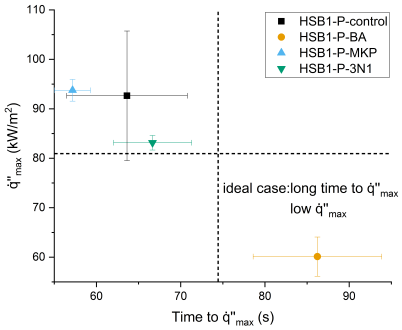

(a) Results for HSB1-P, as seen in Table 7.4a. The dashed lines correspond to $t = 74$ s and $\dot{q}''_{max} = 80.9$ kW/m^2.

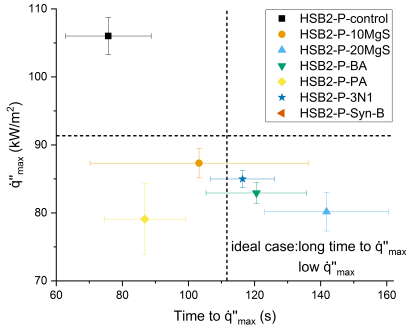

(b) Results for HSB2-P, as seen in Table 7.4b. The dashed lines correspond to $t = 112$ s and $\dot{q}''_{max} = 91.3$ kW/m^2 (sample HSB2-P-Syn-B was not taken into account in the calculation of these median values, and is not shown in the Figure due to its low values).

Figure 7.13: Summary of $\dot{q}''_{max}$ and their times for hemp shiv shiv boards with polysaccharides binder HSB1-P and HSB2-P.

7.5.2 Effect of magnesium sulfate on its own

Time to ignition and mass loss rate

Magnesium sulfate heptahydrate produces water when heated, which dilutes and cools the flame down. Although pyrolysis might have occurred at the same time as the untreated hemp shiv boards HSB2-P-control, it was still expected to observe delayed ignition. Samples HSB2-P-10MgS ignited 112 s after the start of the experiment, which is 32 s later than the control samples, and the flaming period decreased by 16 s. With twice the quantity of $MgSO_4$, HSB2-P-20MgS ignited 68 s after HSB2-P-control and their flaming period was 44 s shorter. The peak of MLR was slightly reduced for both HSB2-P-10MgS and HSB2-P-20MgS, and more so for the latter, which $\dot{m}_{max}$ was the lowest of the HSB2-P series. Although the residual mass at flame out was not significantly different between these two samples and the control one, the final residue after 40 min was 11 wt% and 22 wt% greater for HSB2-P-10MgS and HSB2-P-20MgS respectively than HSB2-P-control. Under those experimental conditions, the presence of $MgSO_4$ successfully acted as a fire retardant by delaying ignition, reducing the peak of MLR, shortening the flaming period, and yielding greater residues, thus limiting the extent of the combustion process of the hemp shiv boards.

Heat release rate and heat of combustion

The peak of HRR dropped from 106.0 kW/m^2 (HSB2-P-control) to 87.3 kW/m^2 and 80.2 kW/m^2 for HSB2-P-10MgS and HSB2-P-20MgS respectively, whilst $q''_{tot,2400}$ decreased from 63.7 MJ/m^2 to 43.1 MJ/m^2 and 39.8 MJ/m^2 once magnesium sulfate was present. Similarly, $\Delta h_{c,eff,fl}$ was reduced from 99.0 kJ/wt% (control) to 74.2 kJ/wt% and 62.1 kJ/wt% for the samples treated with $MgSO_4$. This clearly demonstrates the effect of $MgSO_4$ on the heat released by the systems as water evaporated diluting the flame and cooling it. However, $\Delta h_{c,eff,sm}$ was equivalent between HSB2-P-control and HSB2-P-20MgS, and lower for HSB2-P-10MgS. Considering the standard deviation reported, it is likely that some samples with magnesium sulfate produced much more heat during smouldering than the others. This would suggest that variation within

a same type of sample occurs, which is probably due to the nature of the material tested, e.g. cellulose-based, and as such the exact chemical composition differs from one piece to another. Moreover, in order to better quantify the effect of $MgSO_4$ on the smouldering process, additional test would be required, such as monitoring the heat released under a lower heat flux radiation, so that only combustion by smouldering is observed.

7.5.3 Boron-based compounds

Time to ignition and mass loss rate

Boric acid was used as a fire retardant which similarly to $MgSO_4, 7\,H_2O$ and phosphorus-based compounds is a gaseous phase diluent as it produces water vapour when heated (Equation 7.2). Samples HSB1-P-BA did not contain any magnesium sulfate therefore any effect of the treatment on flammability of the samples is likely to be associated to the action of the boron compounds. Ignition of HSB1-P-BA occurred the latest amongst the HSB1-P series of samples, 25 s after HSB1-P-control, although their flaming period was fairly equivalent to that of the control, and so was their residual mass at flame out. The peak of MLR was also the lowest of the HSB1-P series, at 19×10^{-4} wt%/s, which made it the only type of the series to be present in the bottom right quadrant of Figure 7.12a, corresponding to a longer time to ignition and a relatively low $\dot{m}_{max}$ compared to the other HSB1-P samples. The final residual mass was however 15 wt% greater than that of HSB1-P-control, thus suggesting that the release of water vapour had a greater effect after flame out.

Heat release rate and heat of combustion

The samples only treated with boron-compounds ignited later, flamed less, and also released the least heat during flaming amongst the HSB1-P series. The latter was demonstrated by the lowest peak of HRR (60.1 kW/m^2), and lowest $\Delta h_{c,eff,fl}$ averaging 21.0 kJ/wt%. Over the course of the entire experiment (40 min), the HSB-1-P-BA samples released 15.6 MJ/m^2 on average, as opposed to almost double for the other types

of HSB1-P samples. Smouldering combustion seemed also to be affected by the action of boron-compounds, as the average $\Delta h_{c,eff,sm}$ was calculated at 24.4 MJ/wt%. Such result suggests that boric acid might have continuously decomposed and produced water vapour throughout the experiment, which could have cooled the surrounding atmosphere.

7.5.4 Phosphorus-based compounds: monopotassium phosphate (MKP), ammonium polyphosphate (APP), and phosphoric acid (PA)

Time to ignition and mass loss rate

These three types of phosphorus-based compounds are considered gas diluents when heated. Similarly to HSB1-P-BA, samples HSB1-P-MKP did not contain any $MgSO_4$. These samples exhibited very similar characteristics in terms of TTI, $\dot{m}_{max}$ and associated times than HSB1-P-control. Both types ignited 38 s after being exposed to radiant heat, and reached a value of $\dot{m}_{max}$ greater than 21.2×10^{-4} wt%/s. However, the samples with MKP flamed for over twice as long: either not enough water evaporated from the chemical reactions occurring during the phosphate degradation which would have diluted the flame enough to reduce its extent, or the presence of phosphoric acid catalysed the chemical reactions of degradation, which thus occurred earlier and for longer. Just as HSB1-P-BA, the residual mass of HSB1-P-MKP at the end of the experiment was greater than that observed for the control samples by 8 wt%.

The ammonium polyphosphate solution is commercialised as a flame retardant, and was applied on the hemp shiv similarly to the other fire retardant additives of the HSB2-P type, although no $MgSO_4$ was present. Only one sample of HSB2-P-Syn out of three flamed, whose results are shown in Table 7.2b and its $\dot{m}_{max}$ plotted in Figure 7.12b. Despite yielding the lowest $\dot{m}_{max}$ of the HSB2-P type of hemp shiv boards, HSB2-P-Syn-B ignited quickly compared to the others, after only 41 s. Being a flame retardant, it was expected not to observe any flaming which was the case for two samples. Should only a short flaming period be monitored, which was indeed the fact as it lasted only 36 s, it was anticipated for it to potentially occur once the surface temperature would have been higher, thus much later. The final residue (55.9 wt%) suggests

that the ammonium polyphosphate did not protect the hemp shiv board better from combustion than other treatments, as its value was very close to those obtained for the other samples with $MgSO_4$. Although two samples of HSB2-P-Syn did not undergo flaming ignition, they did sustain a smouldering fire. The samples that did not flame experienced a slower pyrolysis rate when exposed to an external heat flux, but their degradation nonetheless. Indeed, their average final residual mass (not taken into account in Table 7.2b) was measured at 59.7 wt% after 40 min, which is not far off the final residual mass of the sample that flamed. This highlights the complexities of delivering a fire retardant product, which prevents thermal degradation occurring in both flaming and smouldering combustion.

The presence of H_3PO_4 combined with $MgSO_4, 7\,H_2O$ did not seem to delay ignition and and reduce flaming. Ignition of samples HSB2-P-PA occurred 94 s after being exposed to radiant heat, which was 14 s later than the control samples, but 18 s earlier than when only magnesium sulfate is present as additive in the same quantities (HSB2-P-10MgS). However, a slightly lower $\dot{m}_{max}$ was recorded for HSB2-P-PA than HSB2-P-10MgS, thus suggesting that even though flaming occurred, the combustion rate during this period was slightly slower, which would be why the residual mass at flame out was greater to some extent. The addition of phosphoric acid also seemed to decrease the smouldering combustion rate, as the final residual mass was measured at 58.3 wt% for HSB2-P-PA compared to 51.9 wt% and 40.9 wt% for HSB2-P-10MgS and HSB-2-P-control respectively.

Heat release rate and heat of combustion

Samples HSB1-P-MKP produced the most heat during the 40 min of experiment (their $q''_{tot,2400}$ was calculated at 42.4 MJ/m^2), with a peak of HRR equivalent to that of the control samples. This behaviour was therefore seen in the greatest values of $\Delta h_{\text{c,eff}}$ of the series. During flaming, the effective heat of combustion was calculated at 75.3 kJ/wt% (compared to 35.2 kJ/wt% for HSB1-P-control) and 60.6 MJ/wt% during smouldering (compared to 36.4 MJ/wt%). This analysis means that the combustion of a hemp shiv board in which MKP was incorporated actually aggravated the combus-

tion process, as additional exothermic reactions occurred, probably catalysed by the phosphoric acid released.

The sample with ammonium polyphosphate flame retardant which flamed (HSB2-P-Syn-B) indeed presented the lowest value of $\dot{q}''_{max}$ at 40.9 kW/m^2, and lowest $\Delta h_{\text{c,eff,fl}}$ at 14.9 kJ/wt%. It is likely that this additive also released radicals which poisoned the flame, therefore completely impeding flaming for two samples out of three, and reducing it for the remaining one.

The lowest values of $\dot{q}''_{max}$ and $q''_{tot,2400}$ of the HSB2-P series (not taking into account HSB2-P-Syn-B) were obtained for samples HSB2-P-PA, at 79.1 kW/m^2 and 30.4 MJ/m^2 respectively. Compared to HSB2-P-control, the $\Delta h_{\text{c,eff,fl}}$ value calculated for HSB2-P-PA was greatly reduced, as well as $\Delta h_{\text{c,eff,sm}}$. It demonstrates that the heat released during this experiment could be significantly decreased by the combined chemical actions of phosphoric acid, recombination of radicals produced, and magnesium sulfate.

7.5.5 Preventing flaming by mineral addition

Another solution to reduce the thermal degradation bio-materials is to prevent flaming by increasing the quantity of non-combustible material in a sample. The first set of samples with a mineral binder tested in this study was HSB-M. The ratios of MgO to hemp shiv decreased from HSB-M-1 to HSB-M-3 (Table 7.1), so that the effect of magnesia could be demonstrated. Combustion of all HSB-M samples occurred via smouldering only, therefore validating the hypothesis that flaming could be prevented with 25 wt% of the sample being mineral.

The residual mass values of the HSB-M types are reported in Table 7.3. Expectedly, the more MgO in the sample, and the greater the residue, with 87.5 wt% remaining of HSB-M-1 over 2400 s (which contained 33 wt% of MgO), whereas 76.8 wt% of HSB-M-3 were left (the samples were made with 25 wt% of MgO). Considering the compositions of each type of samples (detailed in Table 7.1), it is likely that a significant quantity of hemp shiv present initially pyrolysed via smouldering, whilst the inorganic species MgO mostly remained. In a similar pattern, the more MgO, the smaller the values of $\dot{m}_{avg,2400}$ and $\dot{m}_{max}$, which themselves were one order of magnitude smaller than

those obtained for HSB-P samples, which flamed. Equally, the time to $\dot{m}_{max}$ increased with the MgO content. This behaviour suggests that the presence of magnesia not only stopped flaming, but also prevented the thermal degradation of the samples as a whole.

Multi-layered composite boards (HSB-ML) were manufactured, which did not contain any chemically active fire retardant additives, but the upper 10 mm (directly exposed to the radiant heat flux of the cone) were made with two ratios of earthen clay (Figure 7.2d), which is thought to have a physical action by its inorganic nature, similarly to silica. The multi-layered composites only combusted by smouldering, with no flaming ignition occurring despite the spark igniter, which was also observed for the HSB-M samples. Table 7.3 shows the values of mass loss rate analysis for both types of multi-layered composites. The overall rate of pyrolysis, given by the value of $\dot{m}_{avg,2400}$ was more important for HSB-ML-2:1, with a greater $\dot{m}_{max}$ than HSB-ML-4:1. Consequently, the residue was far greater after 40 min of experiment for the samples with the greater ratio of clay:hemp shiv in the upper layer, which is HSB-ML-4:1. The MLR curves displayed in Figure 7.14 have been smoothed out as the raw mass data was subject to low amplitude variations due to the relatively slow combustion rate, therefore the values displayed on the y-axis are indicative only and do not correspond to those shown in Table 7.3. Samples of type HSB-ML-2:1 combusted faster than 4:1 samples, although the simultaneous release of CO and CO_2 occurred at similar times for the two types of samples, for the first peak for HSB-ML-4:1 shown in Figure 7.14. The $\dot{m}_{max}$ was reached earlier for HSB-ML-2:1: 167 s after the start of test compared to 272 s for samples 4:1 for the first peak.

The case of samples HSB-ML-4:1 is interesting as the MLR curve shows a second peak, at 725 s on average. It is thought that the first peak was reached after the upper layer (which thickness was 10 mm) of the composites, containing earthen clay, ignited by smouldering, whilst the second peak was due to the later smouldering ignition of the bottom part of the composite. It is likely that the clay-rich layer would have insulated the remaining of the composite beneath. This behaviour was not observed for samples HSB-ML-2:1 as heat was probably transferred faster from the clay-rich

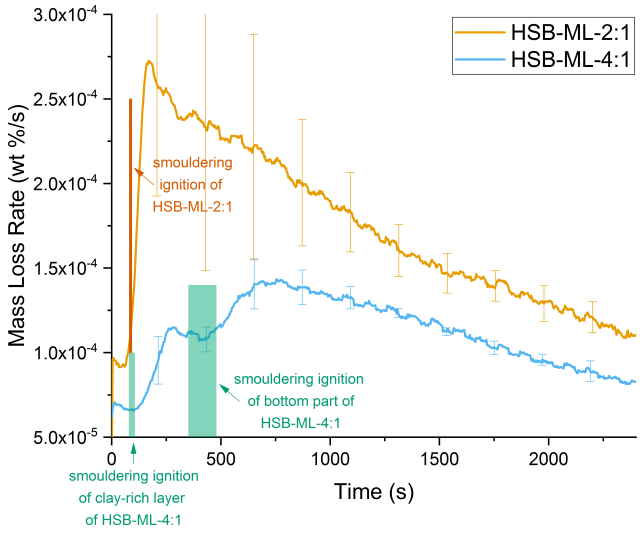

Figure 7.14: Mass Loss Rate of samples HSB-ML-2:1 and HSB-ML-4:1 by cone calorimetry. The shaded rectangles indicate the times of ignition by smouldering for samples HSB-ML-4:1, determined from a sudden increase in concentration of CO. The standard deviations are represented by the error bars to avoid overloading the graph.

layer to the rest of the sample, and thus the peaks might actually overlap. In order to verify this hypothesis, thermocouples could be placed within the sample at different heights and the gradient of temperatures could be monitored.

The HSB-ML samples were made by pressing the clay-rich layer onto the the second, thicker part. The adhesion between these two parts was not strong to withstand under heat exposure, as the clay-rich layer was clearly detached from the remaining of the sample after the experiment. Applying a layer of binder could chemically bond the two parts and thus address this issue compared to relying on physical bonding only, which was created during thermopressing.

Knowing the evolution of the concentration of O_2 permitted to calculate the HRR following the oxygen consumption method of Janssens (1991) for the samples that flamed (HSB-P series). However, only combustion by smouldering occurred for the HSB-M and HSB-ML series as flaming was prevented. Whilst smouldering occurs, the aforementioned method is not always appropriate as the oxygen consumption rate is

much slower than for flaming samples, which was evidenced by the low amplitude of O_2 concentrations in Figure 7.15. This is why the curve plotted from the data of O_2 concentration presented steps instead of a smoother signal, as it was the case for the samples made with polysaccharides binder in Figure 7.9. It was nevertheless possible to determine the ignition via smouldering of the HSB-M and HSB-ML samples, characterised by the release of CO simultaneously with CO_2. The sample of HSB-M which gas analysis is shown in Figure 7.15 yielded much less CO_2 and CO over the duration of the experiment compared to HSB2-P-control, which would suggest that the combustion of bio-materials was slower due to the presence of inorganic material. Figure 7.16 shows a sample of HSB-ML-4:1 15 min after the end of the experiment (external radiant heat flux removed), on which glowing is observed, demonstrating that combustion occurred within the sample, underneath the clay-rich layer. This also suggests the risks associated with the thermal degradation of a combustible material (such as a hemp shiv board) on which a plaster of inorganic material has been bound. It is more challenging to visually determine the combustion of the material as it occurs in depth by smouldering.

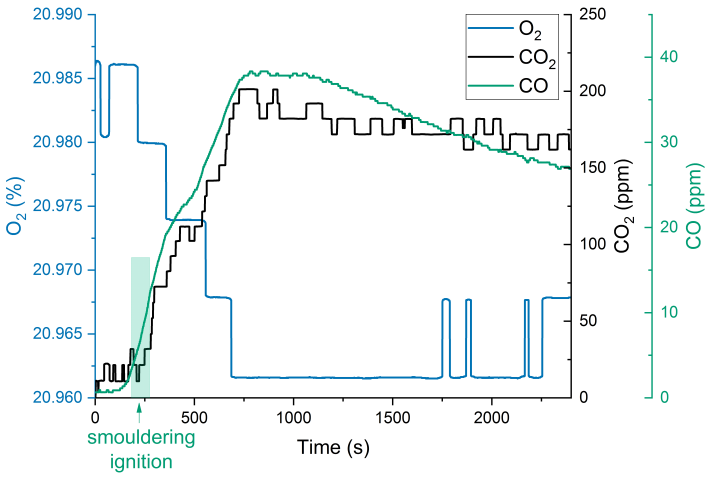

Figure 7.15: Gas analysis of a sample of HSB-M-1 by cone calorimetry. The shaded rectangle corresponds to ignition by smouldering determined from the increased yield of CO.

Figure 7.16: HSB-ML-4:1 sample glowing during smouldering combustion (photograph taken 15 min after removing the sample from the combustion chamber and from under the external radiant heat flux).

7.5.6 Concluding remarks and comparison with silica treatment

The difference between a chemical and physical action of fire retardant additives was described in Chapter 2. To summarise, all additives except silica particles used in the formulations of samples HSB1-P and HSB2-P worked on reducing the mass loss and heat released upon burning by chemical action in either the solid or gaseous phase. As for the inorganic materials, either silica particles present in the composite, either embedded in the binder or on the surface of hemp shiv, the magnesium oxide binder, and earthen clay acted thermally to increase the time to the onset of pyrolysis and reduce the rate of pyrolysis and hence mass loss rate and heat release rate (when it could be evaluated). The inorganic materials are likely to have protected the hemp shiv by absorbing part of the heat, thus less energy was available for pyrolysis.

All samples in the HSB1-P series showed an improvement in terms of mass loss rate and its peak, and final residual mass. The samples with silica particles blended with the binder (HSB1-P-3N1) demonstrated a longer longer time to ignition and thus

time to $\dot{m}_{max}$. However, their flaming period was also longer, which led to smaller residual mass at flame out (87.9 wt%), but an intermediate final residual mass value (34.4 wt%) between those of HSB1-P-BA and HSB1-P-MKP. Eventually, after 40 min of test, the three types of hemp shiv boards HSB1-P with fire retardant additives exhibited a greater residual mass of 34.5 wt% on average, more than 10 wt% over the value obtained for the control samples, which is greater than the quantity of inorganic content. This result suggests the positive influence of the additives on the protection of hemp shiv during the smouldering part of the combustion in terms of mass loss.

The analyses of heat release rate and heat of combustion of this series of samples however suggested that the presence of certain compounds could produce more heat than a hemp shiv board without treatment, which was seen for the MKP samples. The heat released calculated during this part of the combustion process reflects that HSB-1-P-MKP and HSB1-P-3N1 flamed longer. Nevertheless, for similar periods after flame out, HSB1-P-3N1 displayed a lower $\Delta h_{\text{c,eff,sm}}$ than the MKP samples. The difference between a chemically reactive compound such as MKP and silica, is that being inorganic, silica was not released and did not react during combustion. It is supposed that it remained in the residual hemp shiv board and continued to act as a heat sink during smouldering combustion.

The greater influence of silica was observed for the HSB2-P-3N1 samples, when the particles were combined with magnesium sulfate. The addition of silica for HSB2-P-3N1 compared to HSB2-P-10MgS did not affect $\dot{m}_{max}$ (the values obtained for these two types of samples were very close), but it did slightly increase the time to ignition by 11 s, and decreased the flaming period by 14 s. Silica also prevented the combustion of the hemp shiv board to an equivalent extent than HSB2-P-BA and HSB2-P-PA in terms of final residual mass.

No specific fire retardant additives significantly affected the smouldering period, as the $\Delta h_{\text{c,eff,sm}}$ of all the samples were of similar values. It is only supposed that samples with silica particles presented an advantage as silica was likely not to chemically react during the combustion process, and consequently remain unchanged within the combusted hemp shiv boards. This behaviour was especially observed for the series

HSB-M and HSB-ML for which flaming was prevented, but smouldering was sustained. A greater content of MgO induced a slower combustion rate, as measured by greater residual mass after 40 min of external radiant heat exposure, and lower $\dot{m}_{avg,2400}$ values. Observing HSB-ML samples after the experiment also showed that the clay-rich layer insulated the hemp shiv core of the composite, delayed and reduced its thermal degradation but did not stop it. Smouldering occurred in depth, which under real-life scenarios might remain unseen and undetectable. More research is required to understand smouldering, its mechanisms and effects on bio-materials, as commercially available solutions do not often account for this phenomenon.

All the fire retardant additives tested in this study influenced the fire performance of the hemp shiv boards at different extents under the conditions studied. The following effects were observed:

- Delayed ignition;
- Slightly reduced $\dot{m}_{max}$ and its time of occurrence;
- Increased residue after 2400 s of exposure to heat flux of 15 kW/m^2;
- Reduced $\dot{q}''_{max}$ and its time for most formulations, apart from the special case of Synthro®-nyl;
- Reduced q''_{tot} over the length of the test;
- Significantly reduced $\Delta h_{\mathrm{c,eff,fl}}$ for the HSB2-P boards compared to the HSB1-P series, which emphasises the importance of denser panels to limit oxygen ingress;
- Despite the presence of fire retardant additives (chemically active or inorganic materials), smouldering still occurred.

In the case of the presence of silica, this study suggests that combining it with other fire retardant additives, such as $\mathrm{MgSO_4}$ in the case of HSB2-P-3N1, might have cooled the gaseous phase thus decreased the local temperature (action of $\mathrm{MgSO_4}$), absorbed part of the radiant heat (action of silica) which decreased the onset of pyrolysis, limited the egress of volatiles from the hemp shiv board and limited the ingress of oxygen

(physical barrier of silica). It is however interesting to notice that silica itself could slightly delay ignition, lower the pyrolysis rate of hemp shiv board, reduce the heat release rate (HSB1-P-3N1 compared to HSB1-P-control), and also reduce the flaming period and the heat associated with the combustion processes (HSB2-P-3N1 compared to HSB2-P-10MgS).

7.6 Summary and recommendations

Firstly, the combustion of a hemp shiv board made with a polysaccharides binder was compared to that of similar samples containing silica particles, either introduced in the binder, or directly deposited on the surface of hemp shiv. Silica provided an additional protection against heat as they directly covered the surface of hemp shiv (which was evidenced in the SEM images in Figure 5.5) and were combined with magnesium sulfate. Most importantly, the addition of $\mathrm{MgSO_4}$ with commercially available fire retardant delayed ignition via flaming, and lowered the values of $\dot{m}_{max}$, $\dot{q}''_{max}$, $q''_{tot,2400}$, and $\Delta h_{\mathrm{c,eff,fl}}$. Specifically, silica reduced $q''_{tot,2400}$, $\Delta h_{\mathrm{c,eff,fl}}$, and $\Delta h_{\mathrm{c,eff,sm}}$ compared to samples without (HSB2-P-10MgS), which suggests its effect as a heat sink, thus less energy was available for pyrolysis of hemp shiv boards. Although these parameters were altered by the fire retardant additives, all samples still thermally degraded by being exposed to an external radiant heat flux, via flaming and smouldering combustions.

The flaming period was successfully suppressed by introducing significant quantities of mineral in the samples (HSB-M and HSB-ML). The rates of combustion thus were lowered, with the $\dot{m}_{max}$ and $\dot{q}''_{max}$ values greatly reduced compared to those of HSB-P samples. Moreover, the more magnesia present in the sample, the greater the residue after 40 min. It was expected to monitor less heat released with greater MgO contents. The multi-layered samples served as intermediates between the HSB-P type and HSB-M type, with the upper 10 mm of each sample being a mix of hemp shiv and earthen clay, another mineral. Flaming was also suppressed for the HSB-ML samples as the clay-rich layer insulated the rest of the composite from the radiant heat of

the conical heater. This allowed the $\dot{m}$ to be lower the more clay was present (HSB-ML-4:1). However, the HRR calculation method used in this study was based on the oxygen concentrations, which amplitude was too low to correctly calculate the heat released. This analysis could not be performed by this method and could not confirm the hypothesis. The oxygen consumption method to assess the HRR was therefore not appropriate for samples experiencing only smouldering combustion for which the oxygen consumption rate is lower than for flaming.

Complete assessment of hemp shiv boards (and any other materials subject to smouldering) could be undertaken via other methods than cone calorimetry, to monitor in more depth the mechanism of action of a potential fire retardant within the material. Moreover, composites which hemp shiv have been coated with silica particles and which present a sufficient mineral content could be investigated in order to not only suppress flaming, but also provide the water repellence properties demonstrated in Chapter 5. Additionally, indications on the mechanisms of insulation by a layer of mineral plaster could be obtained by placing thermocouples at different heights in a multi-layered composite board to monitor the gradient of temperatures throughout the experiment.

Chapter 8

Conclusions

8.1 Summary of main conclusions

Research in the building sector is now driven towards sustainable and energy-efficient solutions, such as the use of crop by-products. Before such materials are widely adopted, their safe and effective use needs to be ensured. For example, by finding protective treatments against biodegradation and fire whilst maintaining their moisture buffering properties. The research carried out and described in this thesis aimed at finding a unique and multifunctional solution. The work reported herein has demonstrated that silica particles technology could protect bio-materials such as hemp shiv against biodegradation and improve their fire performance. The key findings for this treatment based on silica particles and main conclusions are summarised below.

Chapter 3 described the rational design approach for the synthesis of silica particles of various sizes, between two boundary conditions of water content. A thorough characterisation was carried out, which demonstrated the physical characteristics of the particles between these two boundary conditions. The statistical analysis demonstrated a consistent and reliable manufacturing process for particles which diameter was 30 nm and 110 nm.

In Chapter 4, these silica particles were functionalised, which means that the chemical characteristics of their outer surface was modified. In this study, a hydrophobic silane was used so as to increase the liquid repellent behaviour of the particles when

deposited on glass slides. The repellent characteristics were not altered by immersing coated glass slides in a water bath for 24 h.

Functionalised silica particles were then deposited by immersion on hemp shiv in Chapter 5. Complete coverage of the hemp shiv surface was achieved when the coating process was repeated several times. The treated hemp shiv demonstrated increased hydrophobic properties, for up to 20 min, and retained this characteristic in humid conditions. Composite panels made from untreated and treated hemp shiv were also exposed to warm and humid environment. In these ideal conditions for microbial growth, panels which external surface was not treated with functionalised silica particles demonstrated fungal development after seven days. However, biodegradation was significantly delayed when both the hemp shiv and the external surface of the composites were treated. This exhibited the potential of silica particles to act as a protective layer, whilst maintaining hydrophobic properties even in a humid environment.

Silica was also shown in Chapter 6 to affect the thermal degradation of hemp shiv. The silica particles reduced the rate of pyrolysis with no chemical action from their part. Thermal and flammability analyses suggested that the silica particles acted as a heat sink, which means the thermal mass of the treated hemp shiv was greater, therefore for an equivalent quantity of heat radiating on the hemp shiv, less energy was available for pyrolysis.

Chapter 7 presented hemp shiv composite panels treated with various fire retardant additives, which acted in the gaseous (such as magnesium sulfate heptahydrate) and/or the condensed phase (inorganic materials such as silica). Under external radiant heat exposure, the chemically active fire retardant decomposed producing water vapour which in turn diluted the flame and cooled it, thus reducing flaming. The flaming combustion process could be prevented altogether, especially by introducing inorganic material in the structure of the composite (such as magnesium oxide), but the hemp shiv boards still combusted by smouldering. For an equivalent loading of 3 wt% solid content, silica particles proved to be an interesting alternative to conventional fire retardant additives owing to their physical impact on the combustion

process, rather than chemical.

8.2 Holistic approach

The novelty of the research and work described in the thesis relied on the combination of two functionalities within a unique treatment, namely limiting biodegradation and thermal degradation of hemp shiv. Versatility of functionalised silica particles was demonstrated, generating evidence that this technology has potential for further development for various applications. Both hydrophobicity and fire retardancy could have been even more improved separately. For example, superhydrophobicity could have been achieved and maintained for longer periods, by functionalising the particles with fluoroalkyl silanes. Combustion could also have been significantly reduced by combining into one solution compounds which physically (silica) and chemically (ammonium polyphosphate) impact the combustion rate. Both examples however are based on relatively toxic compounds, which are in the process of being phased out by chemical authorities, probably hindering their future manufacture and availability. The aim here was then to develop a solution which provides hydrophobicity, thus limits biodegradation, and reduces the effects of thermal degradation with a less toxic material than conventional additives.

8.3 Further work

It is important to recall that all experiments were carried out at laboratory scale. Due to the relatively small quantities of silica deposited on each piece of hemp shiv, the fire experiments demonstrated delayed flaming ignition, but not its suppression. For example with increased loadings of silica on hemp shiv within composites, biodegradation could be delayed up to several weeks, whilst still repelling liquid water. Flaming and smouldering could be delayed and their effects limited by the presence of silica. Specifically, flaming was completely prevented for composites with an increased quantity of inorganic material. Should similar experiments be carried out at larger scale, the effects of the silica treatment might not be of the same extent than those

measured during bench-scale analyses.

Silica is thought to be attached to cellulose by hydrogen bonding between the alkoxy groups present on the surface of the particles, and the natural polymer. Various methods of separation were explored to detach the particles from their substrate (the hydrolytic resistance test was one of them), without any success. Achieving this would improve understanding of the bonding mechanism between the two entities, and how to strengthen it, if possible.

Although composites of hemp shiv seemed to maintain their structural integrity under humidity exposure, this aspect was not quantified. The mechanical properties and resilience under load of such structures could be investigated, with the presence of silica expected not to have a detrimental effect on those. In fact, silica is used as filler to strengthen polymeric matrices, therefore the toughness of composites made with silica-coated hemp shiv should be preserved, or even improved.

Before adoption as conventional insulation materials, hemp shiv and bio-materials in general need to comply with standard test methods and certifications existing for the building sector. Currently, very few of these standards account for such materials, as their behaviour under operating conditions (humidity, warmth, fire, rain, etc.) is not yet fully understood and assessable. New testing frameworks are required to be put into place to understand underpinning mechanisms of degradation and their prevention, in order to enable safe use of bio-materials.

Bibliography

Alaee, M. and Wenning, R. J. (2002). "The significance of brominated flame retardants in the environment: Current understanding, issues and challenges". *Chemosphere* 46.5, pp. 579–582. DOI: 10.1016/S0045-6535(01)00224-7.

Alongi, J., Colleoni, C., Rosace, G., and Malucelli, G. (2014). "Sol-gel derived architectures for enhancing cotton flame retardancy: Effect of pure and phosphorus-doped silica phases". *Polymer Degradation and Stability* 99.1, pp. 92–98. DOI: 10.1016/j.polymdegradstab.2013.11.020.

Amziane, S. and Collet, F. (2017). *Bio-aggregates Based Building Materials*. Ed. by S. Amziane and F. Collet. Vol. 23. DOI: 10.1007/978-94-024-1031-0.

Ansell, M. P. and Mwaikambo, L. Y. (2009). "The structure of cotton and oter plant fibres". *Handbook of textile fibre structure. Volume 2: Natural, regenerated, inorganic and specialist fibres*. Ed. by S. J. Eichhorn, J. W. S. Hearle, M. Jaffe, and T. Kikutani. Woodhead Publishing Limited. Chap. 2, pp. 62–94.

Armistead, C. G., Tyler, A. J., Hambleton, F. H., Mitchell, S. A., and Hockey, J. A. (1969). "The surface hydroxylation of silica". *Journal of Physical Chemistry* 73.11, pp. 3947–3953. DOI: 10.1021/j100845a065.

Arnaud, L. and Gourlay, E. (2012). "Experimental study of parameters influencing mechanical properties of hemp concretes". *Construction and Building Materials* 28.1, pp. 50–56. DOI: 10.1016/j.conbuildmat.2011.07.052.

Arup (2017). *The Urban Bio-Loop*. Tech. rep. ARUP.

Assink, R. A. and Kay, B. D. (1984). "1H NMR Studies of the Sol-Gel Transition". *Materials Research Society Symposium Proceedings* 32, pp. 301–306.

ASTM (2013). "D1353-13: Standard Test Method for Nonvolatile Matter in Volatile Solvents for Use in Paint, Varnish, Lacquer, and Related Products", pp. 1–3. DOI: 10.1520/D1353-13.2.

ASTM (2017a). *C739-17. Standard Specification for Cellulosic Fiber Loose-Fill Thermal Insulation*. Tech. rep., pp. 1–10. DOI: 10.1126/science.1171209.

ASTM (2017b). *E1354-17: Standard Test Method for Heat and Visible Smoke Release Rates for Materials and Products Using an Oxygen Consumption Calorimeter*. Tech. rep. DOI: 10.1520/E1354-17.1.8.

Babrauskas, V. (1984). "Development of the cone calorimeter – A bench-scale heat release rate apparatus based on oxygen consumption". *Fire and Materials* 8.2, pp. 81–95. DOI: 10.1002/fam.810080206.

Babrauskas, V. and Stapleton, H. M. (2015). "Halogenated Flame Retardant Use in Residential Settings - SFPE". *Journal of Fire Protection Engineering*.

Bailey, J. K. and Mecartney, M. L. (1992). "Formation of colloidal silica particles from alkoxides". *Colloids and Surfaces* 63.1-2, pp. 131–138. DOI: 10.1016/0166-6622(92)80081-C.

Balci, S., Sezgi, N. A., and Eren, E. (2012). "Boron oxide production kinetics using boric acid as raw material". *Industrial and Engineering Chemistry Research* 51.34, pp. 11091–11096. DOI: 10.1021/ie300685x.

Barati Darband, G., Aliofkhazraei, M., Khorsand, S., Sokhanvar, S., and Kaboli, A. (2018). "Science and Engineering of Superhydrophobic Surfaces: Review of Corrosion Resistance, Chemical and Mechanical Stability". *Arabian Journal of Chemistry*. DOI: 10.1016/j.arabjc.2018.01.013.

Barrett, E. P., Joyner, L. G., and Halenda, P. P. (1951). "The Determination of Pore Volume and Area Distributions in Porous Substances. I. Computations from Nitrogen Isotherms". *Journal of the American Chemical Society* 73, pp. 373–380.

Barthlott, W. and Neinhuis, C. (1997). "Purity of the sacred lotus, or escape from contamination in biological surfaces". *Planta* 202.1, pp. 1–8. DOI: 10.1007/s004250050096.

Bauer, F., Sauerland, V., Ernst, H., Gläsel, H. J., Naumov, S., and Mehner, R. (2003). "Preparation of scratch- and abrasion-resistant polymeric nanocomposites by monomer grafting onto nanoparticles, 4a: Application of MALDI-TOF mass spectrometry to the characterization of surface modified nanoparticles". *Macromolecular Chemistry and Physics* 204.3, pp. 375–383. DOI: 10.1002/macp.200390003.

Birdi, K. S., Vu, D. T., and Winter, A. (1989). "A study of the evaporation rates of small water drops placed on a solid surface". *Journal of Physical Chemistry* 93.9, pp. 3702–3703. DOI: 10.1021/j100346a065.

Bogush, G., Tracy, M., and Zukoski IV, C. (1988). "Preparation of Monodiperse Silica Particles: Control of Size and Mass Fraction". *Journal of Non-Crystalline Solids* 104, pp. 95–106.

Bogush, G. and Zukoski IV, C. (1991). "Studies of the kinetics of the precipitation of uniform silica particles through the hydrolysis and condensation of silicon alkoxides". *Journal of Colloid And Interface Science* 142.1, pp. 1–18. DOI: 10.1016/0021-9797(91)90029-8.

Bourbigot, S. and Duquesne, S. (2007). "Fire retardant polymers: recent developments and opportunities". *Journal of Materials Chemistry* 17.22, pp. 2283–2300. DOI: 10.1039/B702511D.

Bourebrab, M. A., Durand, G. G., and Taylor, A. (2018). "Development of Highly Repellent Silica Particles for Protection of Hemp Shiv Used as Insulation Materials". *Materials* 11.4, pp. 12–18. DOI: 10.3390/ma11010004.

Bourebrab, M. A., Oben, D. T., Durand, G. G., Taylor, P. G., Bruce, J. I., Bassindale, A. R., and Taylor, A. (2018). "Influence of the initial chemical conditions on the rational design of silica particles". *Journal of Sol-Gel Science and Technology* 88.2, pp. 430–441. DOI: 10.1007/s10971-018-4821-9.

Branda, F., Malucelli, G., Durante, M., Piccolo, A., Mazzei, P., Costantini, A., Silvestri, B., Pennetta, M., and Bifulco, A. (2016). "Silica treatments: A fire retardant strategy for hemp fabric/epoxy composites". *Polymers* 8.8, pp. 1–17. DOI: 10.3390/polym8080313.

Bravo, J., Zhai, L., Wu, Z., Cohen, R. E., and Rubner, M. F. (2007). "Transparent superhydrophobic films based on silica nanoparticles". *Langmuir* 23.13, pp. 7293–7298. DOI: 10.1021/la070159q.

Bridger, K., Fairhurst, D., and Vincent, B. (1979). "Nonaqueous silica dispersions stabilized by terminally-grafted polystyrene chains". *Journal of Colloid And Interface Science* 68.1, pp. 190–195. DOI: 10.1016/0021-9797(79)90271-6.

Brinker, C. J. (1988). "Hyrolysis and Condensation of Silicates: Effects on Structure". *Journal of Non-Crystalline Solids* 100.5, pp. 31–50. DOI: 10.1021/ma00210a047.

British Standards Institution (2016). *BS EN 16733:2016. Reaction to fire tests for building products — Determination of a building product's propensity to undergo continuous smouldering*. Tech. rep.

Brohez, S., Delvosalle, C., Marlair, G., and Tewarson, A. (1999). "Soot generation in fires: an important parameter for accurate calculation of heat release". *6th International Symposium on Fire Safety Science*.

Browne, F. (1958). *Theories of the combustion of wood and its control*. Tech. rep. 2136. U.S. Department of Agriculture Forest Service, p. 72.

Brunauer, S., Emmett, P. H., and Teller, E. (1938). "Adsorption of Gases in Multimolecular Layers". *Journal of the American Chemical Society* 60.2, pp. 309–319. DOI: 10.1021/ja01269a023.

California Legislature (2007). *Assembly Bill 706 Fire retardants*.

Campilho, R. (2017). "Recent innovations in biocomposite products". *Biocomposites for High-Performance Applications*. Ed. by D. Ray. Elsevier Ltd. Chap. Recent inn, pp. 275–306. DOI: 10.1016/B978-0-08-100793-8.00010-7.

Carcouët, C. C. M. C., Esteves, A. C. C., Hendrix, M. M., Benthem, R. A. van, and With, G. de (2014). "Fine-Tuning of Superhydrophobicity Based on Monolayers of Well-defined Raspberry Nanoparticles with Variable Dual-roughness Size and Ratio". *Advanced Functional Materials* 24.36, pp. 5745–5752. DOI: 10.1002/adfm.201400111.

Carrot, G., Rutot-Houzé, D., Pottier, A., Degée, P., Hilborn, J., and Dubois, P. (2002). "Surface-initiated ring-opening polymerization: A versatile method for nanoparticle ordering". *Macromolecules* 35.22, pp. 8400–8404. DOI: 10.1021/ma020558m.

Carus, M., Karst, S., Kauffmann, A., Hobston, J., and Bertucelli, S. (2013). "The European Hemp Industry: Cultivation , processing and applications for fibres, shivs and seeds". *European Industrial Hemp Association* 6.

Cassie, A. B. D. and Baxter, S. (1944). "Wettability of porous surfaces". *Transactions of the Faraday Society* 40, pp. 546–551.

Cérézo, V. (2005). "Propriétés mécaniques, thermiques et acoustiques d'un matériau à base de particules végétales : approche expérimentale et modélisation théorique". [In French]. Thèse doctorale. Ecole Nationale des Travaux Publics de l'Etat, p. 247.

Chandra, S., Lata, H., and ElSohly, M. A. (2017). *Cannabis Sativa L. - Botany and Biotechnology*, p. 479.

Cho, E. C., Chang-Jian, C. W., Chen, H. C., Chuang, K. S., Zheng, J. H., Hsiao, Y. S., Lee, K. C., and Huang, J. H. (2017). "Robust multifunctional superhydrophobic coatings with enhanced water/oil separation, self-cleaning, anti-corrosion, and anti-biological adhesion". *Chemical Engineering Journal* 314, pp. 347–357. DOI: 10.1016/j.cej.2016.11.145.

Ciechańska, D., Wesołowska, E., and Wawro, D. (2009). "An introduction to cellulosic fibres". *Handbook of Textile Fibre Structure*. Ed. by S. J. Eichhorn, J. W. S. Hearle, M. Jaffe, and T. Kikutani. Vol. 2. Woodhead Publishing Series in Textiles. Woodhead Publishing. Chap. 1, pp. 3–61. DOI: https://doi.org/10.1533/9781845697310.1.3.

Colson, V., Bourebrab, M. A., Jadeau, O., and Lanos, C. (2019). "Formulation of Noel Fire Retardant Additives for Biobased Insulation Material". *Construction and Building Materials* Submitted.

Colson, V., Le Cunff, T., Jadeau, O., and Lanos, C. (2017). "Industrial scale-up of biobased insulating panel production". *2nd International Conference on Bio-based Building Materials*. Vol. PRO 119.

Combustion Research Corporation (2018). *U-values for common materials*. URL: https://www.combustionresearch.com/U-Values_for_common_materials.html.

Costes, J.-P., Evrard, A., Biot, B., Keutgen, G., Daras, A., Dubois, S., Lebeau, F., and Courard, L. (2017). "Thermal Conductivity of Straw Bales: Full Size Measurements Considering the Direction of the Heat Flow". *Buildings* 7.11. DOI: 10.3390/buildings7010011.

CRC Handbook of Chemistry and Physics (2018). "Thermal Conductivity at Specified Values of Density and Temperature". *CRC Handbook of Chemistry and Physics, 99th Edition (Internet Version 2018)*. Ed. by J. R. Rumble. CRC Press, Taylor & Francis.

Danish Environmental Protection Agency (2016). *Proposal for a restriction. Substance name(s): (3,3,4,4,5,5,6,6,7,7,8,8,8-tridecafluorooctyl)silanetriol and any of its mono-, di- or tri-O-(alkyl) derivatives*. Tech. rep. EChA, pp. 1–122.

Diquélou, Y., Gourlay, E., Arnaud, L., and Kurek, B. (2015). "Impact of hemp shiv on cement setting and hardening: Influence of the extracted components from the aggregates and study of the interfaces with the inorganic matrix". *Cement and Concrete Composites* 55, pp. 112–121. DOI: 10.1016/j.cemconcomp.2014.09.004.

Drysdale, D. (2011). "Steady Burning of Liquids and Solids". *An Introduction to Fire Dynamics*. Third. John Wiley & Sons, Ltd. Chap. 5, pp. 181–223.

Dzis'ko, V., Vishnevskaya, A., and Chesalova, V. (1950). "Effect of Thermal Treatment on the Silica Gel Catalytic Activity". *Russian Journal of Physical Chemistry* 24, pp. 1416–9.

Ebskamp, M. J. M. (2002). "Engineering flax and hemp for an alternative to cotton". *Trends in Biotechnology* 20.6, pp. 229–230. DOI: 10.1016/S0167-7799(02)01953-4.

Effati, E. and Pourabbas, B. (2012). "One-pot synthesis of sub-50nm vinyl- and acrylate-modified silica nanoparticles". *Powder Technology* 219, pp. 276–283. DOI: 10.1016/j.powtec.2011.12.062.

Energy Saving Trust (2006). *Practical refurbishment of solid-walled houses (CE184)*. Tech. rep., pp. 1–32.

European Chemical Agency (2010). *Substance name: Boric acid. Member state committee support document for identification of boric acid as a substance of very high concern because of its CMR properties*. Tech. rep.

European Parliament (2003). "Directive 2003/11/EC of the European parliament and of the council of February 6 2003 amending for the 24th time Council Directive 76/669/EEC relating to restrictions on the marketing and use of certain dangerous substances and preparations (pentabromodiphenyl ether, octabromo- diphenyl ether)". *Official Journal of the European Union* 16.1, pp. 1–46.

European Parliament (2008). "Regulation (EC) 1271/2008 on classification, labelling and packaging of substances and mixtures, amending and repealing Directives 67/548/EEC and 1999/45/EC, and amending Regulation (EC) 1907/2006". *Official Journal of the European Union*. DOI: http://eur-lex.europa.eu/pri/en/oj/dat/2003/l_285/l_28520031101en00330037.pdf.

European Parliament (2010). "Directive 2010/31/EU of the European Parliament and of the Council of 19 May 2010 on the energy performance of buildings (recast)". *Official Journal of the European Union*, pp. 13–35. DOI: doi:10.3000/17252555.L_2010.153.eng.

European Parliament (2012). "Directive 2012/27/EU of the European Parliament and of the Council of 25 October 2012 on energy efficiency". *Official Journal of the European Union* October, pp. 1–56. DOI: 10.3000/19770677.L_2012.315.eng.

Evrard, A. and De Herde, A. (2010). "Hygrothermal Performance of Lime-Hemp Wall Assemblies". *Journal of Building Physics* 34.1, pp. 5–25. DOI: 10.1177/1744259109355730.

Flory, P. J. (1941). "Molecular Size Distribution in Three Dimensional Polymers. I. Gelation". *Journal of the American Chemical Society* 63.11, pp. 3083–3090. DOI: 10.1021/ja01856a061.

Fowkes, F. M. (1964). "Contact Angle, Wettability, and Adhesion". *Advances in Chemistry* 43. DOI: 10.1021/ba-1964-0043.

Georlette, P. (2001). "Applications of halogen flame retardants". *Fire retardant materials*. Ed. by A. R. Horrocks and D. Price. Woodhead Publishing Limited. Chap. 8, pp. 264–292. DOI: 10.1533/9781855737464.264.

Giesche, H. (1994). "Synthesis of monodispersed silica powders I. Particle properties and reaction kinetics". *Journal of the European Ceramic Society* 14.3, pp. 189–204.

Gilman, J. W., Harris, R. H., Shields, J. R., Kashiwagi, T., and Morgan, A. B. (2006). "A study of the flammability reduction mechanism of polystyrene-layered silicate nanocomposite: Layered silicate reinforced carbonaceous char". *Polymers for Advanced Technologies* 17.4, pp. 263–271. DOI: 10.1002/pat.682.

Glé, P., Gourdon, E., and Arnaud, L. (2011). "Acoustical properties of materials made of vegetable particles with several scales of porosity". *Applied Acoustics* 72.5, pp. 249–259. DOI: 10.1016/j.apacoust.2010.11.003.

Gourlay, E. (2014). "Caractérisation expérimentale des propriétés mécaniques et hygrothermiques du béton de chanvre. Détermination de l'impact des matières premières et de la méthode de mise en oeuvre". [In French]. Thèse Doctorale. Ecole Nationale des Travaux Publics de l'Etat.

Gratkowski, M. T., Dembsey, N. A., and Beyler, C. L. (2006). "Radiant smoldering ignition of plywood". *Fire Safety Journal* 41.6, pp. 427–443. DOI: 10.1016/j.firesaf.2006.03.006.

Greasley, S. L., Page, S. J., Sirovica, S., Chen, S., Martin, R. A., Riveiro, A., Hanna, J. V., Porter, A. E., and Jones, J. R. (2016). "Controlling particle size in the Stöber process and incorporation of calcium". *Journal of Colloid and Interface Science* 469, pp. 213–223. DOI: 10.1016/j.jcis.2016.01.065.

Hadden, R. (2011). "Smouldering and self-sustaining reactions in solids: an experimental approach". PhD thesis. The University of Edinburgh.

Haghighatju, F., Hashemipour Rafsanjani, H., and Esmaeilzadeh, F. (2017). "Estimation of the dimension of micropores and mesopores in single walled carbon nanotubes using the method Horvath–Kawazoe, Saito and Foley and BJH equations". *Micro & Nano Letters* 12.1, pp. 1–5. DOI: 10.1049/mnl.2016.0306.

Harris, M. T., Brunson, R. R., and Byers, C. H. (1990). "The base-catalyzed hydrolysis and condensation reactions of dilute and concentrated TEOS solutions". *Journal of Non-Crystalline Solids* 121.1-3, pp. 397–403. DOI: 10.1016/0022-3093(90)90165-I.

Hassan, P. A., Rana, S., and Verma, G. (2015). "Making sense of Brownian motion: Colloid characterization by dynamic light scattering". *Langmuir* 31.1, pp. 3–12. DOI: 10.1021/la501789z.

Hench, L. L. and West, J. K. (1990). "The Sol-Gel Process". *Chemical Reviews* 90.1, pp. 33–72. DOI: 10.1021/cr00099a003.

Hidalgo-Medina, J. P. (2015). "Performance-based methodology for the fire safe design of insulation materials in energy efficient buildings". PhD thesis. The University of Edinburgh (UK).

Hikita, M., Tanaka, K., Nakamura, T., Kajiyama, T., and Takahara, A. (2005). "Superliquid-repellent surfaces prepared by colloidal silica nanoparticles covered with fluoroalkyl groups". *Langmuir* 21.16, pp. 7299–7302. DOI: 10.1021/la050901r.

Hill, C. A. S., Norton, A. J., and Newman, G. (2009). "Natural Fibre Insulation Materials – the Importance of Hygroscopicity in Providing Indoor Climate Control". *11th International Conference on Non-conventional Materials and Technologies, NOCMAT 2009*.

Hirst, E. A. J. (2013). "Characterisation of Hemp-Lime as a Composite Building Material". PhD Thesis. University of Bath (UK).

Horvath, G. and Kawazoe, K. (1983). "Method for the calculation of effective pore size distribution in molecular sieve carbon". *Journal of Chemical Engineering of Japan* 16.6, pp. 470–475. DOI: 10.1252/jcej.16.470.

Hshieh, F.-Y. (1998). "Shielding effects of silica-ash layer on the combustion of silicones and their possible applications on the fire retardancy of organic polymers". *Fire and Materials* 22.2, pp. 69–76. DOI: 10.1002/(SICI)1099-1018(199803/04)22:2<69::AID-FAM640>3.0.CO;2-U.

Huang, X. and Rein, G. (2014). "Smouldering combustion of peat in wildfires: Inverse modelling of the drying and the thermal and oxidative decomposition kinetics".

Combustion and Flame 161.6, pp. 1633–1644. DOI: 10.1016/j.combustflame.2013.12.013.

Huggett, C. (1980). "Estimation of rate of heat release by means of oxygen consumption measurements". *Fire and Materials* 4.2, pp. 61–65. DOI: 10.1002/fam.810040202.

Hussain, A., Calabria-Holley, J., Jiang, Y., and Lawrence, M. (2018). "Modification of hemp shiv properties using water-repellent sol–gel coatings". *Journal of Sol-Gel Science and Technology* 86.1, pp. 187–197. DOI: 10.1007/s10971-018-4621-2.

Hussain, A., Calabria-Holley, J., Schorr, D., Jiang, Y., Lawrence, M., and Blanchet, P. (2018). "Hydrophobicity of hemp shiv treated with sol-gel coatings". *Applied Surface Science* 434, pp. 850–860. DOI: 10.1016/j.apsusc.2017.10.210.

Hyde, E. D., Seyfaee, A., Neville, F., and Moreno-Atanasio, R. (2016). "Colloidal Silica Particle Synthesis and Future Industrial Manufacturing Pathways: A Review". *Industrial and Engineering Chemistry Research* 55.33, pp. 8891–8913. DOI: 10.1021/acs.iecr.6b01839.

Ibrahim, I. a.M., Zikry, a.a.F., and Sharaf, M. a. (2010). "Preparation of spherical silica nanoparticles: Stober silica". *Journal of American Science* 6.11, pp. 985–989. DOI: 10.7537/marsjas061110.133.

Iler, R. K. (1979). *The Chemistry of Silica: Solubility, Polymerization, Colloid and Surface Properties, and Biochemistry*. John Wiley. New York: Wiley.

International Organization for Standardization (2008). *BS ISO 22412:2008. Particle size analysis - Dynamic light scattering (DLS)*.

International Organization for Standardization (2015). *BS ISO 5660-1:2015. Reaction-to-fire tests — Heat release , smoke production and mass loss rate. Part 1 : Heat release rate (cone calorimeter method) and smoke production rate (dynamic measurement)*.

ISOBIO (2015). *Preliminary Economic and Environmental Analysis (access restricted to ISOBIO consortium)*.

IUPAC (1997). "Hydrophobicity". *Compendium of Chemical Terminology, 2nd ed. (the "Gold Book"). Compiled by A. D. McNaught and A. Wilkinson. XML on-line corrected version: http://goldbook.iupac.org (2006-) created by M. Nic, J. Jirat, B. Kosata; updates*

compiled by A. Jenkins. Oxford: Blackwell Scientific Publications. DOI: 10.1351/goldbook.HT06964.

Jafarzadeh, M., Rahman, I. A., and Sipaut, C. S. (2009). "Synthesis of silica nanoparticles by modified sol-gel process: The effect of mixing modes of the reactants and drying techniques". *Journal of Sol-Gel Science and Technology* 50.3, pp. 328–336. DOI: 10.1007/s10971-009-1958-6.

Jańczuk, B. and Białłopiotrowicz, T. (1989). "Surface free-energy components of liquids and low energy solids and contact angles". *Journal of Colloid And Interface Science* 127.1, pp. 189–204. DOI: 10.1016/0021-9797(89)90019-2.

Janssens, M. L. (1991). "Measuring rate of heat release by oxygen consumption". *Fire Technology* 27.3, pp. 234–249. DOI: 10.1007/BF01038449.

Jeevahan, J., Chandrasekaran, M., Britto Joseph, G., Durairaj, R. B., and Mageshwaran, G. (2018). "Superhydrophobic surfaces: a review on fundamentals, applications, and challenges". *Journal of Coatings Technology and Research* 15.2, pp. 231–250. DOI: 10.1007/s11998-017-0011-x.

Jiang, Y., Bourebrab, M. A., Sid, N., Taylor, A., Collet, F., Pretot, S., Hussain, A., Ansell, M., and Lawrence, M. (2018). "Improvement of water resistance of hemp woody substrates through deposition of functionalised silica hydrophobic coating, whilst retaining excellent moisture buffering properties". *ACS Sustainable Chemistry and Engineering* 6, pp. 10151–10161. DOI: 10.1021/acssuschemeng.8b01475.

Jiang, Y., Lawrence, M., Ansell, M. P., and Hussain, A. (2018). "Cell wall microstructure, pore size distribution and absolute density of hemp shiv". *Royal Society Open Science* 5.171945. DOI: 10.1098/rsos.171945.

Jimenez, M., Duquesne, S., and Bourbigot, S. (2006). "Characterization of the performance of an intumescent fire protective coating". *Surface and Coatings Technology* 201, pp. 979–987. DOI: 10.1016/j.surfcoat.2006.01.026.

John, M. J. and Thomas, S. (2008). "Biofibres and biocomposites". *Carbohydrate Polymers* 71.3, pp. 343–364. DOI: 10.1016/j.carbpol.2007.05.040.

Jones, D. (2017). "Introduction to the performance of bio-based building materials". *Performance of Bio-based Building Materials*. Ed. by D. Jones and C. Brischke. Elsevier Ltd. Chap. 1, pp. 1–19. DOI: 10.1016/B978-0-08-100982-6.00001-X.

Kaelble, D. H. (1970). "Dispersion-Polar Surface Tension Properties of Organic Solids". *The Journal of Adhesion* 2.2, pp. 66–81. DOI: 10.1080/0021846708544582.

Kandola, B. K. (2001). "Nanocomposites". *Fire retardant materials*. Chap. 6, pp. 204–219. DOI: 10.1533/9781855737464.204.

Kashiwagi, T., Gilman, J. W., Butler, K. M., Harris, R. H., Shields, J. R., and Asano, A. (2000). "Flame retardant mechanism of silica gel/silica". *Fire and Materials* 24.6, pp. 277–289. DOI: 10.1002/1099-1018(200011/12)24:6<277::AID-FAM746>3.0.CO;2-A.

Kashiwagi, T., Harris, R. H., Zhang, X., Briber, R., Cipriano, B. H., Raghavan, S. R., Awad, W. H., and Shields, J. R. (2004). "Flame retardant mechanism of polyamide 6–clay nanocomposites". *Polymer* 45.3, pp. 881–891. DOI: 10.1016/j.polymer.2003.11.036.

Kashiwagi, T., Morgan, A. B., Antonucci, J. M., VanLandingham, M. R., Harris, R. H., Awad, W. H., and Shields, J. R. (2003). "Thermal and flammability properties of a silica-poly(methylmethacrylate) nanocomposite". *Journal of Applied Polymer Science* 89.8, pp. 2072–2078. DOI: 10.1002/app.12307.

Kashiwagi, T., Shields, J. R., Harris, R. H., and Davis, R. D. (2003). "Flame-retardant mechanism of silica: Effects of resin molecular weight". *Journal of Applied Polymer Science* 87.9, pp. 1541–1553. DOI: 10.1002/app.11967.

Kidalova, L., Stevulova, N., and Terpakova, E. (2015). "Influence of water absorption on the selected properties of hemp hurds composites". *Pollack Periodica* 10.1, pp. 123–132. DOI: 10.1556/Pollack.10.2015.1.12.

Korjenic, A., Petránek, V., Zach, J., and Hroudová, J. (2011). "Development and performance evaluation of natural thermal-insulation materials composed of renewable resources". *Energy and Buildings* 43.9, pp. 2518–2523. DOI: 10.1016/j.enbuild.2011.06.012.

Kymäläinen, H. R. and Sjöberg, A. M. (2008). "Flax and hemp fibres as raw materials for thermal insulations". *Building and Environment* 43.7, pp. 1261–1269. DOI: 10.1016/j.buildenv.2007.03.006.

Lally, T. J. (2005). *Fire-retardant coating, method for producing fire-retardant building materials. Patent N°US729290B2*. DOI: 10.1016/j.(73).

LaMer, V. K. and Dinegar, R. H. (1950). "Theory, production and mechanism of formation of monodispersed hydrosols". *Journal of the American Chemical Society* 72.8, pp. 4847–4854. DOI: 10.1021/ja01167a001.

Lawrence, M., Shea, A., Walker, P., and De Wilde, P. (2013). "Hygrothermal performance of bio-based insulation materials". *Proceedings of the ICE - Construction Materials* 166.4, pp. 257–263. DOI: 10.1680/coma.12.00031.

Lazko, J., Landercy, N., Laoutid, F., Dangreau, L., Huguet, M. H., and Talon, O. (2013). "Flame retardant treatments of insulating agro-materials from flax short fibres". *Polymer Degradation and Stability* 98.5, pp. 1043–1051. DOI: 10.1016/j.polymdegradstab.2013.02.002.

Lenormand, H., Mahieu, A., Leblanc, N., and Vivet, A. (2014). "Nouvelles agroressources pour panneaux de particules 100 % biosourcés". In French. *Colloque 01 Ecomateriaux*.

Levan, S. L. (1984). "Chemistry of Fire Retardancy". *The Chemistry of Solid Wood*. Ed. by R. M. Rowell. Washington, DC: American Chemical Society. Chap. 14, pp. 531–574. DOI: 10.1021/ba-1984-0207.ch014.

Li, S., Wan, Q., Qin, Z., Fu, Y., and Gu, Y. (2015). "Understanding Stöber silicas pore characteristics measured by gas adsorption". *Langmuir* 31.2, pp. 824–832. DOI: 10.1021/la5042103.

Lim, H. M., Lee, J., Jeong, J.-H., Oh, S.-G., and Lee, S.-H. (2010). "Comparative Study of Various Preparation Methods of Colloidal Silica". *Engineering* 02.12, pp. 998–1005. DOI: 10.4236/eng.2010.212126.

Lin, J., Siddiqui, J. A., and Ottenbrite, R. M. (2001). "Surface Modification of Inorganic Oxide Particles with Silane Coupling Agent and Organic Dyes". *Polymer for advanced technologies* 292.February 2000, pp. 285–292. DOI: 10.1002/pat.064.

Liu, Y.-l., Hsu, C.-y., and Wang, M.-l. (2003). "A novel approach of chemical functionalization on nano-scaled silica". *Nanotechnology* 14, pp. 813–819.

Lowell, S., Shields, J. E., Thomas, M. A., and Thommes, M. (2004). *Characterization of Porous Solids and Powders: Surface Area, Pore Size and Density*. Ed. by B. Scarlett. Particle T. Springer, Dordrecht, The Netherlands, pp. XIV, 350. DOI: 10.1007/978-1-4020-2303-3.

Lyon, R. E. (2000). "Heat Release Kinetics". *Fire and Materials* 24.4, pp. 179–186. DOI: 10.1002/1099-1018(200007/08)24:4<179::AID-FAM736>3.0.CO;2-V.

Madorsky, S. L. (1964). *Thermal degradation of organic polymers*. eng. Polymer reviews; v.7. New York: Interscience Publishers.

Magniont, C., Escadeillas, G., Coutand, M., and Oms-Multon, C. (2012). "Use of plant aggregates in building ecomaterials". *European Journal of Environmental and Civil Engineering* 16.sup1, s17–s33. DOI: 10.1080/19648189.2012.682452.

Malvern Instruments (2014). *Dynamic Light Scattering: An Introduction in 30 Minutes*. Technical note.

Mantanis, G. I. and Young, R. A. (1997). "Wetting of wood". *Wood Science and Technology* 31.5, pp. 339–353. DOI: 10.1007/BF01159153.

Marmur, A. (2004). "The lotus effect: Superhydrophobicity and metastability". *Langmuir* 20.9, pp. 3517–3519. DOI: 10.1021/la036369u. eprint: la036369u (10.1021).

Marmur, A. (2009). "Solid-Surface Characterization by Wetting". *Annual Review of Materials Research* 39.1, pp. 473–489. DOI: 10.1146/annurev.matsci.38.060407.132425.

Matsoukas, T. and Gulari, E. (1988). "Dynamics of growth of silica particles from ammonia-catalyzed hydrolysis of tetra-ethyl-orthosilicate". *Journal of Colloid And Interface Science* 124.1, pp. 252–261. DOI: 10.1016/0021-9797(88)90346-3.

McLaggan, M. S. (2016). "Novel fire testing frameworks for Phase Change Materials and hemp-lime insulation". PhD thesis. The University of Edinburgh (UK).

Mercado Roca, L. A. (2005). "Resinas Epoxi Sililadas Retardantes a la llama. Síntesis, Caracterización y Propiedades". [In Spanish]. PhD thesis. Universitat Rovira i Virgili, Tarragona, Spain.

Mngomezulu, M. E., John, M. J., Jacobs, V., and Luyt, A. S. (2014). "Review on flammability of biofibres and biocomposites". *Carbohydrate Polymers* 111, pp. 149–182. DOI: 10.1016/j.carbpol.2014.03.071.

Mokhothu, T. H. and John, M. J. (2015). "Review on hygroscopic aging of cellulose fibres and their biocomposites". *Carbohydrate Polymers* 131, pp. 337–354. DOI: 10.1016/j.carbpol.2015.06.027.

Museovirasto (2000). "Lämmöneristyksen parantaminen". [In Finnish]. *Korjauskortisto*, pp. 1–12.

Nagao, D., Satoh, T., and Konno, M. (2000). "A generalized model for describing particle formation in the synthesis of monodisperse oxide particles based on the hydrolysis and condensation of tetraethyl orthosilicate". *Journal of Colloid and Interface Science* 232.1, pp. 102–110. DOI: 10.1006/jcis.2000.7195.

Napierska, D., Thomassen, L. C., Lison, D., Martens, J. A., and Hoet, P. H. (2010). "The nanosilica hazard: another variable entity". *Particle and Fibre Toxicology* 7.1, p. 39. DOI: 10.1186/1743-8977-7-39.

NORDTEST (1988). *NT FIRE 035. Building Products: Flammability and Smouldering Resistance of Loose-fill Thermal Insulation*. Tech. rep.

Nunes, L. (2017). "Nonwood bio-based materials". *Performance of Bio-based Building Materials*. Ed. by D. Jones and C. Brischke. Elsevier Ltd. Chap. 3, pp. 97–186. DOI: 10.1016/B978-0-08-100982-6.00003-3.

Nykter, M. (2006). "Microbial Quality of Hemp (Cannabis sativa L.) and Flax (Linum usitatissimum L.) from Plants to Thermal Insulation". PhD thesis. University of Helsinki (Finland).

Ohlemiller, T. J. (1995). "Smoldering Combustion". *SFPE Handbook of Fire Protection Engineering*. Second edition. Chap. 11, pp. 171–179. DOI: 10.1007/978-1-4939-2565-0_19.

Owens, D. K. and Wendt, R. C. (1969). "Estimation of the Surface Free Energy of Polymers". *Journal of Applied Polymer Science* 13, pp. 1741–1747.

Pacheco-Torgal, F. and Jalali, S. (2011). "Cementitious building materials reinforced with vegetable fibres: A review". *Construction and Building Materials* 25.2, pp. 575–581. DOI: 10.1016/j.conbuildmat.2010.07.024.

Palmer, K. N. (1957). "Smouldering combustion in dusts and fibrous materials". *Combustion and Flame* 1.2, pp. 129–154. DOI: 10.1016/0010-2180(57)90041-X.

Palumbo, M., Lacasta, A. M., Navarro, A., Giraldo, M. P., and Lesar, B. (2017). "Improvement of fire reaction and mould growth resistance of a new bio-based thermal insulation material". *Construction and Building Materials* 139, pp. 531–539. DOI: 10.1016/j.conbuildmat.2016.11.020.

Park, S. K., Kim, K. D., and Kim, H. T. (2002). "Preparation of silica nanoparticles: Determination of the optimal synthesis conditions for small and uniform particles". *Colloids and Surfaces A: Physicochemical and Engineering Aspects* 197.1-3, pp. 7–17. DOI: 10.1016/S0927-7757(01)00683-5.

Perro, A., Reculusa, S., Bourgeat-Lami, E., Duguet, E., and Ravaine, S. (2006). "Synthesis of hybrid colloidal particles: From snowman-like to raspberry-like morphologies". *Colloids and Surfaces A: Physicochemical and Engineering Aspects* 284-285, pp. 78–83. DOI: 10.1016/j.colsurfa.2005.11.073.

Posthumus, W., Magusin, P. C. M. M., Brokken-Zijp, J. C. M., Tinnemans, A. H. A., and Linde, R. van der (2004). "Surface modification of oxidic nanoparticles using 3-metha-cryloxypropyltrimethoxysilane." *Journal of colloid and interface science* 269.1, pp. 109–116. DOI: 10.1016/j.jcis.2003.07.008.

Purser, D. (2001). "Toxicity of fire retardants in relation to life safety and environmental hazards". *Fire retardant materials*. Ed. by A. R. Horrocks and D. Price. Woodhead Publishing Limited. Chap. 3, pp. 69–127. DOI: 10.1533/9781855737464.69.

Rabel, W. (1971). "Einige Aspekte der Benetzungstheorie und ihre Anwendung auf die Untersuchung und Veränderung der Oberflächeneigenschaften von Polymeren". *Farbe und Lacke* 77.10, pp. 997–1005.

Rahman, I. A. and Padavettan, V. (2012). "Synthesis of Silica nanoparticles by Sol-Gel: Size-dependent properties, surface modification, and applications in silica-

polymer nanocompositesa review". *Journal of Nanomaterials* 2012. DOI: 10.1155/2012/132424. eprint: 132424.

Rao, K. S., El-Hami, K., Kodaki, T., Matsushige, K., and Makino, K. (2005). "A novel method for synthesis of silica nanoparticles". *Journal of Colloid and Interface Science* 289.1, pp. 125–131. DOI: 10.1016/j.jcis.2005.02.019.

Rein, G. (2009). "Smouldering Combustion Phenomena in Science and Technology". *International Review of Chemical Engineering* 1, pp. 3–18. DOI: http://hdl.handle.net/1842/2678.

Roberts, A. F. (1970). "A review of kinetics data for the pyrolysis of wood and related substances". *Combustion and Flame* 14.2, pp. 261–272. DOI: 10.1016/S0010-2180(70)80037-2.

Roenner, N., Hutheesing, K., Fergusson, A., and Rein, G. (2017). "Simultaneous improvements in flammability and mechanical toughening of epoxy resins through nano-silica addition". *Fire Safety Journal* 91.February, pp. 200–207. DOI: 10.1016/j.firesaf.2017.03.010.

Rouquerol, J., Avnir, D., Fairbridge, C., Everett, D., Haynes, J., Pernicone, N., Ramsay, J., Sing, K., and Unger, K. (1994). "Recommendations for the characterization of porous solids". *Pure and Applied Chemistry* 66.8, pp. 1739–1758.

Saito, A. and Foley, H. C. (1991). "Curvature and parametric sensitivity in models for adsorption in micropores". *AIChE Journal* 37.3, pp. 429–436. DOI: 10.1002/aic.690370312.

Sato-Berrú, R., Saniger, J. M., Flores-Flores, J., and Sanchez-Espíndola, M. (2013). "Simple Method for the Controlled Growth of SiO2 Spheres". *Journal of Materials Science and Engineering A* 3.4, pp. 237–242.

Schartel, B. (2010). "Phosphorus-based flame retardancy mechanisms-old hat or a starting point for future development?" *Materials* 3.10, pp. 4710–4745. DOI: 10.3390/ma3104710.

Scheidema, M. N. and Taskinen, P. (2011). "Decomposition thermodynamics of magnesium sulfate". *Industrial and Engineering Chemistry Research* 50.16, pp. 9550–9556. DOI: 10.1021/ie102554f.

Sedlbauer, K. (2001). "Vorhersage von Schimmelpilzbildung auf und in Bauteilen". PhD thesis. Universität Stuttgart, pp. 1–105.

Seyfaee, A., Neville, F., and Moreno-Atanasio, R. (2015). "Experimental Results and Theoretical Modeling of the Growth Kinetics of Polyamine-Derived Silica Particles". *Industrial & Engineering Chemistry Research* 54.9, pp. 2466–2475. DOI: 10.1021/acs.iecr.5b00093.

Shea, A., Lawrence, M., and Walker, P. (2012). "Hygrothermal performance of an experimental hemp–lime building". *Construction and Building Materials* 36, pp. 270–275. DOI: 10.1016/j.conbuildmat.2012.04.123.

Sigma-Aldrich (2016). *Trimethoxy(propyl)silane*. URL: https://www.sigmaaldrich.com/catalog/product/aldrich/662275?lang=en&region=GB.

Sing, K., Everett, D., Haul, R., Moscou, L., Pierotti, R., Rouquerol, J., and Siemieniewska, T. (1985). "Reporting physisorption data for gas/solid systems with special reference to the determination of surface area and porosity (Recommendations 1984)". *Pure and Applied Chemistry* 57.4, pp. 603–619. DOI: 10.1351/pac198557040603. eprint: bk-27.

Small, E. (2017). "Classification of Cannabis sativa L. in Relation to Agricultural, Biotechnological, Medical and Recreational Utilization". *Cannabis Sativa L. - Botany and Biotechnology*. Ed. by S. Chandra, H. Lata, and M. A. ElSohly. Chap. 1, pp. 1–62.

Steen-Hansen, A., Mikalsen, R. F., and Jensen, U. E. (2018). "Smouldering Combustion in Loose-Fill Wood Fibre Thermal Insulation: An Experimental Study". *Fire Technology* 54.6, pp. 1585–1608. DOI: 10.1007/s10694-018-0757-4.

Sterling, E., Arundel, A., and Sterling, T. (1985). "Criteria for Human Exposure to Humidity in Occupied Buildings". *ASHRAE Transactions* 91, pp. 611–622.

Stetefeld, J., McKenna, S. A., and Patel, T. R. (2016). "Dynamic light scattering: a practical guide and applications in biomedical sciences". *Biophysical Reviews* 8.4, pp. 409–427. DOI: 10.1007/s12551-016-0218-6. eprint: 0005074v1.

Stöber, W., Fink, A., and Bohn, E. (1968). "Controlled growth of monodisperse silica spheres in the micron size range". *Journal of Colloid and Interface Science* 26.1, pp. 62–69. DOI: 10.1016/0021-9797(68)90272-5.

Stockmayer, W. H. (1944). "Theory of molecular size distribution and gel formation in branched polymers: II. General cross linking". *The Journal of Chemical Physics* 12.4, pp. 125–131. DOI: 10.1063/1.1723922.

Tan, C. G., Bowen, B. D., and Epstein, N. (1987). "Production of monodisperse colloidal silica spheres: Effect of temperature". *Journal of Colloid And Interface Science* 118.1, pp. 290–293. DOI: 10.1016/0021-9797(87)90458-9.

Tavisto, M., Kuisma, R., Pasila, A., and Hautala, M. (2003). "Wetting and wicking of fibre plant straw fractions". *Industrial Crops and Products* 18.1, pp. 25–35. DOI: 10.1016/S0926-6690(03)00017-7.

Taylor, A., Durand, G. G., Alvarez Tirado, M., Sid, N., and Mycock, S. (2017). "Functionalisation Method for Metal Oxide Particles. WO2017/093759A1."

Thomas, J. C. (1987). "The determination of log normal particle size distributions by dynamic light scattering". *Journal of Colloid and Interface Science* 117.1, pp. 187–192.

Thomsen, A. B., Rasmussen, S., Bohn, V., Nielsen, K. V., and Thygesen, A. (2005). *Hemp raw materials : The effect of cultivar , growth conditions and pretreatment on the chemical composition of the fibres*. Tech. rep. Forskningscenter Risø, pp. 6–30.

Topuz, B., Şimşek, D., and Çiftçioğlu, M. (2015). "Preparation of monodisperse silica spheres and determination of their densification behaviour". *Ceramics International* 41.1, pp. 43–52. DOI: 10.1016/j.ceramint.2014.07.112.

Torero, J. L. (2016). "Flaming Ignition of Solid Fuels". *SFPE Handbook of Fire Protection Engineering*. Ed. by M. Hurley. Fifth edition. Chap. 21, pp. 633–661. DOI: 10.1007/978-1-4939-2565-0_21.

Tran Le, A. D., Maalouf, C., Mai, T. H., Wurtz, E., and Collet, F. (2010). "Transient hygrothermal behaviour of a hemp concrete building envelope". *Energy and Buildings* 42.10, pp. 1797–1806. DOI: 10.1016/j.enbuild.2010.05.016.

Troitzsch, J. H. (1998). "Overview of Flame Retardants". *Chimica Oggi / Chemistry Today* 16.January/February 1998.

Tsai, H. J. and Lee, Y. L. (2007). "Facile method to fabricate raspberry-like particulate films for superhydrophobic surfaces". *Langmuir* 23.25, pp. 12687–12692. DOI: 10.1021/la702521u.

Tsuyumoto, I. and Oshio, T. (2009). "Development of fire resistant laminated wood using concentrated sodium polyborate aqueous solution". *Journal of Wood Chemistry and Technology* 29.4, pp. 277–285. DOI: 10.1080/02773810903033721.

Upton, G. and Cook, I. (1996). *Understanding Statistics*. Oxford University Press.

Viel, M., Collet, F., and Lanos, C. (2018). "Chemical and multi-physical characterization of agro-resources' by-product as a possible raw building material". *Industrial Crops and Products* 120.December 2017, pp. 214–237. DOI: 10.1016/j.indcrop.2018.04.025.

Vignon, M. R., Garcia-Jaldon, C., and Dupeyre, D. (1995). "Steam explosion of woody hemp chenevotte". *International Journal of Biological Macromolecules* 17.6, pp. 395–404. DOI: 10.1016/0141-8130(96)81852-6.

Wakelyn, P. J. (2008). "Environmentally friendly flame resistant textiles". *Advances in Fire Retardant Materials*. Ed. by A. R. Horrocks and D. Price. Woodhead Publishing Limited. Chap. 9, pp. 188–212. DOI: 10.1533/9781845694701.1.188.

Wang, D., Peng, L., Zhu, G., Fu, F., Zhou, Y., and Song, B. (2014). "Improving the sound absorption capacity of wood by microwave treatment". *BioResources* 9.4, pp. 7504–7518. DOI: 10.15376/biores.9.4.7504-7518.

Wang, H.-C., Wu, C.-Y., Chung, C.-C., Lai, M.-H., and Chung, T.-W. (2006). "Analysis of Parameters and Interaction between Parameters in Preparation of Uniform Silicon Dioxide Nanoparticles Using Response Surface Methodology". *Industrial & Engineering Chemistry Research* 45, pp. 8043–8048. DOI: 10.1021/ie060299f.

Ward, M. H., Colt, J. S., Deziel, N. C., Whitehead, T. P., Reynolds, P., Gunier, R. B., Nishioka, M., Dahl, G. V., Rappaport, S. M., Buffler, P. A., and Metayer, C. (2014). "Residential levels of polybrominated diphenyl ethers and risk of childhood acute lymphoblastic leukemia in California". *Environmental Health Perspectives* 122.10, pp. 1110–1116. DOI: 10.1289/ehp.1307602.

Weaver, J. (1918). "The Quadrat Method in Teaching Ecology". *The Plant World* 21.11, pp. 267–283.

Wenzel, R. N. (1936). "Resistance of solid surfaces to wetting by water". *Industrial and Engineering Chemistry* 28.8, pp. 988–994. DOI: 10.1021/ie50320a024.

Wilkie, C. A. and Morgan, A. B. (2008). "Nanocomposites I: Current developments in nanocomposites as novel flame retardants". *Advances in Fire Retardant Materials*. Ed. by A. R. Horrocks and D. Price. Woodhead Publishing Limited. Chap. 5, pp. 95–123. DOI: 10.1533/9781845694701.1.95.

Witkowski, A., Stec, A. A., and Hull, T. R. (2016). "Thermal Decomposition of Polymeric Materials". *SFPE Handbook of Fire Protection Engineering*. Ed. by M. Hurley. Fifth edition. Chap. 7, pp. 167–254. DOI: 10.1007/978-1-4939-2565-0_7,.

Wojdyla, A. M., Durand, G., Taylor, A., and Boyd, I. (2015). "Advanced low-energy durable coatings". *International Journal of Energy Research* 39, pp. 165–171. DOI: 10.1002/er.

Xue, C. H., Li, Y. R., Zhang, P., Ma, J. Z., and Jia, S. T. (2014). "Washable and wear-resistant superhydrophobic surfaces with self-cleaning property by chemical etching of fibers and hydrophobization". *ACS Applied Materials and Interfaces* 6.13, 10153–10161. DOI: 10.1021/am501371b.

Yang, H., Yan, R., Chen, H., Lee, D. H., and Zheng, C. (2007). "Characteristics of hemicellulose, cellulose and lignin pyrolysis". *Fuel* 86.12-13, pp. 1781–1788. DOI: 10.1016/j.fuel.2006.12.013.

Zhuravlev, L. T. (1993). "Surface characterization of amorphous silica - a review of work from the former USSR". *Colloids and Surfaces A: Physicochemical and Engineering Aspects* 74.1, pp. 71–90. DOI: 10.1016/0927-7757(93)80399-Y.

Zhuravlev, L. T. (2000). "The surface chemistry of amorphous silica. Zhuravlev model". *Colloids and Surfaces A: Physicochemical and Engineering Aspects* 173.1-3, pp. 1–38. DOI: 10.1016/S0927-7757(00)00556-2.